Final Report

for

# A STUDY OF LOW-COST RELIABLE ACTUATORS FOR LIGHT AIRCRAFT

KU-FRL-351

NASA Grant NSG 1421

Part A: Chapters 1 - 8

Jan Roskam
Principal Investigator

Prepared by: Han Eijsink
Mark Rice

April 1978

TABLE OF CONTENTS

TABLE OF CONTENTS (continued)

TABLE OF CONTENTS (continued)

## SYMBOLS

| Symbol | Meaning | Dimension |
|---|---|---|
| $A_p$ | Piston Area | $in^2$ |
| $A_v$ | Valve Area | $in^2$ |
| a | Number of parallel paths through the armature | |
| b | Wing Span | ft |
| $C_{D_1}$ | Steady state drag coefficient | |
| $C_d$ | Discharge Coefficient | |
| $C_h$ | Hinge Moment Coefficient | |
| $C_{L_\alpha} = \frac{\partial C_L}{\partial \alpha}$ | Variation of lift coefficient with angle of attack | $deg^{-1}$ or $rad^{-1}$ |
| $C_{L_{\delta_E}}$ | Variation of lift coefficient with elevator deflection | $deg^{-1}$ or $rad^{-1}$ |
| $C_{\ell_p} = \frac{\partial C_\ell}{\partial (\frac{pb}{2U_1})}$ | Variation of rolling moment coefficient with roll rate | $rad^{-1}$ |
| $C_{\ell_{\delta_A}} = \frac{\partial C_\ell}{\partial \delta_A}$ | Variation of rolling moment coefficient with aileron deflection | $rad^{-1}$ |
| $C_{m_q}$ | Variation of pitching moment coefficient with pitch rate | $rad^{-1}$ |
| $C_{m_\alpha}$ | Variation of pitching moment coefficient with angle of attack | $rad^{-1}$ |
| $C_{m_{\dot{\alpha}}}$ | Variation of pitching moment coefficient with rate of change of angle of attack | $rad^{-1}$ |
| $C_{m_{\delta_E}}$ | Variation of pitching moment coefficient with elevator deflection | $rad^{-1}$ |

SYMBOLS (continued)

| Symbol | Meaning | Dimension |
|---|---|---|
| $C_q$ | Flow Coefficient | |
| c | Chord | ft |
| $\bar{c}$ | Mean Aerodynamic Chord | ft |
| E | Supply Voltage | Volt |
| $E_g$ | Voltage generated in an electric motor | Volt |
| $F_L$ | Load Force | lbf |
| G | Gearing Ratio (ratio of motor rpm to output rpm) | |
| g | Gravitational Acceleration | $ft/sec^2$ |
| H | Transfer Function | |
| h | Linear actuator moment arm | in |
| I | Moment of Inertia | $in\text{-}lbf\text{-}sec^2$ |
| I | Current | Ampere |
| $I_{xx}$ | Airplane moment of inertia about the X-axis | $slug\text{-}ft^2$ |
| $I_{yy}$ | Airplane moment of inertia about the Y-axis | $slug\text{-}ft^2$ |
| J | Total inertia reflected to motor | $in\text{-}lbf\text{-}sec^2$ |
| $J_L$ | Load Inertia | $in\text{-}lbf\text{-}sec^2$ |
| $J_R$ | Rotor Inertia | $in\text{-}lbf\text{-}sec^2$ |
| K | Error Amplifier Gain | Volt/deg |
| $K_E$ | Voltage Constant | Volt/rad/sec |
| $K_p$ | Pilot Gain | deg/deg |
| $K_T$ | Torque Constant | in-lbf/Amp |

SYMBOLS (continued)

| Symbol | Meaning | Dimension |
|---|---|---|
| $K_v$ | Valve Gain | $in^2/in$ |
| k | Constant defined in (B.2-8) | $in^2/sec$ |
| $k_c$ | Load Torque Constant | in-lbf/rad |
| L | Inductance | Henry |
| $L_p$ | Dimensional variation of rolling moment with roll rate (See Table 6.1) | $sec^{-1}$ |
| $L_{\delta_A}$ | Dimensional variation of rolling moment with aileron deflection (See Table 6.1) | $sec^{-2}$ |
| M | Hinge Moment | in-lbf |
| $M_A$ | Product of elevator area and elevator centroid-to-hingeline distance | $in^3$ |
| $M_E$ | Elevator centroid-to-hingeline distance | in |
| $M_L$ | Load Moment | in-lbf |
| $M_q$ | Dimensional variation of pitching moment with pitch rate (See Table 6.1) | $sec^{-1}$ |
| $M_\alpha$ | Dimensional variation of pitching moment with angle of attack (See Table 6.1) | $sec^{-2}$ |
| $M_{\dot{\alpha}}$ | Dimensional variation of pitching moment with rate of change of angle of attack (See Table 6.1) | $sec^{-1}$ |
| $M_{\delta_E}$ | Dimensional variation of pitching moment with elevator deflection (See Table 6.1) | $sec^{-2}$ |
| $M_2$ | Mass in exhaust volume | $lbf\text{-}sec^2/in$ |
| $\dot{M}_2$ | Exhaust mass flow rate | lbf-sec/in |
| m | Airplane Mass | slugs |

SYMBOLS (continued)

| Symbol | Meaning | Dimension |
|---|---|---|
| $m_e$ | Equivalent Mass | $lbf\text{-}sec^2/in$ |
| n | Rotor Rotational Speed | rpm |
| $P_e$ | Ambient Pressure | psi |
| $P_L$ | Load Pressure | psi |
| $P_{PK}$ | Peak Power Output | hp |
| $P_s$ | Supply Pressure | psi |
| $P_1$ | Actuator Supply Pressure | psi |
| $P_2$ | Actuator Exhaust Pressure | psi |
| $\dot{P}_2$ | Rate of change in exhaust pressure | psi/sec |
| p | Number of poles in an electric motor | |
| p | Roll Rate | rad/sec |
| q | Flow Rate (Chapter 5, Appendix B.3) | $in^3/sec$ |
| q | Pitch Rate (Chapter 6) | rad/sec |
| $q_s$ | Supply Flow Rate | $in^3/sec$ |
| $q_1$ | Actuator supply flow rate | $in^3/sec$ |
| $\bar{q}_1$ | Steady state dynamic pressure | $lbf/ft^2$ |
| $q_2$ | Actuator exhaust flow rate | $in^3/sec$ |
| R | Gas Constant | $in^2/sec^2\text{-}R$ |
| R | Resistance | Ω |
| r | Rotary actuator piston radius | in |

SYMBOLS (continued)

| Symbol | Meaning | Dimension |
|---|---|---|
| $r_p$ | Rotary actuator moment arm | in |
| S | Wing Area | $ft^2$ |
| $S_a$ | Aileron Area | $ft^2$ |
| $S_e$ | Elevator Area | $ft^2$ |
| s | Laplace Operator | $sec^{-1}$ |
| T | Torque | in-lbf |
| T | Computer Time | sec |
| $T_c$ | Concurrent Load Torque | in-lbf |
| $T_{IL}$ | Inertial Load Torque | in-lbf |
| $T_L$ | Pilot lead time constant | sec |
| $T_m$ | Motor Torque | in-lbf |
| $T_{max}$ | Maximum Output Torque | in-lbf |
| $T_s$ | Stall Torque | in-lbf |
| $T_2$ | Actuator Exhaust Temperature | R |
| t | Time | sec |
| $U_1$ | Steady state forward velocity | ft/sec |
| $V_{max}$ | Maximum voltage | Volt |
| $V_2$ | Actuator Exhaust Volume | $in^3$ |
| $\dot{V}_2$ | Rate of change of exhaust volume | $in^3/sec$ |
| W | Weight | lbf |

SYMBOLS (continued)

| Symbol | Meaning | Dimension |
|---|---|---|
| $x$ | Actuator Piston Displacement | in |
| $\dot{x}$ | Actuator Piston Velocity | in/sec |
| $\ddot{x}$ | Actuator Piston Acceleration | $in/sec^2$ |
| $x_c$ | Command Displacement | in |
| $Z$ | Number of armature conductors | |
| $Z_s$ | Z-axis of stability axes system | |
| $Z_\alpha$ | Dimensional variation of $Z_s$-force with angle of attack (See Table 6.1) | $ft-sec^{-2}$ |
| $Z_{\delta_E}$ | Dimensional variation of $Z_s$-force with elevator deflection (See Table 6.1) | $ft-sec^{-2}$ |
| $\alpha$ | Angle of Attack | deg or rad |
| $\alpha$ | Time Scaling Factor | |
| $\gamma$ | Specific Heat Ratio | |
| $\delta$ | Control Surface Deflection | deg or rad |
| $\dot{\delta}$ | Control Surface Rate of Deflection | deg/sec or rad/sec |
| $\ddot{\delta}$ | Control Surface Angular Acceleration | $deg/sec^2$ or $rad/sec^2$ |
| $\delta_A$ | Aileron Deflection | deg or rad |
| $\delta_E$ | Elevator Deflection | deg or rad |
| $\delta_c$ | Command Deflection | deg or rad |
| $\varepsilon$ | Error Signal | deg or rad |
| $\zeta$ | Damping Constant | |

SYMBOLS (continued)

| Symbol | Meaning | Dimension |
|---|---|---|
| $\eta$ | Efficiency | |
| $\theta$ | Pitch Attitude Angle | deg or rad |
| $\theta$ | Rotor Displacement Angle | rad |
| $\dot{\theta}$ | Rotor Rotational Speed | rad/sec |
| $\ddot{\theta}$ | Rotor Angular Acceleration | $rad/sec^2$ |
| $\rho$ | Density | $lbf\text{-}sec^2/in^4$ |
| $\tau$ | Pilot reaction time delay constant | sec |
| $\tau_a$ | Actuator Time Constant | sec |
| $\Phi$ | Flux per Pole | Wb |
| $\phi$ | Roll Angle | deg or rad |
| $\omega$ | Rotor Rotational Speed | rad/sec |
| $\omega$ | Bandwidth | rad/sec |
| $\omega_n$ | Undamped Natural Frequency | rad/sec |

Subscripts

| | |
|---|---|
| a | Aileron |
| e | Elevator |
| h | Horizontal Tail |
| S. P. | Short Period |

# CHAPTER 1

## INTRODUCTION

This report is the result of a study conducted by the University of Kansas Flight Research Laboratory for the National Aeronautics and Space Administration under Grant Number NSG 1421, "A Study of Low Cost, Reliable Actuators for Single Engine Light Aircraft." The study has been conducted from June 15, 1977, to March 15, 1978.

An analysis involving electro-mechanical, electro-pneumatic and electro-hydraulic actuators has been performed to study which are compatible for use in the primary and secondary flight controls of a single engine light aircraft. Actuator characteristics under investigation include cost, reliability, weight, force, volumetric requirements, power requirements, response characteristics and heat accumulation characteristics.

Actuators are a necessity for positioning the control surfaces of large commercial and military aircraft. By having the actuator controlled by an electrical signal, an automatic control system can be used to position the control surface. Using simple, low-cost actuators and with recent advances in electronics, such as micro-computers, it should be possible to develop an automatic flight control system for a single engine light aircraft in an acceptable price range.

This study has compared the basic types of actuators for performance characteristics in positioning a control surface model and then mathematically evaluated each actuator in an aircraft to get the closed loop dynamic response characteristics. Conclusions have then been made as to the suitability of each actuator type for use in an aircraft.

# CHAPTER 2

# CONTROL SURFACE MODEL DERIVATION

This chapter provides a description of the control surface model that has been used to allow a comparison of the actuator types; furthermore it describes the characteristics of the control surfaces of the aircraft used in the closed loop analysis of Chapter 6.

Section 2.1 describes the geometry, inertia characteristics and flight conditions used for the control surface model. Sections 2.2 to 2.4 do the same for the control surfaces of the aircraft.

## 2.1 CONTROL SURFACE

To evaluate each actuator for purposes of comparison, a typical horizontal tail configuration for a light aircraft has been used. The elevator on the horizontal tail is normally the largest single control surface under the highest loading and determines the maximum actuator size needed. Frictional forces in cable driven control systems are typically only several pounds; and since load forces exceed 500 pounds, friction will be considered negligible in this analysis.

Two flight conditions have been used to provide data for sizing the actuators and comparing their performance. A maximum load condition was used to size the actuator for stall force, and a cruise load condition was used to evaluate time response.

### 2.1.1 CONTROL SURFACE GEOMETRY AND MASS

Reference 1 is being used to determine the aerodynamic coefficients for the hinge moments of the control surface. An aspect ratio of 4.5 and a surface area of 40 square feet is typical for a horizontal tail on a light single engine aircraft and is used for the planform. A 30% chord elevator has been used with no sweep at the hingeline axis, the

same planform as tested in Reference 1. The horizontal tail planform is shown in Figure 2.1, and dimensions are outlined in Table 2.1.

The weight of the control surface is obtained using empirical methods in Reference 2, and the weight of the elevator is estimated to be 12 pounds. To calculate the inertia, the control surface is assumed to be a flat plate with its hingeline axis on one edge. The following equation is used:

$$I = \frac{c^2 W}{3g} \tag{2.1}$$

For a linear actuator this inertia must be converted to an equivalent mass for the equation of motion by using the following relation illustrated in Figure 2.2:

$$\frac{x}{h} = \sin \delta \doteq \delta \tag{2.2}$$

$$F_L h = I\ddot{\delta} \tag{2.3}$$

$$F_L = m_e \ddot{x} \tag{2.4}$$

$$m_e = \frac{I}{h^2} \tag{2.5}$$

### 2.1.2 CONTROL SURFACE FLIGHT CONDITIONS

A graph from Reference 1 showing the variation in hinge moment coefficient with change in angle of attack and control surface deflection is shown in Fig. 2.3. The planform geometry is the same as for the control surface model and was run in tests at a Mach number of 0.21 in Reference 1. This Mach number will be used at sea level for the maximum load condition. For the cruise load a typical altitude for a single engine light aircraft of 6000 feet and a cruise Mach number of 0.18 (117 knots) has been used. The two flight conditions are summarized in Table 2.2. An angle of attack of -10° (according to Figure

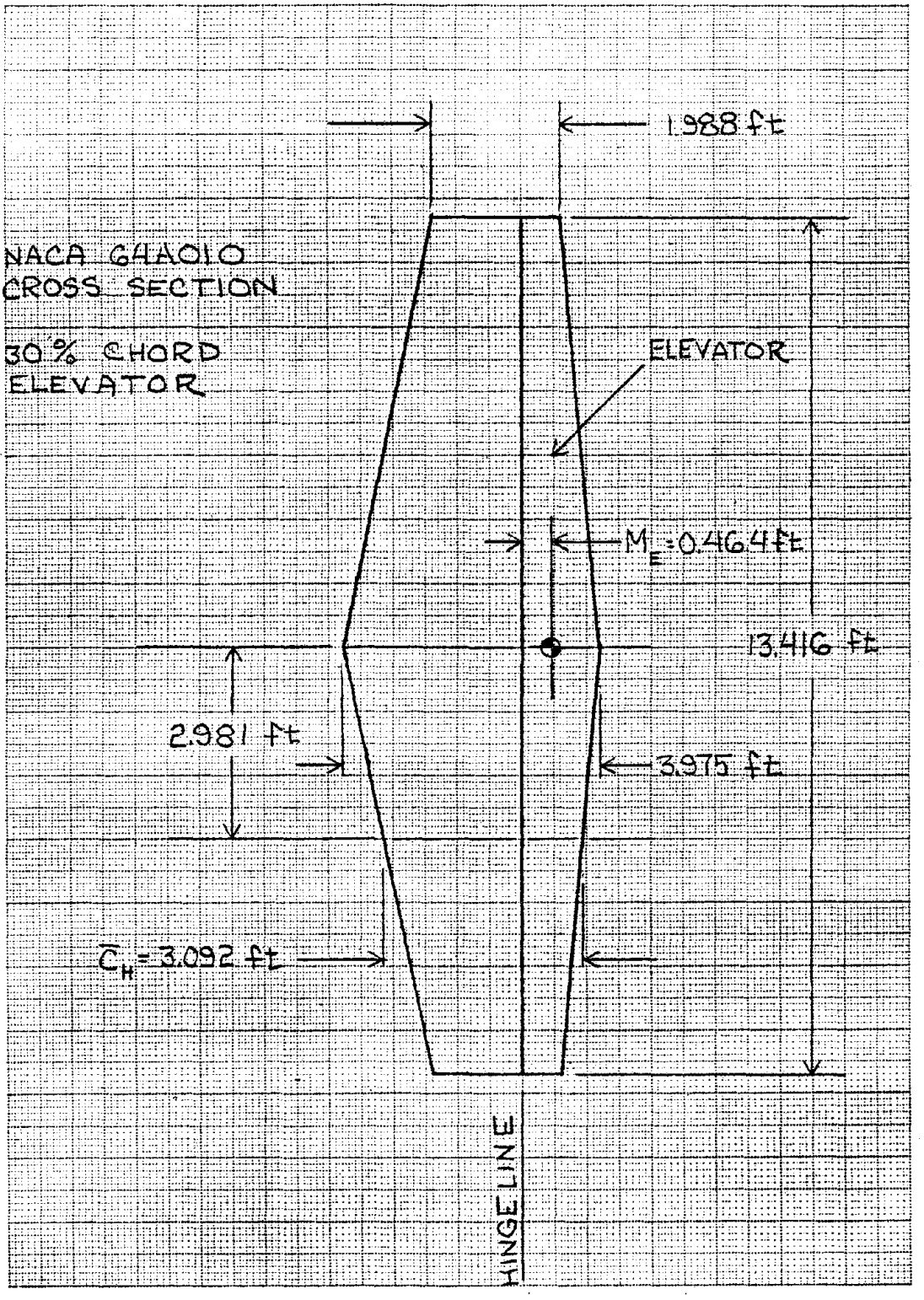


| | | | | | |
|---|---|---|---|---|---|
| CALC | | | REVISED | DATE | Figure 2.1: Control Surface Model Planform Geometry |
| CHECK | | | MSR | | |
| APPD | | | | | |
| APPD | | | | | UNIVERSITY OF KANSAS |
| | | | | | PAGE 4 |

Table 2.1 - Control Surface Dimensions

| | |
|---|---|
| Horizontal Tail Area | 40.00 $ft^2$ |
| Aspect Ratio | 4.5 |
| Span | 13.416 ft |
| Taper Ratio | 0.5 |
| Horizontal Tail MAC | 3.092 ft |
| Horizontal Tail Root Chord | 3.975 ft |
| Horizontal Tail Tip Chord | 1.988 ft |
| Elevator Chord Percentage | 30% |
| Elevator Area | 12.00 $ft^2$ |
| Elevator MAC | 0.928 ft |
| Elevator Average Chord | 0.894 ft |
| Hingeline Angle | 0° |
| Leading Edge Angle | 11.7° |
| Hingeline to Elevator Centroid Distance | 0.464 ft |
| Elevator Area Moment ($M_A$) | 5.565 $ft^3$ |
| Elevator Weight | 12 lb |
| Elevator Hingeline Inertia | 1.192 lb in $sec^2$ |
| Linear Actuator Moment Arm | 4.0 in |
| Equivalent Mass (Linear Actuator) | 0.0745 lb $sec^2$/in |

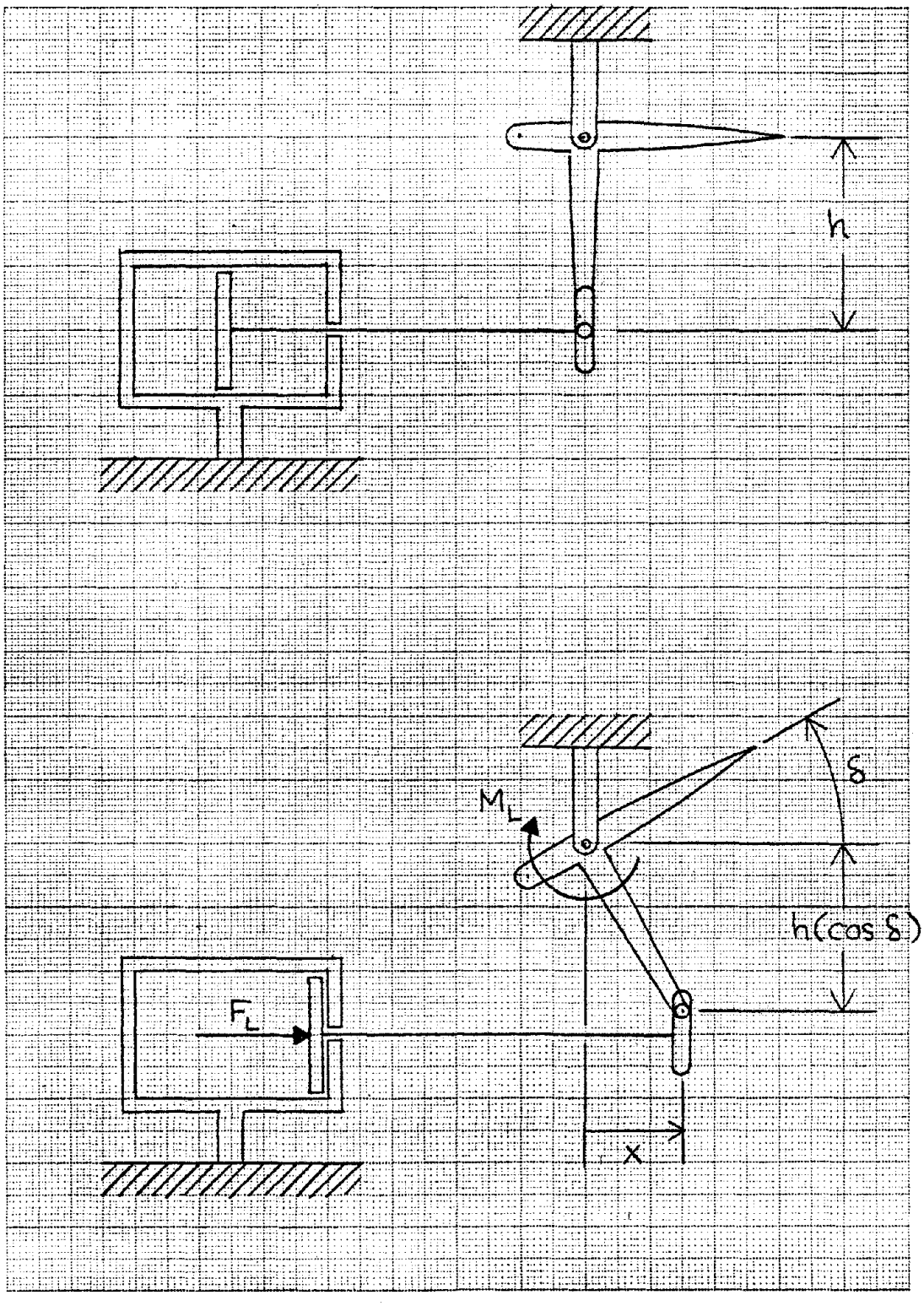


| | | | | |
|---|---|---|---|---|
| CALC | | | REVISED | DATE |
| CHECK | | | | |
| APPD | | | | |
| APPD | | | | |
| | | | | |

Figure 2.2: Linear Actuator Geometry

UNIVERSITY OF KANSAS

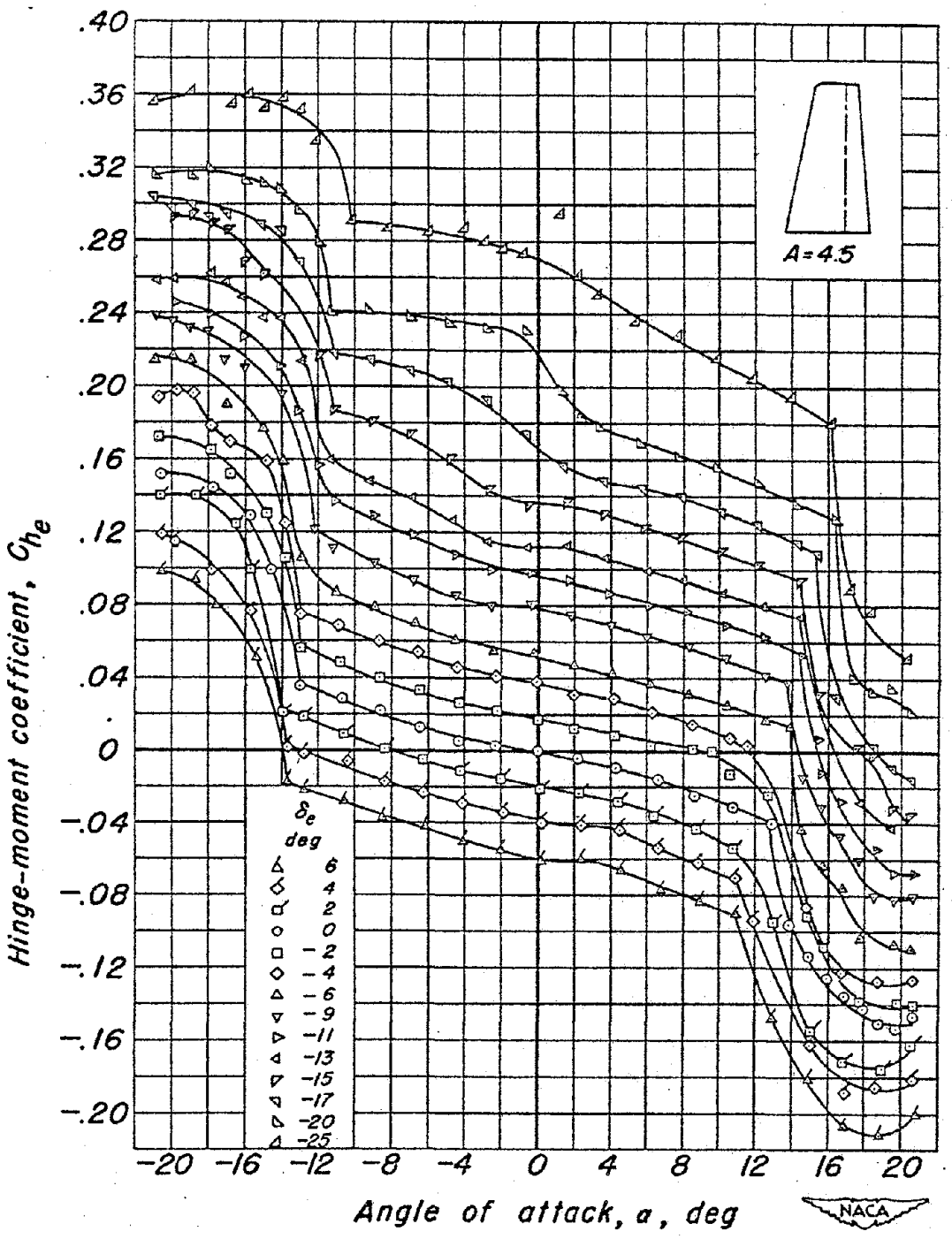


Hinge-moment coefficient.

| | | | | | |
|---|---|---|---|---|---|
| CALC | | | REVISED | DATE | Figure 2.3: Control Surface Model Hinge Moment Coefficients |
| CHECK | | | MSR | | |
| APPD | | | | | |
| APPD | | | | | UNIVERSITY OF KANSAS |
| | | | | | PAGE 7 |

Table 2.2 - CONTROL SURFACE MODEL FLIGHT CONDITIONS

| | Cruise Load | Maximum Load |
|---|---|---|
| Altitude | 6000 ft | Sea Level |
| Mach Number | 0.18 | 0.21 |
| Airspeed | 117 knots | 119 knots |
| Dynamic Pressure | 38.46 $lb/ft^2$ | 65.33 $lb/ft^2$ |
| Angle of Attack | 0° | -10° |

| Deflection Angle | Linear Displacement | Hinge Moment Coefficient | Hinge Moment | Axial Load Force |
|---|---|---|---|---|
| $\delta$ | x | $C_{h_e}$ | $M_L$ | $F_L$ |
| deg | in | | in-lbf | lbf |
| **Cruise Load** | | | | |
| 0 | 0. | 0. | 0. | 0. |
| 2 | 0.140 | 0.017 | 87. | 21.8 |
| 4 | 0.279 | 0.036 | 185. | 46.3 |
| 6 | 0.418 | 0.051 | 262. | 65.8 |
| 9 | 0.626 | 0.078 | 401. | 101.5 |
| 11 | 0.763 | 0.096 | 493. | 125.5 |
| 13 | 0.900 | 0.112 | 576. | 147.8 |
| 15 | 1.035 | 0.136 | 699. | 181.0 |
| 17 | 1.169 | 0.166 | 853. | 223.0 |
| 20 | 1.368 | 0.216 | 1110. | 295.3 |
| 25 | 1.690 | 0.270 | 1388. | 382.8 |
| **Maximum Load** | | | | |
| 0 | 0. | 0.025 | 218. | 54.5 |
| 2 | 0.140 | 0.044 | 384. | 96.0 |
| 4 | 0.279 | 0.064 | 559. | 140.0 |
| 6 | 0.418 | 0.082 | 716. | 180.0 |
| 9 | 0.626 | 0.109 | 951. | 240.8 |
| 11 | 0.763 | 0.131 | 1143. | 291.0 |
| 13 | 0.900 | 0.153 | 1336. | 342.8 |
| 15 | 1.035 | 0.184 | 1606. | 415.5 |
| 17 | 1.169 | 0.217 | 1894. | 495.3 |
| 20 | 1.368 | 0.241 | 2103. | 559.5 |
| 25 | 1.690 | 0.290 | 2531. | 698.3 |

2.3) has been used for the maximum load condition to apply an initial load at a zero deflection angle. The cruise flight condition has an angle of attack of 0° for no initial load on the control surface, such as in a trimmed elevator. A zero load condition where only inertial forces are present has also been evaluated. This loading condition is similar to deflecting a control surface on a stationary aircraft.

The hinge moment coefficients of Reference 1 are converted to the control surface hinge moments by the following relationship:

$$M_L = 2C_{h_e} q M_A \tag{2.6}$$

The variable q is free-stream dynamic pressure, and $M_A$ is the product of the elevator area and the distance from its centroid to the hingeline axis. For a rotary actuator, assuming no gearing, this is the applied load, but for a linear actuator this must be converted to an axial force. Figure 2.2 illustrates the following relationship to determine the axial load force:

$$F_L = \frac{M_L}{h \cos \delta} \tag{2.7}$$

The moment arm h has been selected as 4 inches. Studies into an optimum moment arm would involve control surface structural properties and the dynamics of the entire aircraft and is beyond the scope of this analysis. This moment arm was chosen as one that would result in a reasonably sized actuator for the applied loads. The control surface moments and forces are in tabular form in Table 2.2 and in graphical form in Figure 2.4.

When the pilot wants to deflect a control surface, he moves some control device inside the cockpit. This requires a finite amount of time, and a step input for this movement or "command input" would be

unrealistic. A ramp input from a zero deflection angle to the final deflection angle in 0.1 seconds has been used. After 0.1 seconds the command input is held constant at the final deflection angle. A longer time interval for the initial ramp input would decrease the time response of the actuator excessively, as the actuator can be at over half its final deflection after the first tenth of a second. Each time response graph shows the command input as a solid line with an arrow.

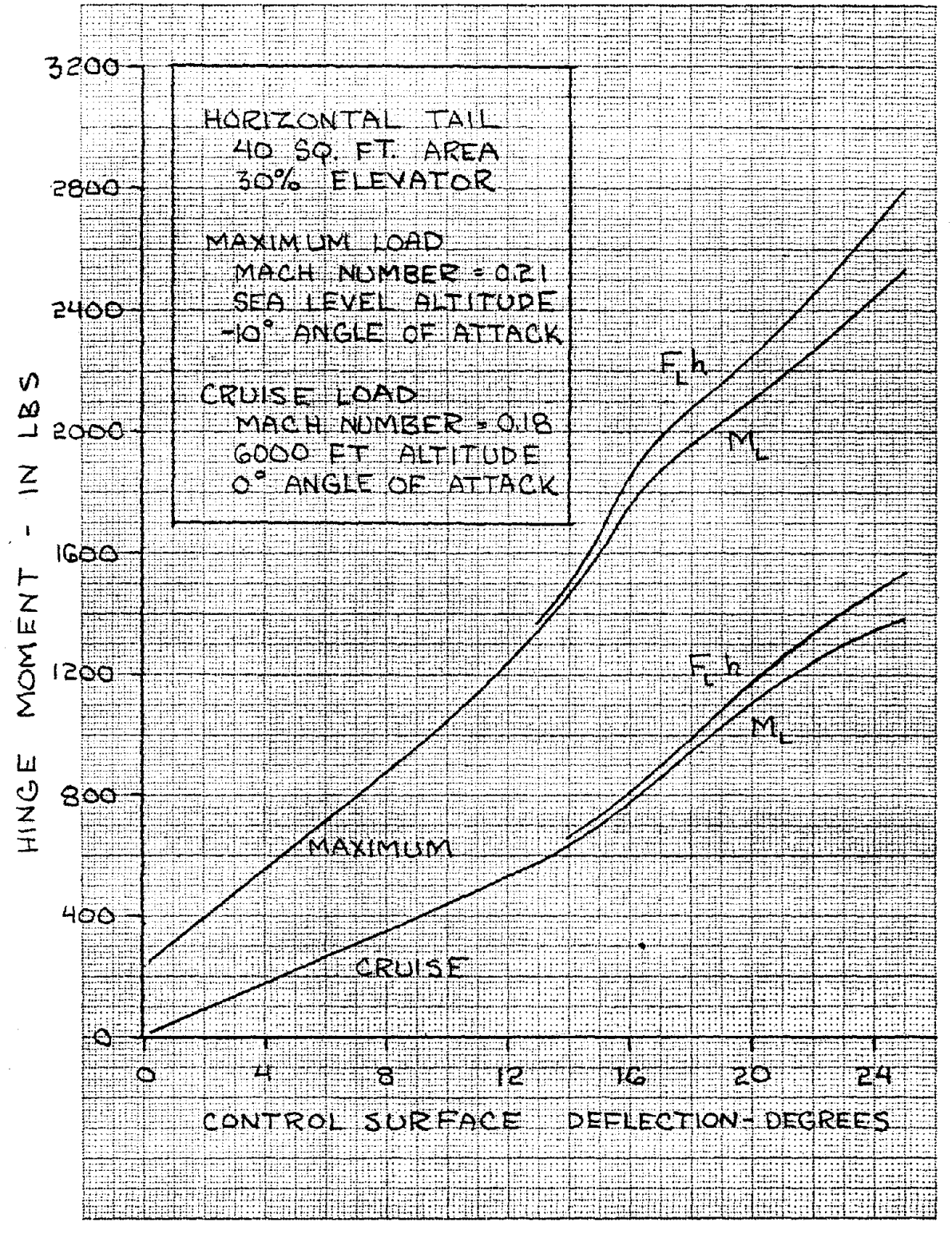


| | | | | | | |
|---|---|---|---|---|---|---|
| CALC | | | REVISED | DATE | Figure 2.4: Control Surface Model Hinge Moments | |
| CHECK | | | MSR | | | |
| APPD | | | | | | |
| APPD | | | | | | |
| | | | | | UNIVERSITY OF KANSAS | PAGE 11 |

## 2.2 HINGE MOMENT DATA AND CONTROL SURFACE INERTIAS OF A LIGHT SINGLE-ENGINE AIRPLANE

In the flight control system analysis to be performed in Chapter 6, this airplane will be referred to as airplane A. A threeview of this airplane is given in Figure 2.5, while Table 2.3 contains data on geometry and flight conditions. The control surface geometry is given below; the areas are aft hinge line areas.

Elevator: $S_e = 15.46\ ft^2$

$\bar{c}_e = 1.49\ ft$

Aileron: $S_a = 6.95\ ft^2$ (one aileron)

$\bar{c}_a = 1.2\ ft$

The hinge moment curves presented in Figures 2.6-2.9 have been derived from wind tunnel data (Reference 3) applied to the flight conditions from Table 2.1. Aileron hinge moment curves are those for the right aileron; deflection is positive for a right turn. Elevator deflection is positive for trailing edge down.

Hinge moments are calculated according to:

$$M_e = C_{h_e} \cdot 1/2\, \rho V^2 S_e \bar{c}_e \tag{2.8}$$

and:

$$M_a = C_{h_a} \cdot 1/2\, \rho V^2 S_a \bar{c}_a \tag{2.9}$$

for elevator and aileron, respectively.

The aileron hinge moment curves (Figure 2.8 and 2.9) may look a bit strange, but that can be explained as follows. Positive right aileron deflection means a trailing edge up deflection, and this is easier to do than a deflection downwards because the static pressure

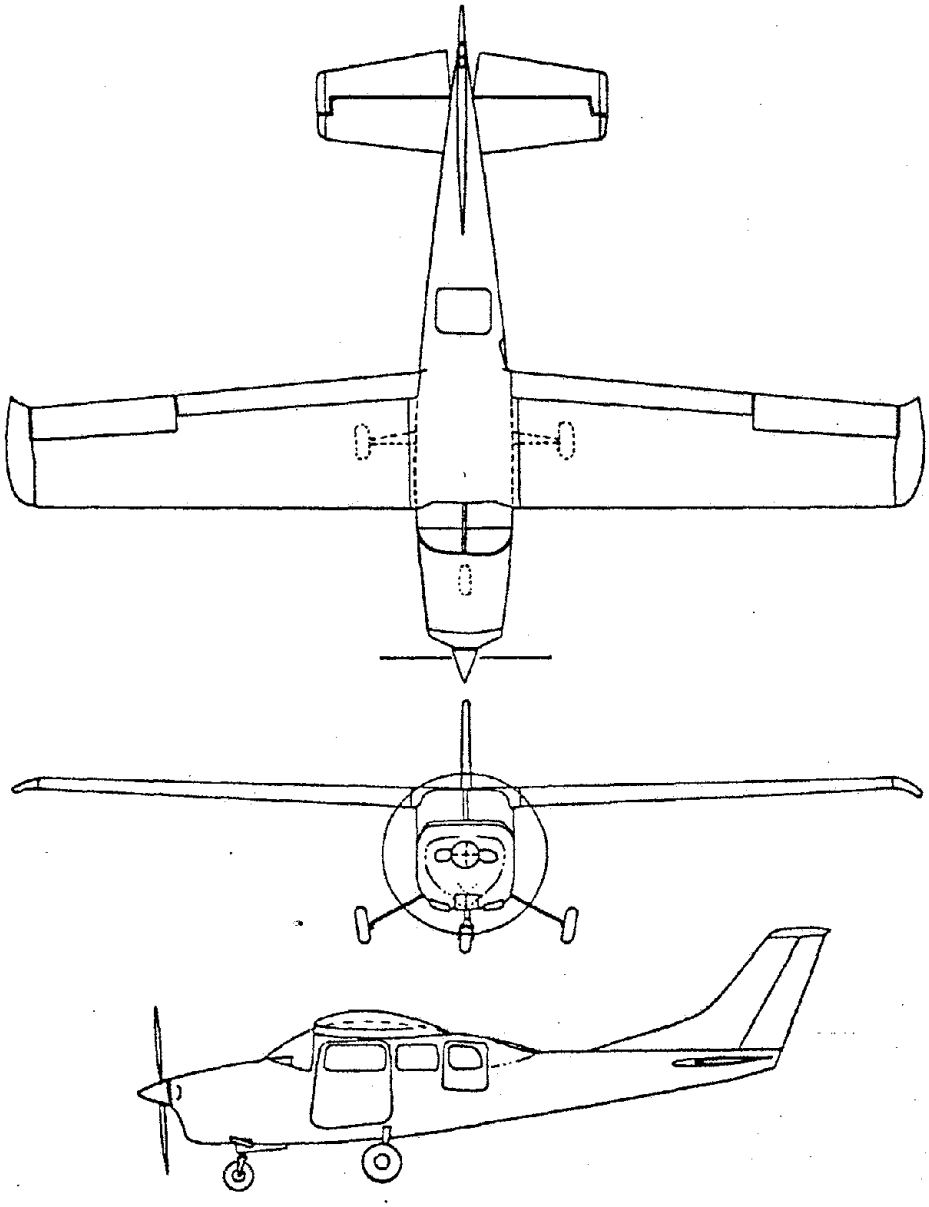

Figure 2.5: Airplane A Threeview

Table 2.3 Data on Airplane A

| | |
|---|---|
| **BASELINE DATA** | |
| WING AREA | 180 $FT^2$ |
| WING SPAN | 36.75 FT |
| WING MAC | 4.95 FT |
| WEIGHT | 2650 LBS |
| **CRUISE CONDITION** | |
| ALTITUDE | 5000 FT |
| AIRSPEED | 130 KNOTS |
| DYNAMIC PRESSURE | 49.5 $LB/FT^2$ |
| **APPROACH CONDITION** | |
| ALTITUDE | 0 FT |
| AIRSPEED | 63 KNOTS |
| DYNAMIC PRESSURE | 13.6 $LB/FT^2$ |

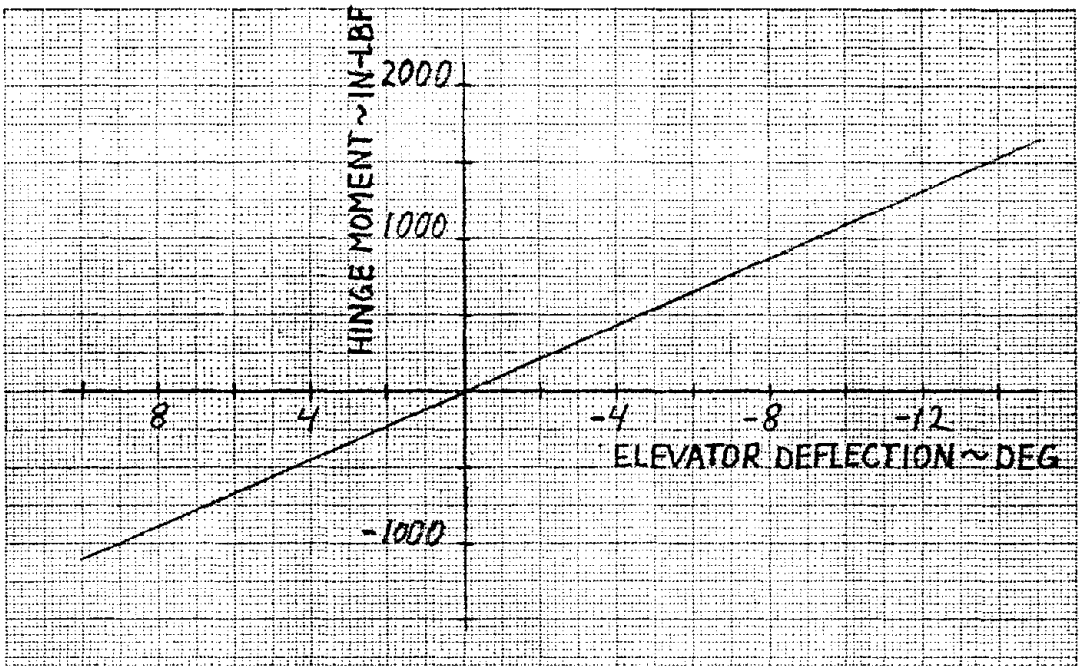


Figure 2.6 Elevator hinge moments for Airplane A (cruise)

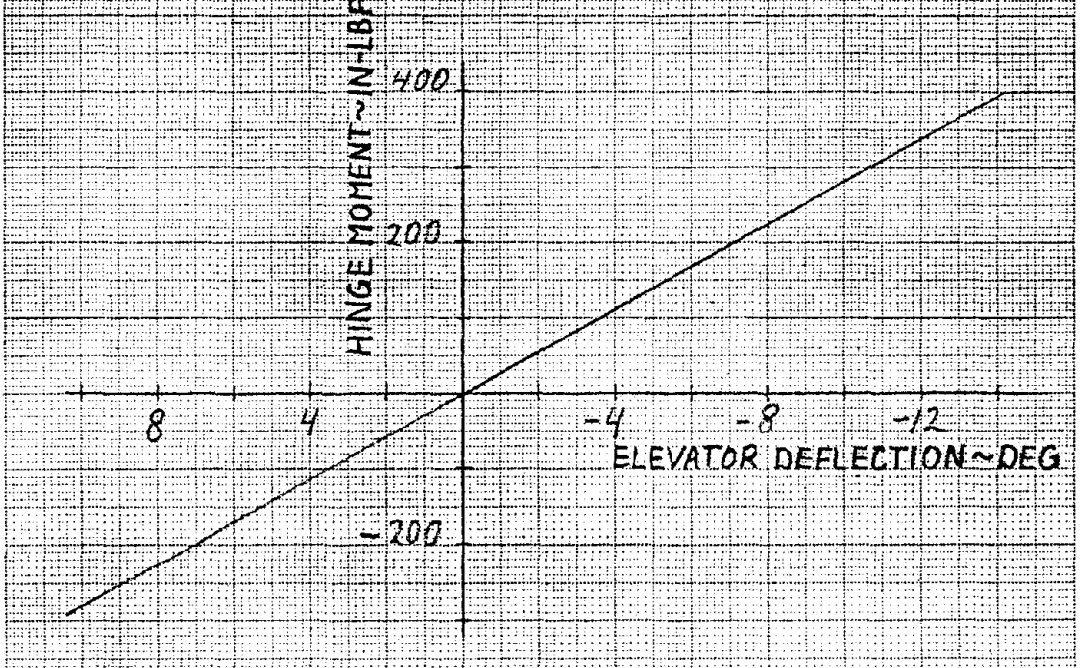


Figure 2.7 Elevator hinge moments for Airplane A (approach)

| | | | | | | |
|---|---|---|---|---|---|---|
| CALC | HE | | REVISED | DATE | | |
| CHECK | | | | | | |
| APPD | | | | | | |
| APPD | | | | | | |
| | | | | | UNIVERSITY OF KANSAS | PAGE 15 |

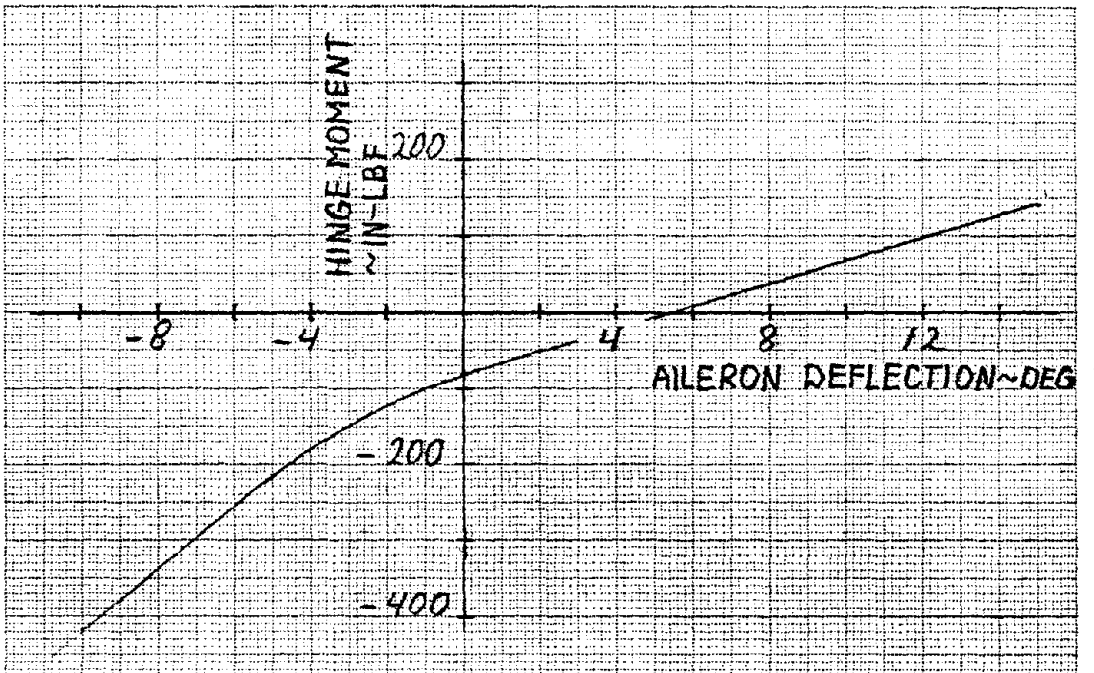


Figure 2.8 Aileron hinge moments for Airplane A (cruise)

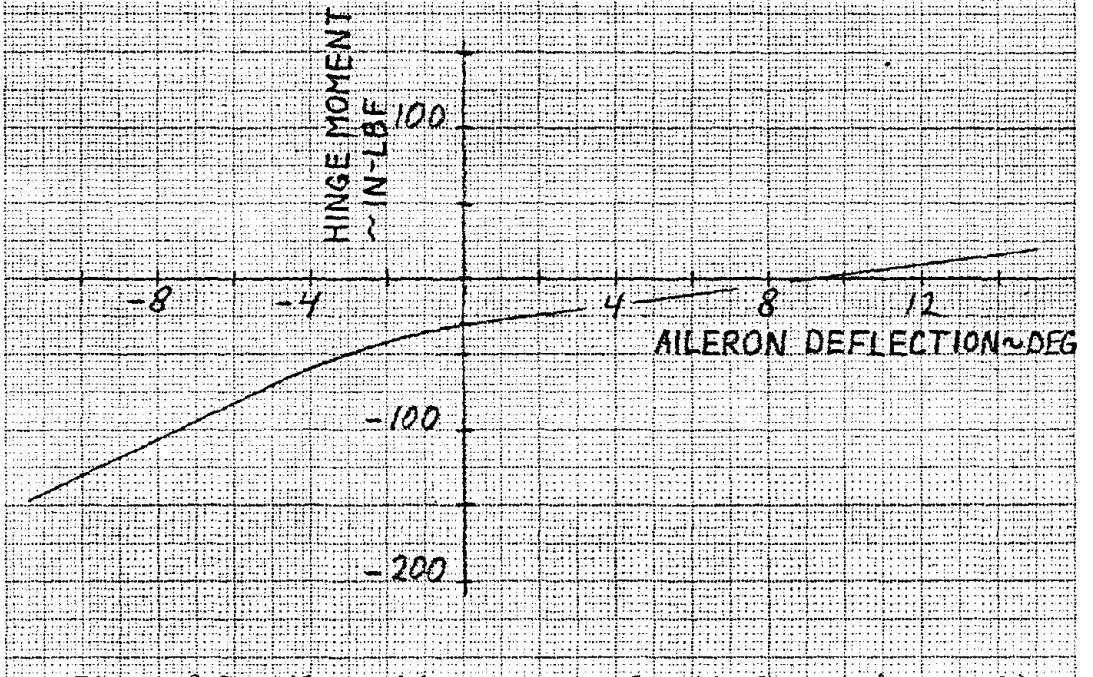


Figure 2.9 Aileron hinge moments for Airplane A (approach)

under the wing is higher than that over the wing. Furthermore, the wing is flown at some angle of attack so the air blows against the lower side of the control surface causing a small hinge moment at zero deflection. If there is one actuator driving both ailerons, this has no effect because the ailerons deflect in opposite directions; but on two actuators driving each separately, it has.

In Section 4.3.2 an electro-pneumatic actuator will be sized to fit on this airplane. To do this, not only the control surface hinge moments must be known but also their inertias about the hingeline. An estimation of these inertias will be given below.

Tailweight of this airplane is about 61 lbs (Reference 2 ). Assume the horizontal tail weight to be two-thirds of this, then stabilizer plus elevator weigh about 40 lbs. Assume further that the mass of the horizontal tail is evenly distributed. Elevator area is 37% of the area of the horizontal tail (Reference 3 ), so then elevator weight becomes approximately 15 lbs. The inertia is then [ with (2.1) ]:

$$I_E = \frac{c^2}{3}\,\frac{W}{g} = 0.3447 \text{ lbf-ft-sec}^2$$
$$= 4.1364 \text{ lbf-in-sec}^2$$

Assume also that the aileron has the same weight per unit area as the elevator, then the weight of one aileron becomes $\frac{6.95}{15.46} \times 15 =$ 6.7 lbs. Aileron inertia is then:

$$I_A = \frac{c^2}{3}\,\frac{W}{g} = 0.0999 \text{ lbf-ft-sec}^2$$
$$= 1.1985 \text{ lbf-in-sec}^2$$

These are only rough estimates, but no better data are currently available.

With these data approximate actuator-plus-control surface transfer functions can be derived in Section 4.3.2; these transfer functions will then be used in Section 6.2 for some flight control system analysis on this airplane.

## 2.3 HINGE MOMENT DATA AND CONTROL SURFACE INERTIAS FOR A LIGHT TWIN

In Section 6.3 this airplane will be referred to as airplane B. A threeview of this airplane is given in Figure 2.10, while Table 2.4 contains geometry and flight condition data. The control surface geometry is as follows (areas are aft hinge line areas):

Stabilator: $S_e = 19.5\ ft^2$

$\bar{c}_e = 2.7\ ft$

Aileron: $S_a = 5.8\ ft^2$ (one aileron)

$\bar{c}_a = 1.0\ ft$

The hinge moment curves given in Figures 2.11-2.14 have been derived from wind tunnel data (Reference 4) applied to the flight conditions given in Table 2.4. Aileron hinge moment curves are those for the right aileron; deflection is positive for a right turn. This airplane has no stabilizer-elevator combination but a stabilator, an all moving horizontal tail; deflection is positive for trailing edge down. The hinge moments have been calculated according to (2.8) and (2.9) for stabilator and aileron, respectively.

Stabilator hinge moments (Figure 2.11 and 2.12) are very high, but the control surface effectiveness is also much higher than for a stabilizer-elevator combination. This means that much less deflection is needed for a given moment change about the Y-axis of the airplane.

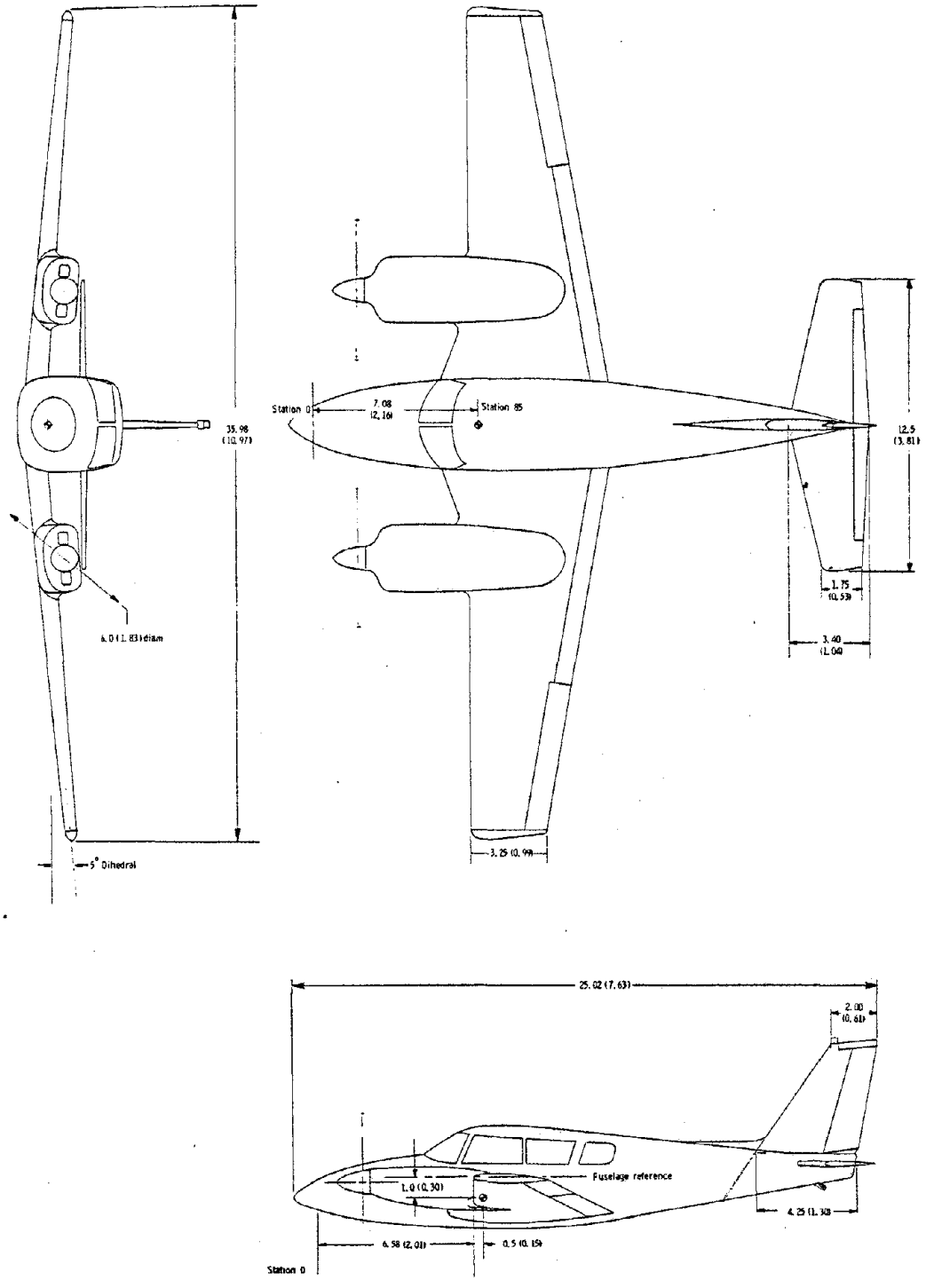


Figure 2.10: Airplane B Threeview

Table 2.4 Data on Airplane B

| | |
|---|---|
| **BASELINE DATA** | |
| WING AREA | 178 $FT^2$ |
| WING SPAN | 35.98 FT |
| WING MAC | 5.0 FT |
| WEIGHT | 3220 LBS |
| **CRUISE CONDITION** | |
| ALTITUDE | 7000 FT |
| AIRSPEED | 146 KNOTS |
| DYNAMIC PRESSURE | 58.2 $LB/FT^2$ |
| **APPROACH CONDITION** | |
| ALTITUDE | 0 FT |
| AIRSPEED | 70 KNOTS |
| DYNAMIC PRESSURE | 16.6 $LB/FT^2$ |

| | | | | | | |
|---|---|---|---|---|---|---|
| CALC | HE | 78/3/4 | REVISED | DATE | | |
| CHECK | | | | | | |
| APPD | | | | | | |
| APPD | | | | | | |
| | | | | | UNIVERSITY OF KANSAS | PAGE 20 |

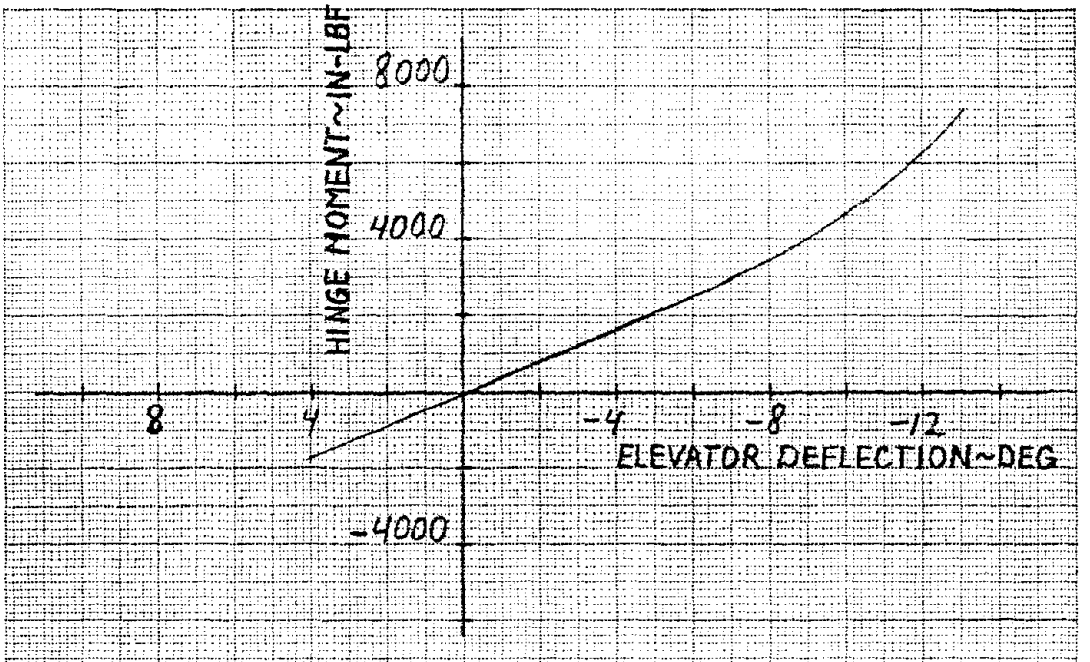


Figure 2.11 Elevator hinge moments for Airplane B (cruise)

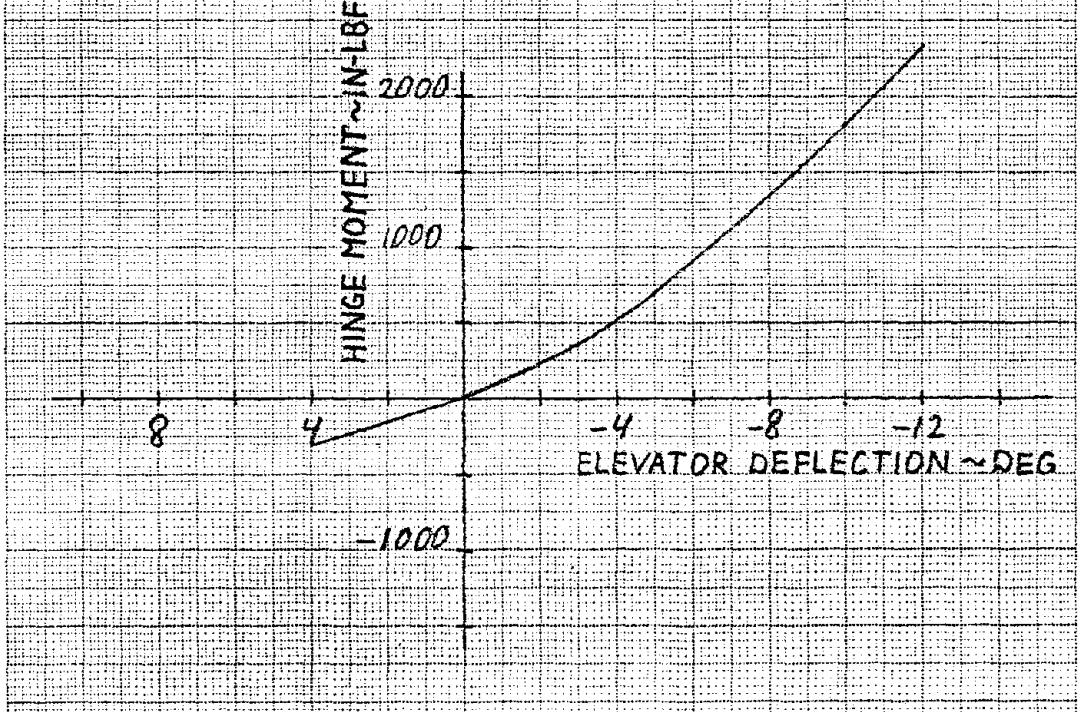


Figure 2.12 Elevator hinge moments for Airplane B (approach)

| | | | | |
|---|---|---|---|---|
| CALC | HE | | REVISED | DATE |
| CHECK | | | | |
| APPD | | | | |
| APPD | | | | |
| | | | | |

UNIVERSITY OF KANSAS

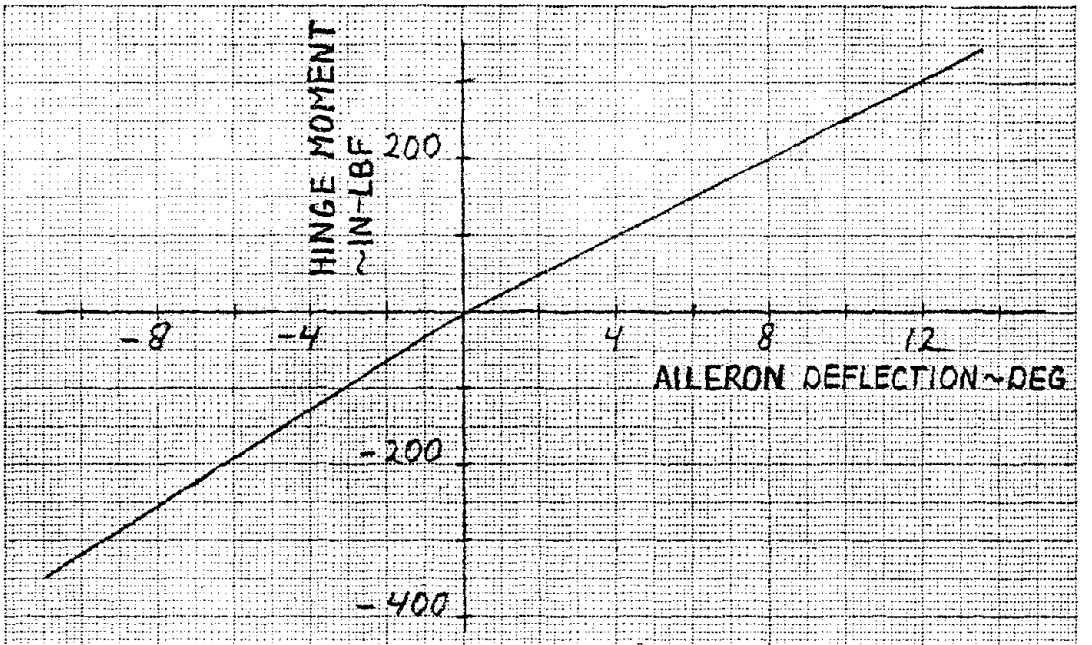


Figure 2.13 Aileron hinge moments for Airplane B (cruise)

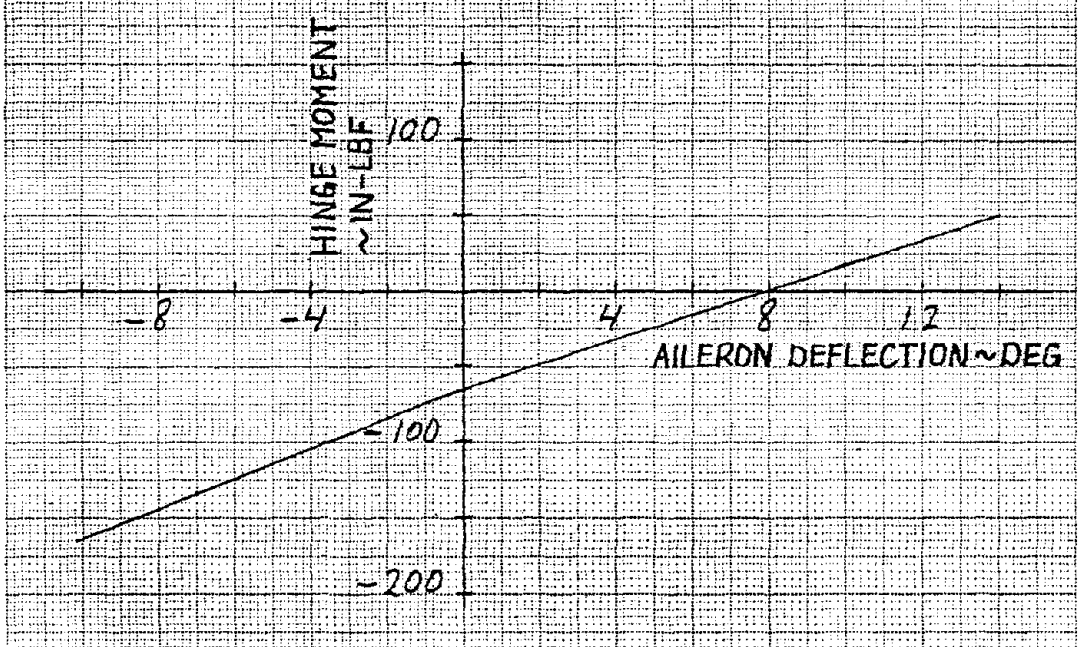


Figure 2.14 Aileron hinge moments for Airplane B (approach)

| | | | | | | |
|---|---|---|---|---|---|---|
| CALC | HE | | REVISED | DATE | | |
| CHECK | | | | | | |
| APPD | | | | | | |
| APPD | | | | | | |
| | | | | | UNIVERSITY OF KANSAS | PAGE 22 |

For the reason explained in Section 2.2, the slopes for positive and negative aileron deflections (Figure 2.13 and 2.14) are different.

Control surface weights are estimated as follows: from Reference 2 it can be found that the tail weight of a similar light twin is 2.44% of MTOW. For this airplane, MTOW is 5200 lbs, so the estimated tail-weight becomes 127 lbs. The horizontal tail will be assumed to weigh two-thirds of this: W = 84.6 lb.

For calculating the inertia about the hingeline, formula (2.1) can be applied two times: on time on the area before the hingeline and one time on the aft hingeline area. The results can simply be added. The hingeline will be assumed to lay on 25% of the chord line.

Part one (area before hingeline):

$$I_{E_1} = \frac{c_1^2}{3}\,\frac{W_1}{g} = 0.0998 \text{ ft-lbf-sec}^2$$
$$= 1.1971 \text{ in-lbf-sec}^2$$

in which:

$$c_1 = 0.25\ \bar{c}_e \text{ and } W_1 = 0.25\ W$$

Part two (aft hingeline area):

$$I_{E_2} = \frac{c_2^2}{3}\,\frac{W_2}{g} = 2.6931 \text{ ft-lbf-sec}^2$$
$$= 32.3169 \text{ in-lbf-sec}^2$$

So total inertia about the hingeline becomes:

$$I_E = I_{E_1} + I_{E_2} = 33.5140 \text{ in-lbf-sec}^2$$

Aileron weight is estimated as horizontal tail weight times the ratio of the control surfaces; this comes to 15.1 lbs. The inertia can then again be calculated with (2.1):

$$I_A = \frac{c^2}{3}\frac{W}{g} = 0.1564 \text{ ft-lbf-sec}^2$$

$$= 1.18773 \text{ in-lbf-sec}^2$$

This information will be used in Section 3.3.2 where an electro-mechanical actuator will be sized for this airplane. Approximate actuator-plus-control surface transfer functions can then be derived which will be used in the flight control system analysis on this airplane (Section 6.3).

## 2.4 HINGE MOMENT DATA AND CONTROL SURFACE INERTIAS FOR A TWIN-ENGINE TURBOPROP

In the flight control system analysis of Chapter 6, this airplane will be referred to as airplane C. A threeview of this airplane can be seen in Figure 2.15; Table 2.5 contains data on geometry and flight conditions. The control surface geometry is as follows (areas are aft hinge line areas):

Elevator: $S_e = 26.39 \text{ ft}^2$

$\bar{c}_e = 1.29 \text{ ft}$

Aileron: $S_a = 6.95 \text{ ft}^2$ (one aileron)

$\bar{c}_a = 0.9 \text{ ft}$

Equations (2.8) and (2.9) are used to calculate the hinge moment curves given in Figures 2.16-2.19; appropriate hinge moment data have been taken from Reference 5. Sign conventions on control surface deflections are the same as in Section 2.2.

Control surface weight data are taken from Reference 6. Elevator weight is 66 lbs; inertia about the hingeline is [with (2.1)]:

$$I_E = \frac{c^2}{3}\frac{W}{g} = 1.1379 \text{ ft-lbf-sec}^2$$

$$= 13.6546 \text{ in-lbf-sec}^2$$

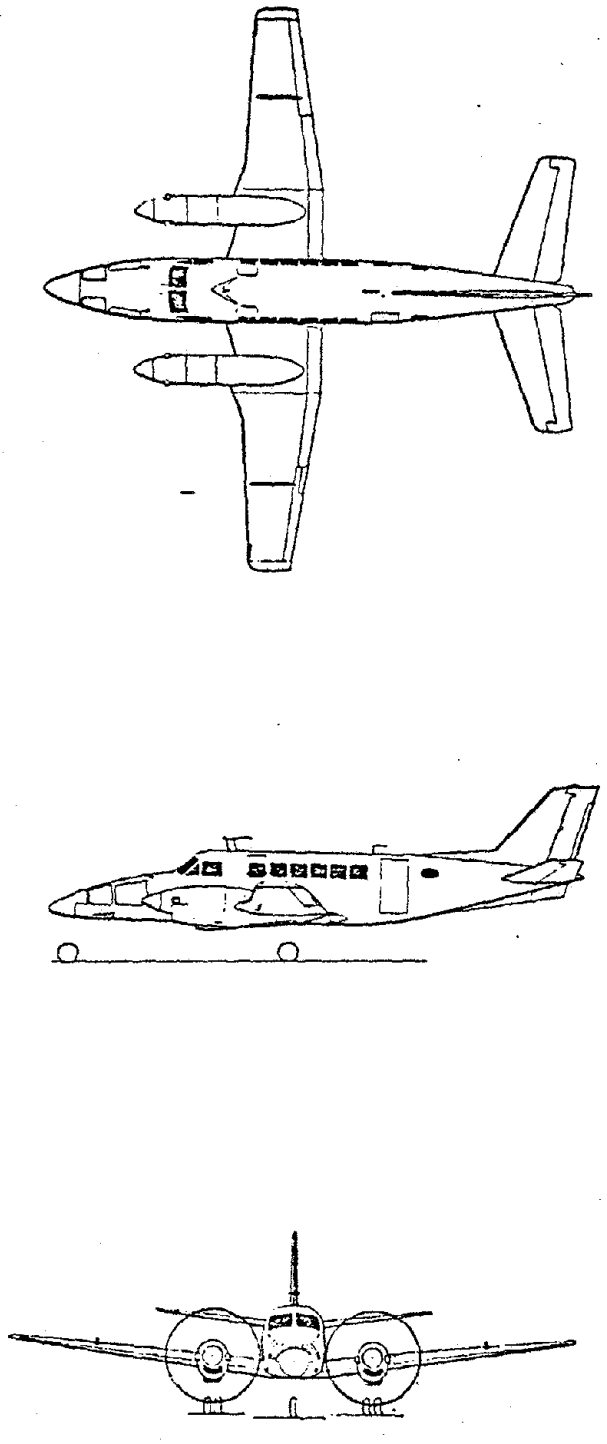

Figure 2.15: Airplane C Threeview

Table 2.5 Data on Airplane C

| | |
|---|---|
| **BASELINE DATA** | |
| WING AREA | 280 $FT^2$ |
| WING SPAN | 46 FT |
| WING MAC | 6.5 FT |
| WEIGHT | 11,000 LBS |
| **CRUISE CONDITION** | |
| ALTITUDE | 20,000 FT |
| AIRSPEED | 266 KNOTS |
| DYNAMIC PRESSURE | 128.4 $LB/FT^2$ |
| **APPROACH CONDITION** | |
| ALTITUDE | 0 FT |
| AIRSPEED | 101 KNOTS |
| DYNAMIC PRESSURE | 34.4 $LB/FT^2$ |

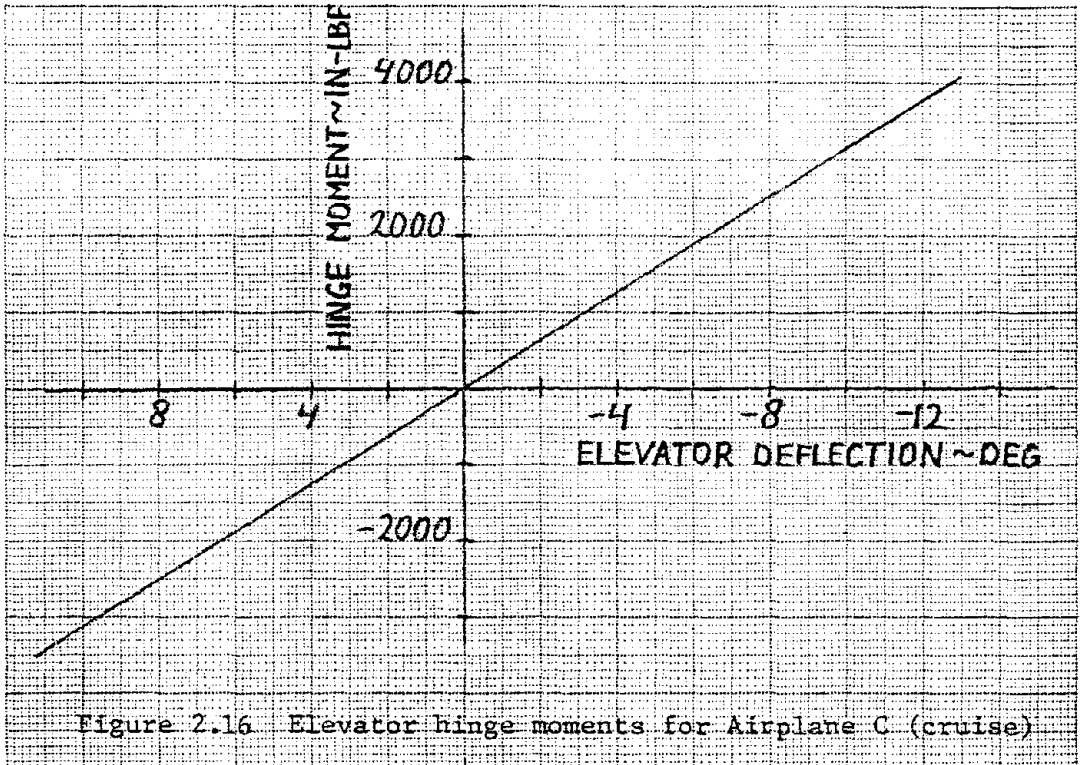


Figure 2.16 Elevator hinge moments for Airplane C (cruise)

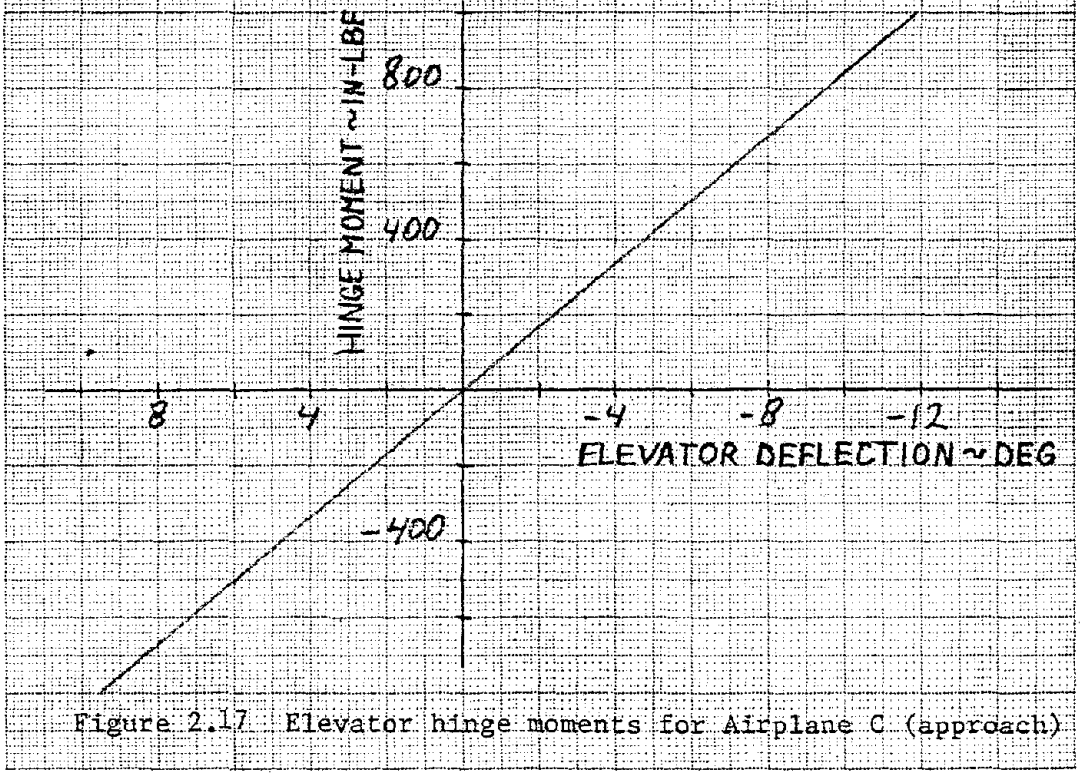


Figure 2.17 Elevator hinge moments for Airplane C (approach)

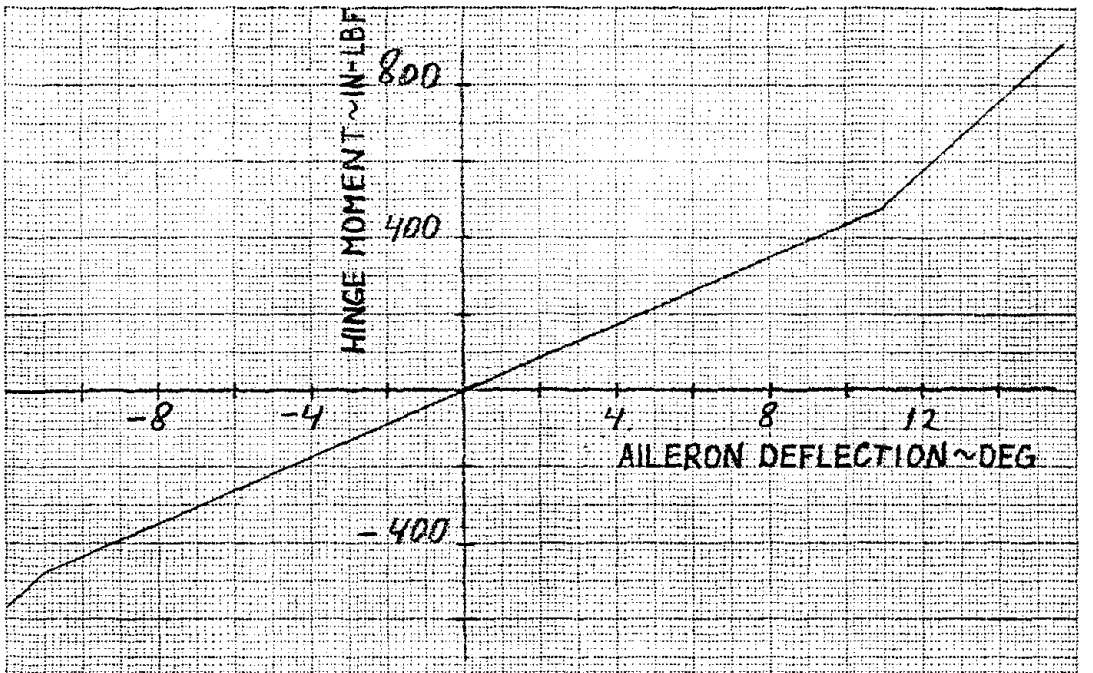


Figure 2.18 Aileron hinge moments for Airplane C (cruise)

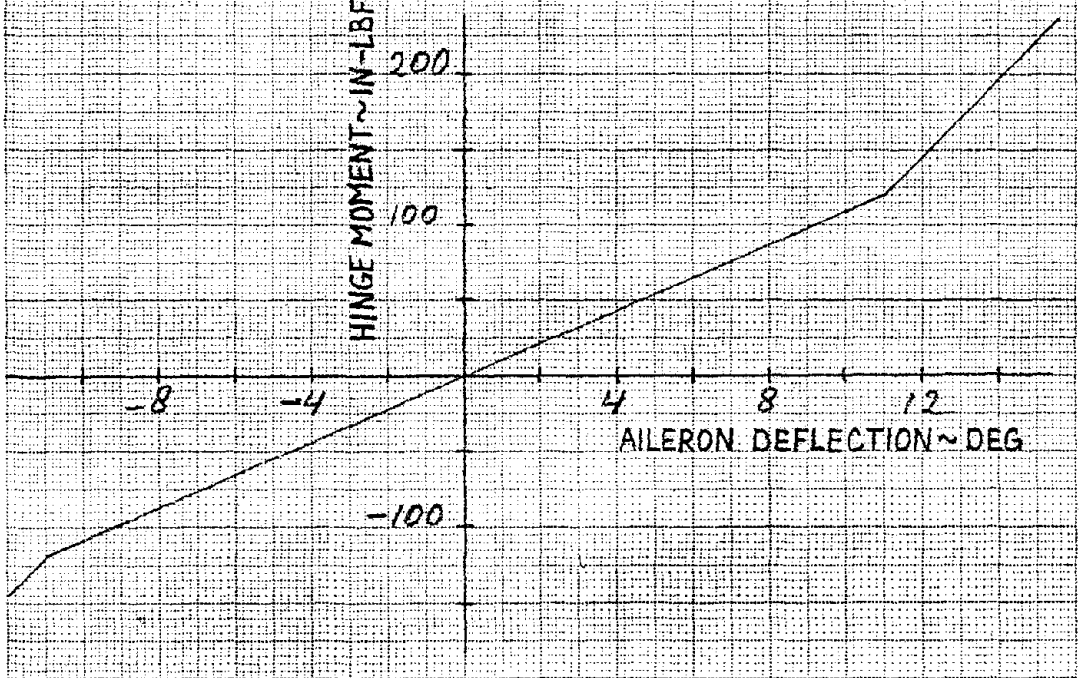


Figure 2.19 Aileron hinge moments for Airplane C (approach)

The weight of one aileron is 14.5 lbs; inertia about the hingeline is:

$$I_A = \frac{c^2}{3}\,\frac{W}{g} = 0.1217 \text{ ft-lbf-sec}^2$$

$$= 1.4602 \text{ in-lbf-sec}^2$$

These data will be used in Section 5.3.2 where an electro-hydraulic actuator will be sized for this airplane. The results of the calculations in that section will then be used in Section 6.4 for the flight control system analysis on this airplane.

References for Chapter 2

1. Dods, J. B. and Tinling, B. E., "Summary of Results of a Wind-tunnel Investigation of Nine Related Horizontal Tails," NACA TN 3497, July 1955.

2. Torenbeek, E., "Synthesis of Subsonic Airplane Design," Delft University Press, The Netherlands, 1976.

3. Carter, C. R., Greer, H. D., Shivers, J. P. and Fink, M. P., "Wind-Tunnel Investigation of Static Longitudinal and Lateral Characteristics of a Full-Scale Mockup of a Light Single-Engine High-Wing Airplane," NASA TN D-7149, May 1973.

4. Fink, M. P. and Freeman, D. C., Jr., "Full-Scale Wind-Tunnel Investigation of Static Longitudinal and Lateral Characteristics of a Light Twin-Engine Airplane," NASA TN D-4983, January 1969.

5. Agnihotri, A. K., "Aerodynamic Data for KU/Beech AACS Test Bed (PD 280)," KU/FRL Report 324 , September 1972.

6. An., "Model PD 280 Weight Distribution and Inertia Data," KU/FRL Report 327, September 1972.

# CHAPTER 3

# ELECTRO-MECHANICAL ACTUATORS

Electro-mechanical actuation is widely used for flap and retractable landing gear systems in small and medium size general aviation aircraft. However, with the development of powerful rare earth-cobalt magnets, this type of actuator has also become available for transport and combat airplanes.

A pulse width modulation amplifier can be used to drive an electro-mechanical actuator; the rate of deflection is proportional to the applied voltage. The control system can be implemented with either analog or digital techniques, the latter becoming increasingly popular.

Section 3.1 deals with electro-mechanical actuation in general. In Section 3.2 a mathematical model for this type of actuator is derived; Section 3.3 then gives time response characteristics for the control surface model described in Section 2.1 and for the stabilator and aileron of Airplane B. Linear approximations of these Airplane B time responses are used in Section 6.3 for the flight control system analysis.

## 3.1 CHARACTERISTICS

In a Direct Current electric motor, torque is generated by the interaction between two different magnetic fields: one of the magnets, one of the conductor windings. The latter magnetic field is caused by current going through the conductor; by changing the current, the strength of this field is also changed.

The magnets of a conventional DC motor are placed in the stator while the rotor consists of conductor windings with associated back

iron to accomodate transmission of magnetic flux. The obtained torque depends on the angle between the two magnetic fields. To get maximum torque for a given current, this angle must be maintained close to 90 degrees. This is accomplished by commutation: when the rotor rotates, the brushes are continually switched to different sets of windings in the rotor.

Because Rare Earth (Samarium)-Cobalt magnets have a much higher energy product (defined as the maximum value of demagnetizing field times induction) than the Alnico magnets normally used in conventional DC motors, it is possible to use them as the rotor. A comparison between the energy products of different magnetic materials is given in Figure 3.1.

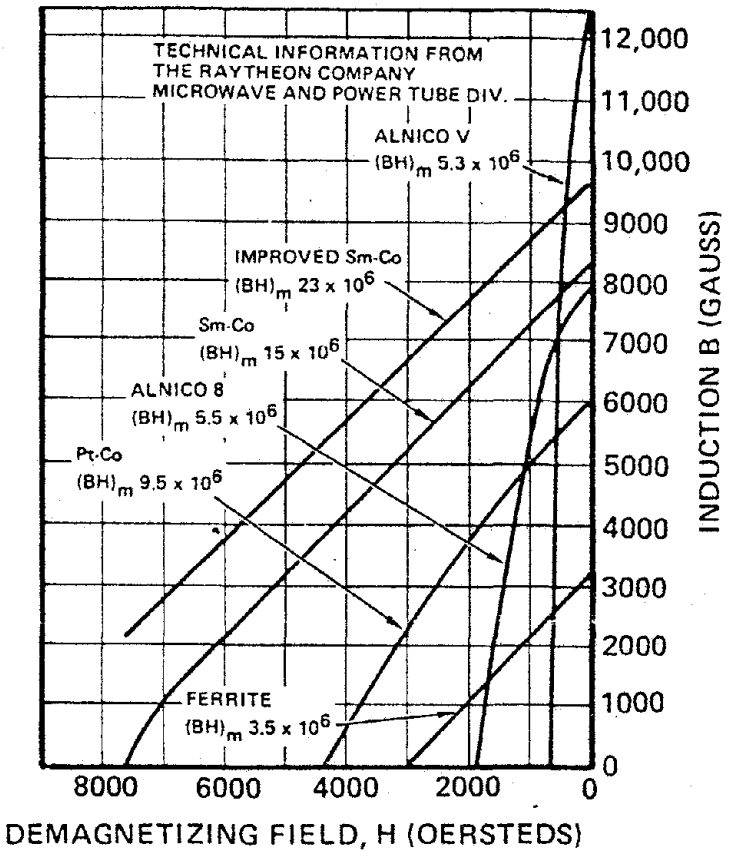


Figure 3.1: Magnetic Characteristics of Different Materials

Wound rotor configurations have a speed limit due to the tensile strength of copper and the attachment of copper to armature. A high energy rotating permanent magnet can have a smaller diameter than a wound rotor. Samarium-Cobalt magnets have modest mechanical properties (Ref. 1) but due to their high volumetric efficiency room for additional high strength materials is available; increased speeds are possible.

Since the conductor windings are now in the stator, brushes are not needed and commutation can be done electronically, as in Figure 3.2, as a function of sensed rotor position. This sensing can be done optically, for example (Ref. 2).

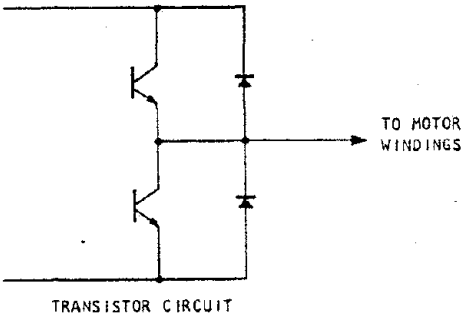


Figure 3.2: Transistor Commutation Circuit

The motor rotation speed can be regulated by varying the average DC voltage supplied to the motor by the electronic commutator. Pulse-width modulation techniques are used to generate the required average voltage.

Thermal control is much better than for a wound rotor configuration because the heat generated in the windings can be transferred to the external motor surface very easily.

There are situations in which a wound rotor would be preferred to a wound stator. This is illustrated in Figure 3.3, taken from Ref. 1. There is a trade-off between response and power; for actuation systems the rotating magnet is the best choice.

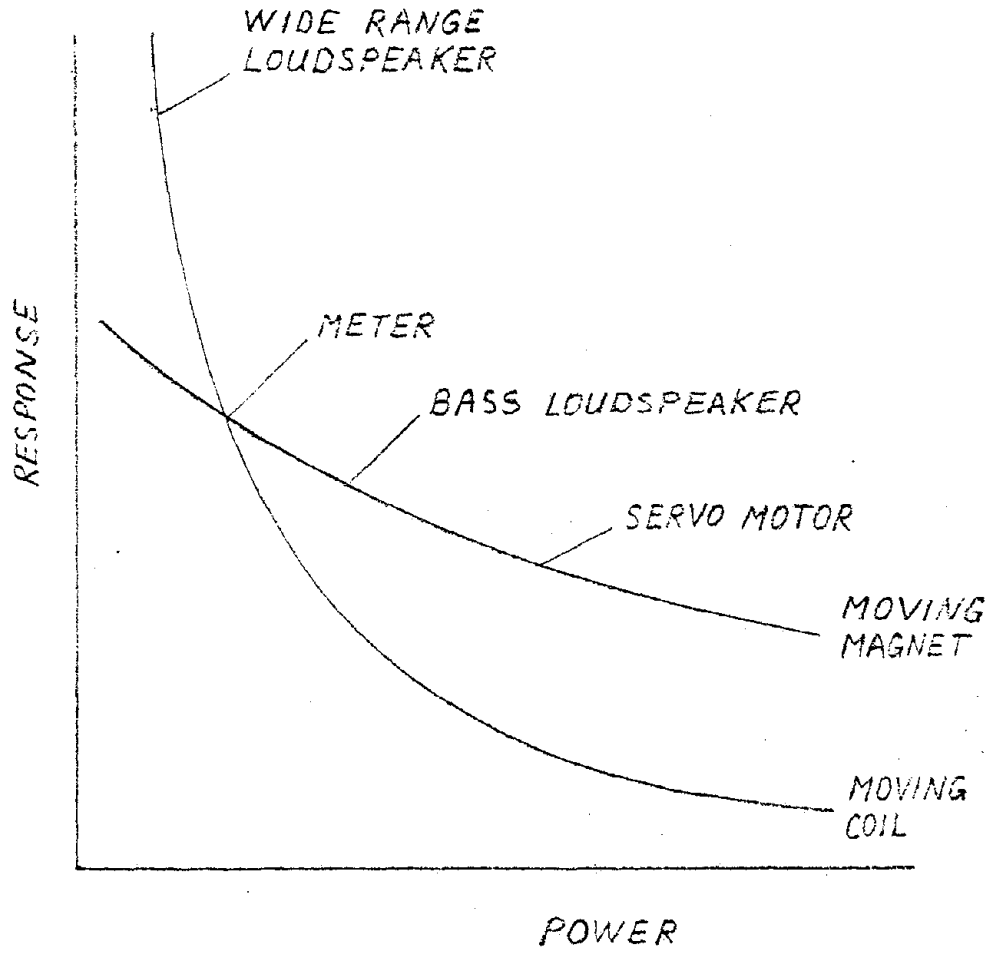


Figure 3.3: Comparison of Device Parameters

There are several possibilities for the implementation of the brushless DC motor. Figure 3.4 compares conventional and surface wound types, while Figure 3.5 shows alternative rotor magnet arrangements (see Ref. 3).

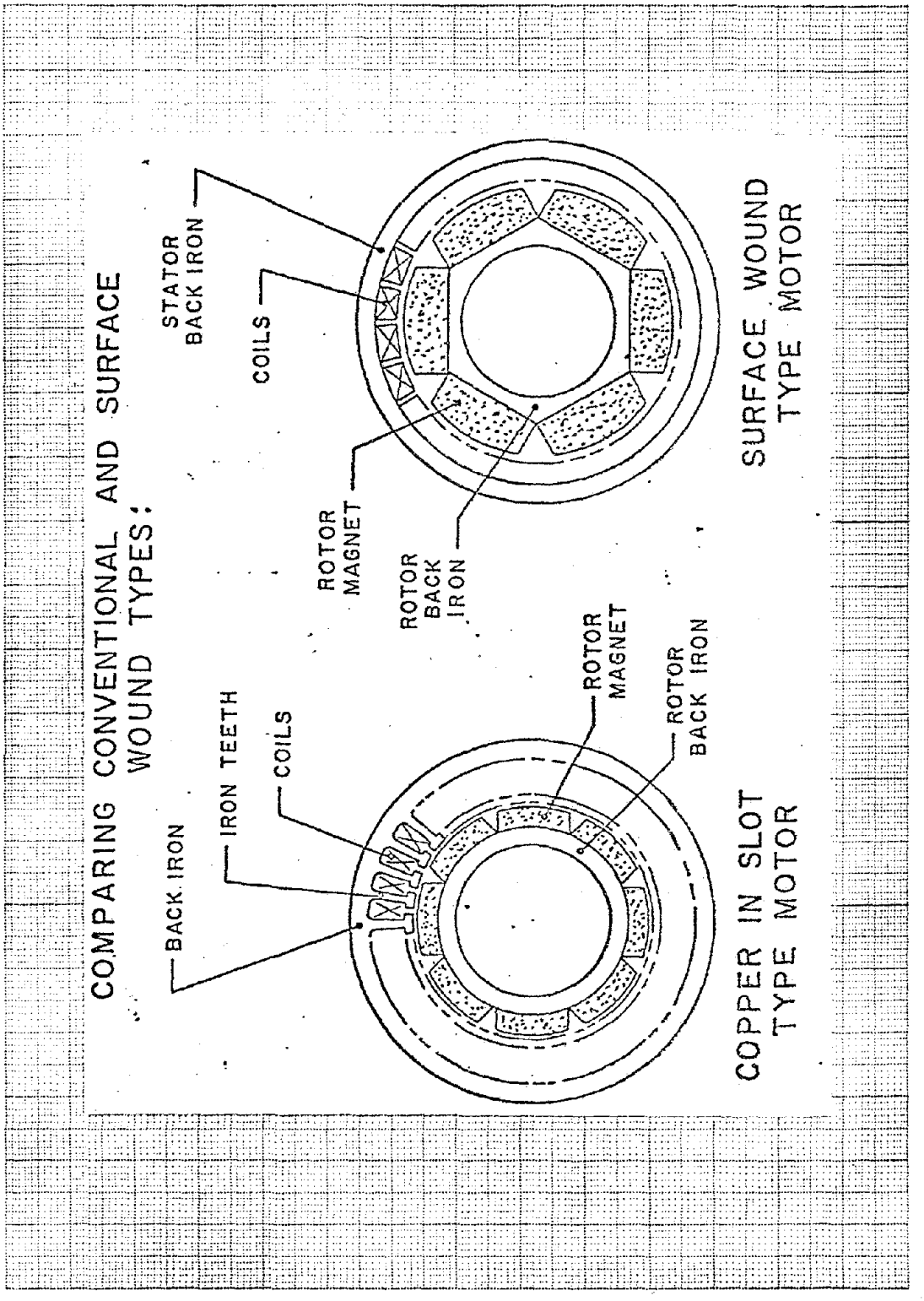


| | | | | |
|---|---|---|---|---|
| CALC | HE | | REVISED | DATE |
| CHECK | | | | |
| APPD | | | | |
| APPD | | | | |
| | | | | |

Figure 3.4: Conventional and Surface Wound Types

UNIVERSITY OF KANSAS

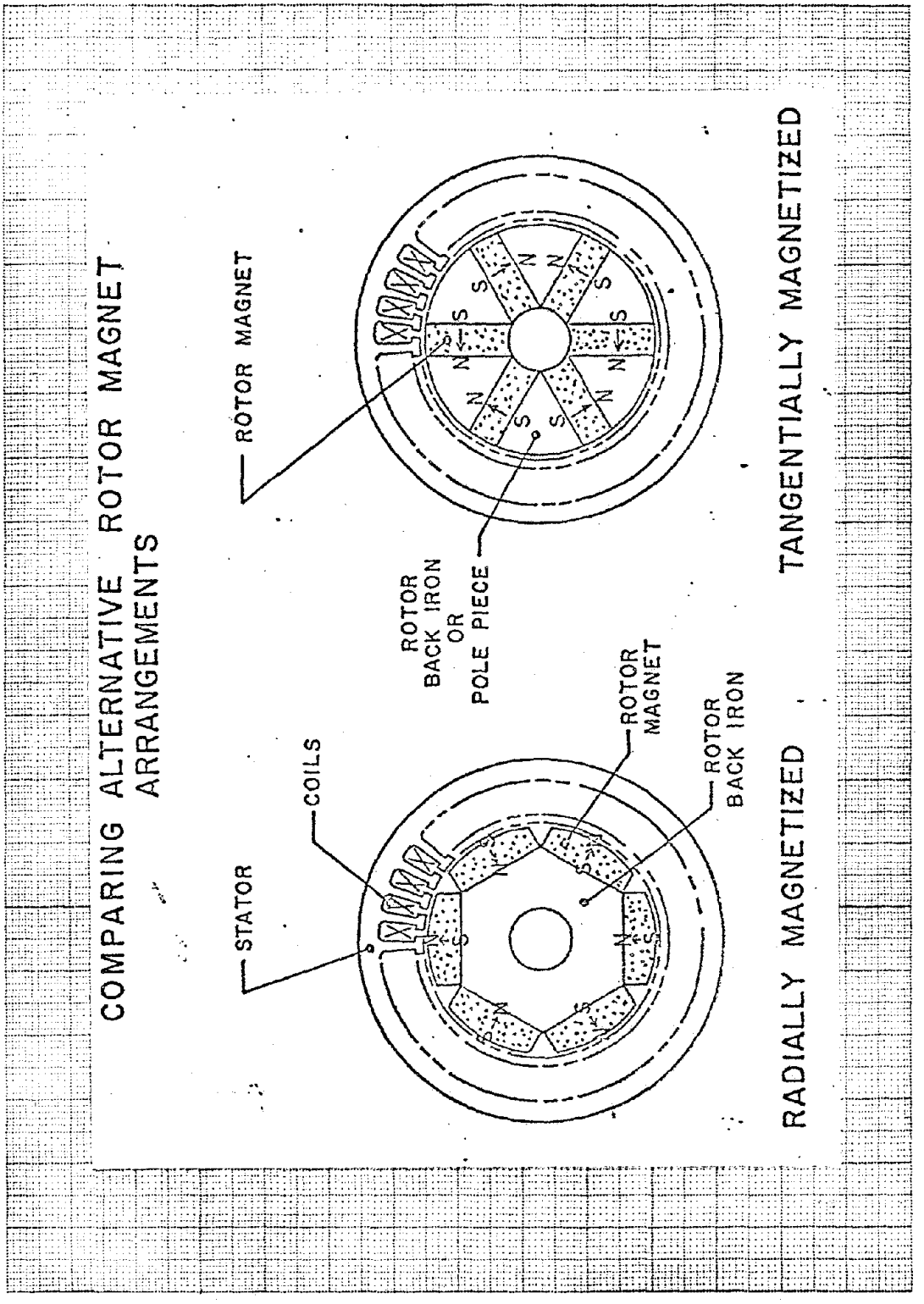


| CALC | HE | | REVISED | DATE |
|---|---|---|---|---|
| CHECK | | | | |
| APPD | | | | |
| APPD | | | | |
| | | | | |

Figure 3.5: Alternative Rotor Magnet Arrangements

UNIVERSITY OF KANSAS

For a brushless DC motor, the torque per ampere is basically constant from no-load to stall and comes close to the theoretical maximum that can be attained for a given no-load speed and rated voltage. This theoretical maximum can be expressed as follows (Ref. 2):

$$\frac{T}{I} = \frac{84.5 \times \text{rated voltage}}{\text{no-load speed (rpm)}} \quad \text{in-lbf/Amp} \qquad (3.1)$$

From this it can be seen that there are two ways to go with this type of actuator:

1. Drive the load directly with a low speed motor,
2. Use a high speed motor and gear down the output.

It might seem that the first option is the way to go, but the same torque per ampere (except for gearing ratio efficiency) can be obtained with the second and the geared unit will be smaller and lighter. Also, in the case of the high speed motor, the load inertia will have little influence on motor acceleration because of the gearing ratio.

The efficiency of Samarium Cobalt actuators is higher than that of comparable actuators using Alnico magnets. The maximum theoretical efficiency is the ratio of operating speed to the no-load speed. Therefore, it is important to operate these actuators at speeds near no-load. To achieve this, the design stall torque output must be much higher than what is normally needed. The applied current can then be limited to control torque output, and the motor operates at speeds near no-load.

Actuator weight is inversely proportional to the number of poles of the magnets used, but small actuators with a large number of poles are difficult to manufacture. Usually there are six to eight poles.

Uniformity of torque depends on how many different sets of windings there are, the more the better. However, the number of

switches needed for commutation increases when there are more sets of windings. A three-phase winding is a reasonable compromise (Ref. 2).

Motor no-load speed can be selected by varying the number of windings and wire size to fit a given requirement.

## 3.2 MATHEMATICAL MODELS

There are two important constants involved in setting up a model for an electromechanical actuator: the back emf* voltage constant and the torque constant. Both depend on the same machine parameters.

The voltage generated in an electric DC motor can be expressed as follows (Ref. 4):

$$E_g = p \Phi \frac{Z}{a} \frac{n}{60} \tag{3.2}$$

$$= \frac{p}{2\pi} \Phi \frac{Z}{a} \omega \tag{3.3}$$

$$= K_E \omega \quad \text{(Volts)} \tag{3.4}$$

in which:

$$K_E = \frac{p}{2\pi} \frac{Z}{a} \Phi \qquad \text{(Volt/rad/sec)} \tag{3.5}$$

The torque generated by an electric DC motor can be written in the following way (Ref. 3.2):

$$T = 8.847 \frac{p}{2\pi} \frac{Z}{a} \Phi I \text{ (in - lbf)} \tag{3.6}$$

$$= K_T I \tag{3.7}$$

in which:

$$K_T = 8.847 \frac{p}{2\pi} \frac{Z}{a} \Phi \qquad \text{(in-lbf/Amp)} \tag{3.8}$$

In comparing (3.5) with (3.8) it can be seen that $K_T = 8.847 K_E$. The number 8.847 is a unit conversion factor.

---

*emf: electromotive force

$K_T$ and $K_E$ will be higher for a Samarium Cobalt actuator than for one with Alnico magnets because of the higher flux $\Phi$ per pole (other things being equal). This is very favorable for the mechanical time constant, as will be seen later.

Electrically, the motor can be represented as shown in Figure 3.6:

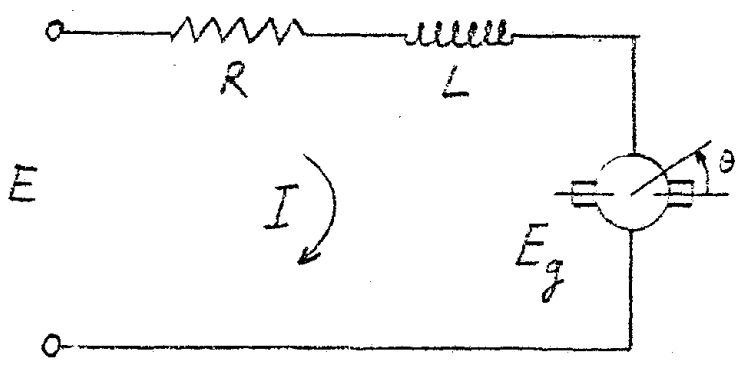


Figure 3.6: Schematic Representation of a DC Motor Driving Its Own Inertia

The voltage and torque equations for this motor are (Ref. 2):

$$E = IR + \dot{I}L + E_g \tag{3.9}$$

$$T = K_T I \tag{3.7}$$

$$T_L = J_R \ddot{\theta} \tag{3.10}$$

Substitution of (3.4) in (3.9), with $\omega = \dot{\theta}$, yields:

$$E = IR + \dot{I}L + K_E \dot{\theta} \tag{3.11}$$

The torque developed by the motor must be equal to the torque required to accelerate the rotor:

$$K_T I = J_R \ddot{\theta} \tag{3.12}$$

These equations are expressed in the time domain. In the frequency domain they become (applying the Laplace transform and assuming zero initial conditions):

$$E = IR + sIL + K_E\, s\theta \tag{3.13}$$

$$K_T\, I = J_R\, s^2\theta \tag{3.14}$$

The current can be eliminated from these equations as follows:

$$I = \frac{E - K_E\, s\theta}{R + sL} \tag{3.15}$$

Substitute this in (3.14):

$$K_T \frac{E - K_E\, s\theta}{R + sL} = J_R\, s^2\theta \tag{3.16}$$

$$E \frac{K_T}{R + sL} = \theta \left\{J_R\, s^2 + \frac{K_T\, K_E}{R + sL}\, s\right\} \tag{3.17}$$

$$\frac{\theta}{E} = \frac{\dfrac{K_T}{R + sL}}{J_R\, s^2 + \dfrac{K_T\, K_E}{R + sL}} \tag{3.18}$$

$$\frac{\theta}{E} = \frac{K_T}{J_R s^2(R + sL) + K_T K_E s} \tag{3.20}$$

$$\frac{\theta}{E} = \frac{1}{\frac{1}{K_T}(J_R L\, s^3 + J_R\, R\, s^2) + K_E\, s} \tag{3.21}$$

This is the open loop transfer function relating rotor angular displacement to applied voltage.

Equation (3.21) can be simplified a little in the following manner:

$$\frac{\theta}{E} = \frac{1}{K_E\, s\, \left(\dfrac{J_R L}{K_T K_E}\, s^2 + \dfrac{J_R R}{K_T K_E}\, s + 1\right)} \tag{3.22}$$

If $\frac{L}{R} << \frac{J_R R}{K_E K_T}$, in which:

$\frac{L}{R}$ is called the electrical time constant and:

$\frac{J_R R}{K_E K_T}$ is called the mechanical time constant, then:

$$\frac{\theta}{E} \approx \frac{1}{K_E\, s\, (\frac{J_R R}{K_E K_T}\, s + 1)\, (\frac{L}{R}\, s + 1)} \tag{3.23}$$

A typical value for the electrical time constant is 0.5 milliseconds, while the mechanical time constant for a brushless DC motor may range from 6 to 10 milliseconds (Ref. 5). This implies that (3.23) generally will be valid.

The mechanical time constant is much smaller for a Samarium-Cobalt actuator than for an actuator using Alnico magnets, and there are two reasons for this:

1. Values of $K_E$ and $K_T$ are higher for a Samarium-Cobalt actuator than for one using Alnico magnets;
2. Rotor inertia is smaller in the case of a Samarium-Cobalt actuator.

The electrical time constants of a Samarium-Cobalt actuator and of one using Alnico Magnets have the same order of magnitude.

An expression for the actuator plus control surface transfer function will now be derived, assuming that the control curface hinge moment increases linearly with deflection. The actuator is of the rotary type (hingeline actuation). The equations for the electrical part of the system are as before:

$$T = K_T I \tag{3.7}$$

$$E = IR + \dot{I}L + K_E\dot{\theta} \tag{3.11}$$

The load consists of three parts: rotor inertia, load inertia, and aerodynamic load.

$$T_{L_1} = J_R \ddot{\theta} \tag{3.24}$$

$$T_{L_2} = J_L \ddot{\delta} + k_c \delta \tag{3.25}$$

$\ddot{\theta}$ and $\ddot{\delta}$ are related in the following manner: $\ddot{\theta} = G \ddot{\delta}$, so

$$T_{L_1} = J_R G \ddot{\delta} \tag{3.26}$$

The load caused by the control surface is reflected to the motor through the gearing ratio; then the torque developed by the motor must be equal to

$$K_T I = J_R G \ddot{\delta} + \frac{1}{G\eta} (J_L \ddot{\delta} + k_c \delta) \tag{3.27}$$

Expressing equations (3.11) and (3.27) in the frequency domain yields (with zero initial conditions):

$$E = IR + sIL + K_E s\theta \tag{3.13}$$

$$K_T I = J_R G s^2 \delta + \frac{1}{G\eta} (J_L s^2 \delta + k_c \delta)$$

$$= (J_R G + \frac{J_L}{G\eta}) s^2 \delta + \frac{k_c}{G\eta} \delta$$

$$= G (J_R + \frac{J_L}{G^2\eta}) s^2\delta + \frac{k_c}{G\eta} \delta \tag{3.28}$$

$J_R + \frac{J_L}{G^2\eta}$ is the total inertia reflected to the motor. If the gearing ratio is large enough, then the effective load inertia is only a small

percentage of the rotor inertia which is favorable for the mechanical time constant.

Call $J_R + \frac{J_L}{G^2\eta} = J$; then (3.28) becomes:

$$K_T I = GJ\, s^2\, \delta + \frac{k_c}{G\eta}\, \delta \tag{3.29}$$

Eliminating the current from (3.13) and (3.29) yields:

$$K_T \frac{E - K_E\, s\, G\delta}{R + sL} = \left(GJ\, s^2 + \frac{k_c}{G\eta}\right) \delta \tag{3.30}$$

or:

$$\frac{K_T E}{R + sL} = \left(GJ\, s^2 + \frac{K_T K_E G}{R + sL}\, s + \frac{k_c}{G\eta}\right) \delta \tag{3.31}$$

The $\frac{\delta}{E}$ transfer function can now be written explicitly as:

$$\frac{\delta}{E} = \frac{\frac{K_T}{R + sL}}{GJs^2 + \frac{K_T K_E G}{R + sL}\, s + \frac{kc}{G\eta}}$$

$$= \frac{1}{\frac{G}{K_T}\,(JLs^3 + JRs^2) + K_E G s + \frac{k_c}{K_T G\eta}\,(R + sL)}$$

$$= \frac{1}{\frac{G}{K_T}\,(JLs^3 + JRs^2) + \left(K_E G + \frac{k_c L}{K_T G\eta}\right)s + \frac{k_c R}{K_T G\eta}} \tag{3.32}$$

This is the open loop transfer function relating control surface deflection to applied voltage. It can be simplified a bit as follows: because L is very small (usually in the order of $10^{-3}$ Henry or less) and G rather large (at least a few hundred), the $\frac{k_c L}{K_T G\eta}$ term in (3.32) is negligible compared to $K_E G$ and the transfer function becomes:

$$\frac{\delta}{E} = \frac{1}{\frac{G}{K_T}\left( JLs^3 + JRs^2\right) + K_E Gs + \frac{k_c R}{K_T G \eta}} \tag{3.33}$$

The closed loop transfer function can be derived from the following block diagram:

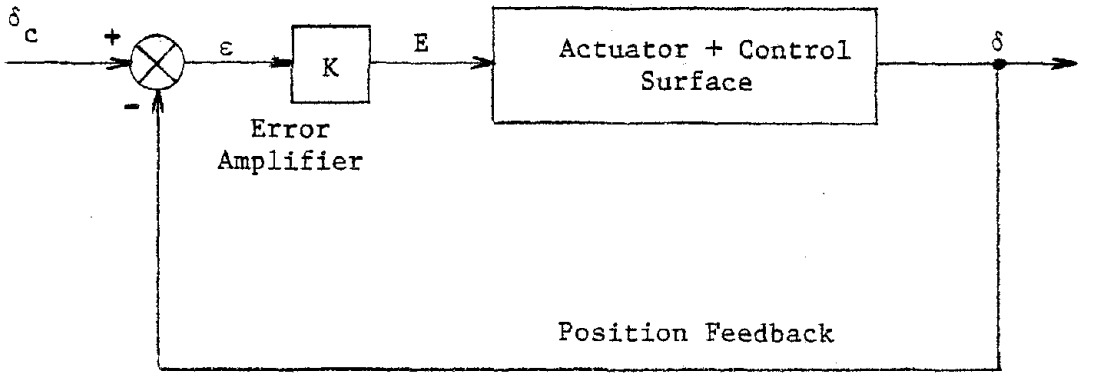


Figure 3.7 - Actuator closed loop block diagram

$$\frac{\delta}{\delta_c} = \frac{K}{\frac{G}{K_T}\left(JLs^3 + JRs^2\right) + K_E Gs + \frac{k_c R}{K_T G \eta} + K} \tag{3.34}$$

Phase compensation in the feedback path may be needed if the closed loop damping is not high enough. If K lies in a range that can cause E to be greater than the rated actuator voltage for certain error signals, a voltage limiter must be incorporated. If that is the case, then this model is no longer valid for situations in which $K \cdot |\varepsilon| > E_{max}$. In such a case the behavior of the system can be studied with an analog computer.

Gearing ratio selection is very important; it must be made in such a way that both torque and frequency response requirements are met. However, a practical limitation can be that typical no-load speeds of Samarium-Cobalt actuators range from 5000 to 30000 rpm (Ref. 2).

The following approach is adopted from Ref. 1.

Motor torque is equal to:

$$T_m = J_R \ddot{\theta} \tag{3.35}$$

Motor acceleration torque equals:

$$T_m = \frac{T_{max} - (T_{IL} + T_c)}{G\eta} \tag{3.36}$$

$T_{max}$ is the maximum output torque and is the larger of:

1. $T_s$ (stall torque)
2. $2\ (T_{IL} + T_c)$ (inertial load and concurrent load)
3. $T_r$ (running load)

Substitution of (3.36) in (3.35) yields:

$$\frac{T_{max} - (T_{IL} + T_c)}{G\eta} = J_R \ddot{\theta} \tag{3.37}$$

Since $\ddot{\theta} = G\ddot{\delta}$, it follows that:

$$T_{max} - (T_{IL} + T_c) = J_R G^2 \eta \ddot{\delta} \tag{3.38}$$

$$G = \sqrt{\frac{T_{max} - (T_{IL} + T_c)}{J_R \ddot{\delta} \eta}} \tag{3.39}$$

The value of $\ddot{\delta}$ can be obtained from the frequency response requirement. For example, consider a sinusoidal output operating into an inertial load:

$$\delta = \delta_o \sin \omega t \ ; \ \delta_{max} = \delta_o \tag{3.40}$$

$$\dot{\delta} = \omega \delta_o \cos \omega t \ ; \ \dot{\delta}_{max} = \omega\delta_o \tag{3.41}$$

$$\ddot{\delta} = -\omega^2\delta_o \sin \omega t; \ \ddot{\delta}_{max} = -\omega^2\delta_o \tag{3.42}$$

For known maximum control surface rate of deflection and bandwidth $\omega$, $\ddot{\delta}$ can be calculated. A maximum value of $\dot{\delta}$ could be something like 100 deg/sec; choice of bandwidth is more or less free.

Values of stall torque, inertial load and concurrent loads can be calculated from the hinge moment and inertia characteristics for a given control surface. Values of running loads can depend on friction, which is ignored here, so running loads will be assumed to be zero.

An estimation of rotor inertia can be made from the peak power output of the actuator; because the torque speed relationship is a straight line from no-load to stall, the peak power output occurs at one-half motor stall torque and one-half no-load speed for a motor without current limiting. In practice, however, the torque output is limited to what is needed, which is only a fraction of motor stall torque. In this case the peak power output occurs at the maximum output torque $T_{max}$:

$$P_{PK} = \frac{T_{max} \times \dot{\delta}}{550} \quad \text{(hp)} \tag{3.43}$$

$T_{max}$ should be expressed in ft-lbf and $\dot{\delta}$ (the control surface rate of deflection at $T_{max}$) in rad/sec. When $P_{PK}$ increases, motor length and diameter also increase and so does rotor inertia. An estimation can be made with Table 3.1 and Figure 3.8.

Table 3.1 Relationship between Motor Length and Peak Power Output (Ref. 2)

| $P_{PK}$ (hp) | Motor Length (in) |
|---|---|
| 0 - 0.15 | 2.9 |
| 0.15 - 0.50 | 3.8 |
| 0.50 - 0.75 | 4.2 |
| 0.75 - 1.5 | 5.2 |

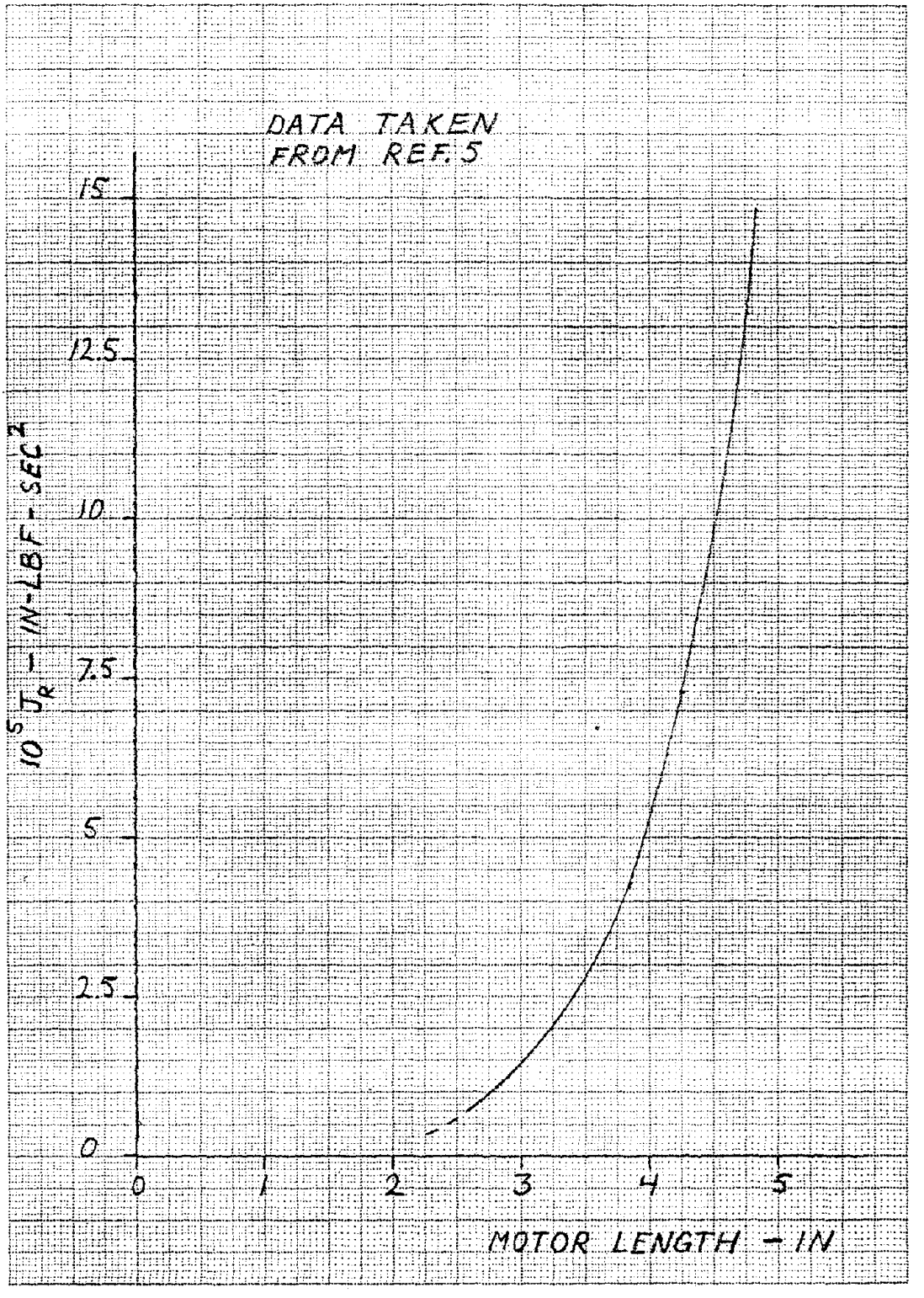


| | | | | | |
|---|---|---|---|---|---|
| CALC | HE | | REVISED | DATE | Figure 3.8: Approximation of Rotor Inertia from Motor Length |
| CHECK | | | | | |
| APPD | | | | | |
| APPD | | | | | |
| | | | | | UNIVERSITY OF KANSAS |

The variation in peak power outpout for a given motor length is mainly caused by different numbers of windings per coil in the stator (different no-load speeds). When the motor length increases, the motor diameter increases also; since rotor inertia is proportional to rotor length and to the square of rotor radius, the relationship of Figure 3.8 is not linear.

Once the gearing ratio is known, $K_T$ can be estimated from (3.1) for a given supply voltage and from $K_T$, $K_E$. Estimations must also be made of motor resistance, motor inductance and gearing ratio efficiency.

The complete servoloop can be implemented with either an analog or a digital controller system. The advantage of an analog system is simplicity, but it is not adaptable to changes in system requirements. A precision RC network (if necessary) is needed in the feedback path but it is relatively unreliable (Ref. 2). The main advantages of a digital controller are versatility, simple hardware, its adaptability to failure and cost competitiveness. A disadvantage is that software design is required.

For applications where the control surface must be held in a certain position for a longer period of time (e.g. for a trim), either a no-back or a brake can be used. A no-back is a device that allows power to pass from the input to the output without appreciable losses, and acts as a brake to prevent power being transferred from the output back to the input. The energy absorbed in the no-back appears as friction heating. A motor brake, however, will be designed for holding torque and not for power dissipation; and position holding is achieved with less increase in weight than with a no-back. Actuation of the

brake will require control logic in conjunction with that of the motor operation.

An example Bode plot for a Samarium-Cobalt actuator is shown in Figure 3.9. The command signal has an amplitude of 1.5 deg; the load is a moment of 200 in-lbf.

## 3.3 DESIGN EXAMPLES

The electromechanical actuator will be evaluated for two cases: on the control surface model, described in Section 2.1, and on a light twin-engine airplane, described in Section 2.3. The evaluation on the control surface model is meant to obtain a comparison with the other actuator types, and the aircraft evaluation will be used in the control system analysis in Section 6.3.

### 3.3.1 CONTROL SURFACE MODEL

Data on the control surface model are presented in Section 2.1 and will be used here for sizing the actuator.

Design stall torque: $T_s = 2550$ in-lbf

Inertia: $J_L = 1.192$ in-lbf-sec$^2$

A no-load rate of 100 deg/sec will be chosen for the control surface. At the stall torque a rate of 75 deg/sec will be taken. This is more or less an arbitrarily chosen value. For a higher rate at the stall torque, a larger actuator is needed, while a lower rate reduces the efficiency to intolerably low values.

With (3.43) the peak power output can be calculated to be 0.51 hp. Table 3.1 shows that motor length is about 4 inches; since there is some overlap in power output between different motor lengths (depending on number of windings in the stator), a motor length of 3.8 inches is estimated. With Figure 3.8 an estimated rotor inertia of $4.275 \cdot 10^{-5}$ in-lbf-sec$^2$ is found.

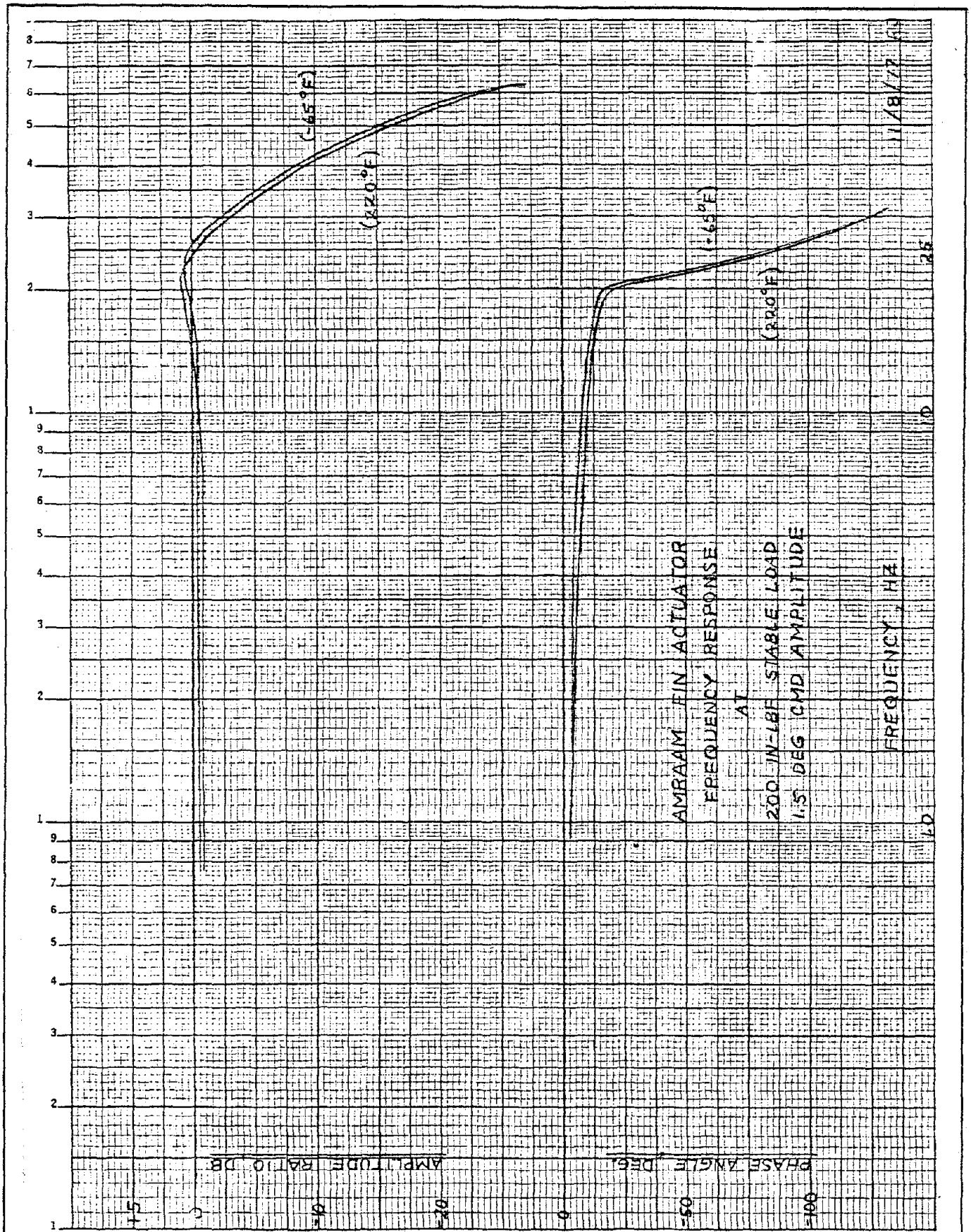


| | | | | |
|---|---|---|---|---|
| CALC | HE | | REVISED | DATE |
| CHECK | | | | |
| APPD | | | | |
| APPD | | | | |
| | | | | |

Figure 3.9: Sm-Co Actuator Example Bode Plot

UNIVERSITY OF KANSAS

To find the right gearing ratio, a bandwidth must be chosen for the frequency response. A value of $\omega$ = 50 rad/sec is taken here, but other values are possible. From (3.40), (3.41) and (3.42) the deflection associated with this bandwidth can be calculated to be 2 degrees; control surface acceleration becomes:

$$\ddot{\delta} = 87.25 \text{ rad/sec}^2$$

The inertial load is then:

$$T_{IL} = 104.7 \text{ in-lbf}$$

For the concurrent load, the hingemoment associated with a 2 deg. deflection under maximum load condition will be taken (see Figure 2.4). This yields:

$$T_c = 400 \text{ in-lbf}$$

With an estimated gearing ratio efficiency of 0.9, the gearing ratio can be calculated according to (3.39):

$$G = 780$$

This yields for the rotor no-load speed:

$$\dot{\theta} = 1362 \text{ rad/sec} = 13000 \text{ rpm}$$

The theoretical maximum $K_T$-value can be calculated with (3.1): $K_T$ = 0.1820 in-lbf/Amp for a rated voltage of 28 V. For Samarium-Cobalt motors, the $K_T$ value is about 5% less (Ref. 2):

$$K_T = 0.1729 \text{ in-lbf/Amp.}$$

With the relation $K_T = 8.847\ K_E$ the value of $K_E$ is calculated to be:

$$K_E = 0.0195 \text{ Volt/rad/sec}$$

The output torque per Ampere is equal to $K_T$ multiplied by gearing ratio and gearing ratio efficiency which yields a value of 121.4 in-

lbf/Amp. The maximum current needed is then:

$$I_{max} = \frac{T_s}{121.4} = 21 \text{ Amp.}$$

Motor resistance is estimated as R = 0.3Ω (Ref. 5). With the typical electrical time constant value of 0.5 millisec, this yields an inductance of L = 0.00015 Henry.

A commercially available Sm-Co actuator with similar characteristics is shown in Figure 7.6.

Time responses have been obtained with an analog computer (see Appendix B.1) for the loading conditions described in Section 2.1.2. Figure 3.10 shows the inertia loading time response, while the time responses for cruise load and maximum load are presented in Figure 3.11 and Figure 3.12, respectively. It can be seen that the load has hardly any influence on the time response. There are some changes in steady state error, but those are not very large.

The frequency response is a lot slower than the 50 rad/sec used above. However, it must be kept in mind that the amplitude associated with this frequency is only 2 degrees, so for larger amplitudes the frequency response will naturally be worse.

The time responses for a smaller control surface deflection of 10 deg are shown in Figure 3.13 for two different error amplifier gains. An open loop time response can be seen in Figure 3.14 for maximum load condition. To compare the time histories of the Sm-Co actuator with those of the electro-pneumatic and electro-hydraulic actuators, see Sections 4.3 and 5.3, respectively.

### 3.3.2 AIRCRAFT MODEL

The light twin-engine airplane (Airplane B) has been used for evaluation of aircraft response characteristics with a Samarium-Cobalt

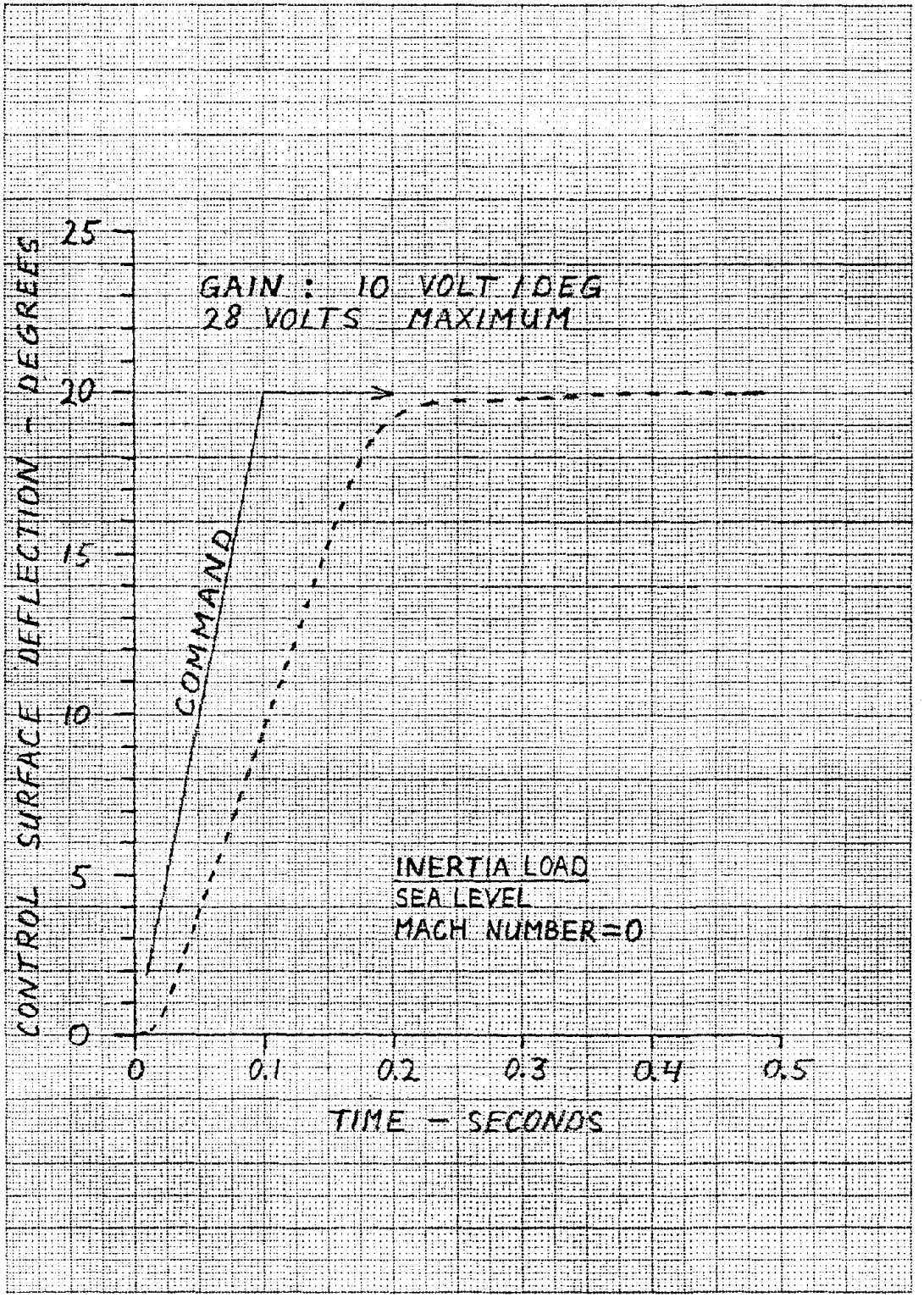


| | | | | | |
|---|---|---|---|---|---|
| CALC | HE | | REVISED | DATE | Figure 3.10: Sm-Co Actuator - Inertia Load, Closed Loop |
| CHECK | | | | | |
| APPD | | | | | |
| APPD | | | | | |
| | | | | | UNIVERSITY OF KANSAS |

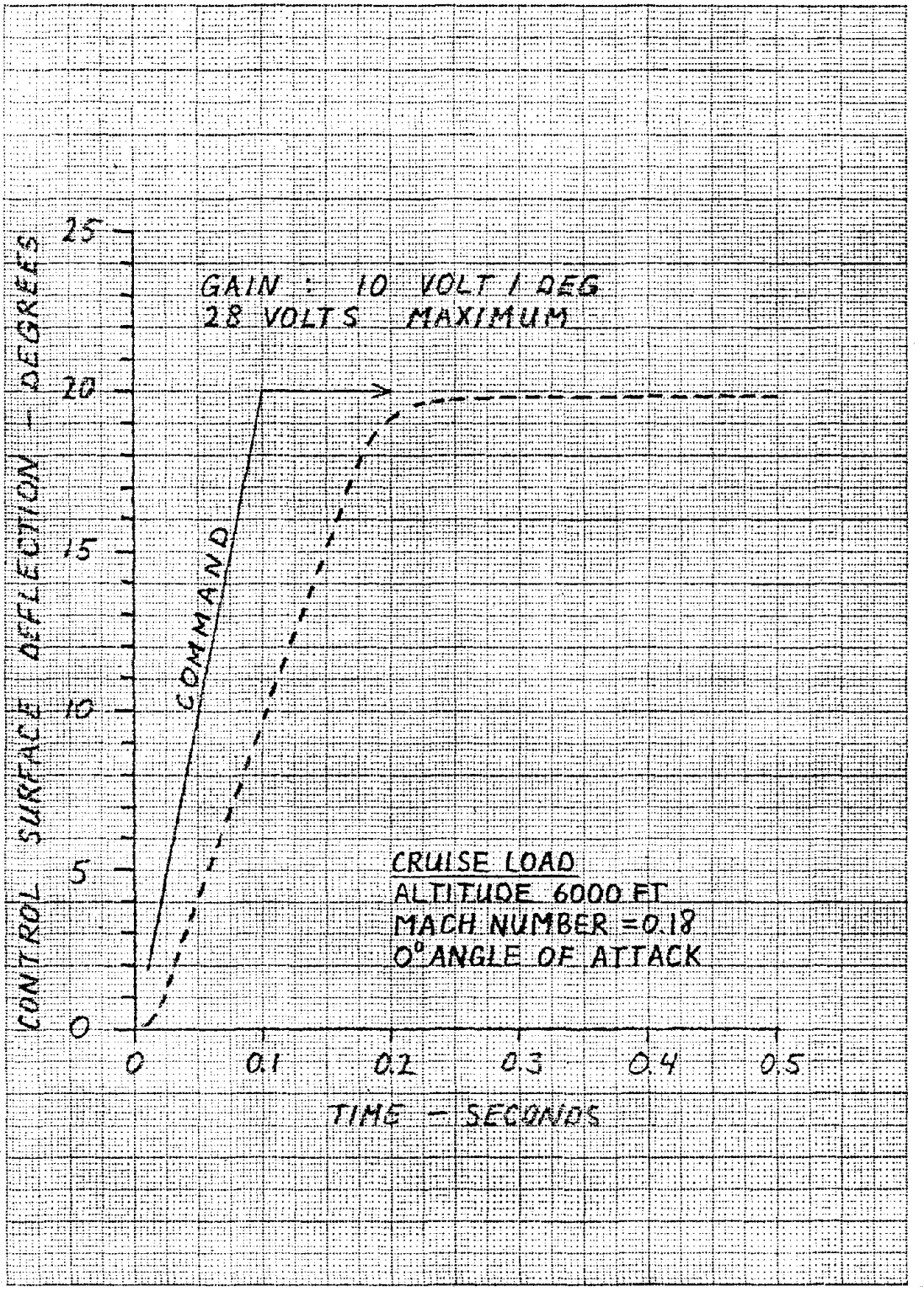


| | | | | | |
|---|---|---|---|---|---|
| CALC | HE | | REVISED | DATE | Figure 3.11: Sm-Co Actuator - Cruise Load, Closed Loop |
| CHECK | | | | | |
| APPD | | | | | |
| APPD | | | | | |
| | | | | | UNIVERSITY OF KANSAS |

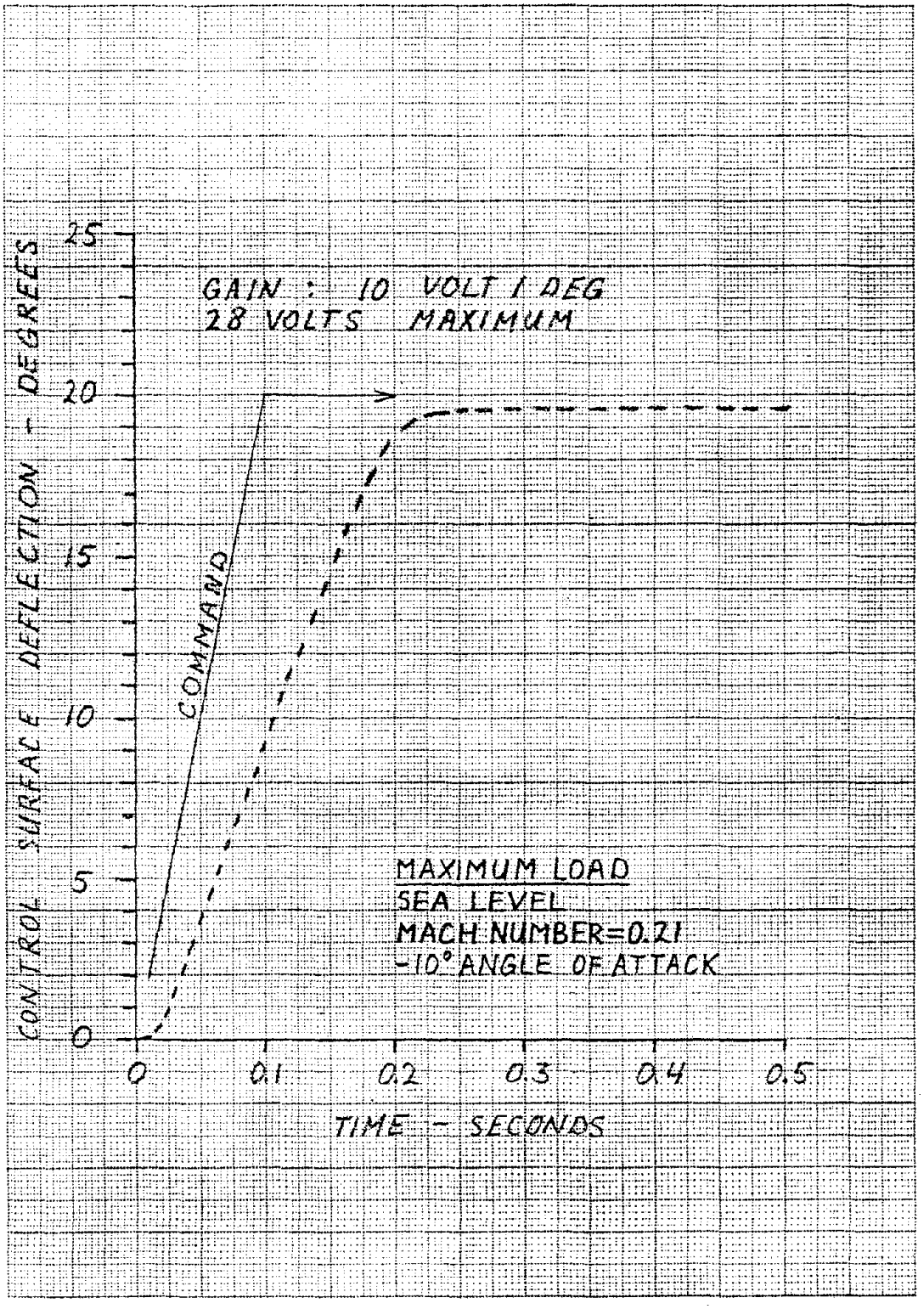


| | | | | | | |
|---|---|---|---|---|---|---|
| CALC | HE | | REVISED | DATE | Figure 3.12: Sm-Co Actuator - Maximum Load, Closed Loop | |
| CHECK | | | | | | |
| APPD | | | | | | |
| APPD | | | | | | |
| | | | | | UNIVERSITY OF KANSAS | PAGE 55 |

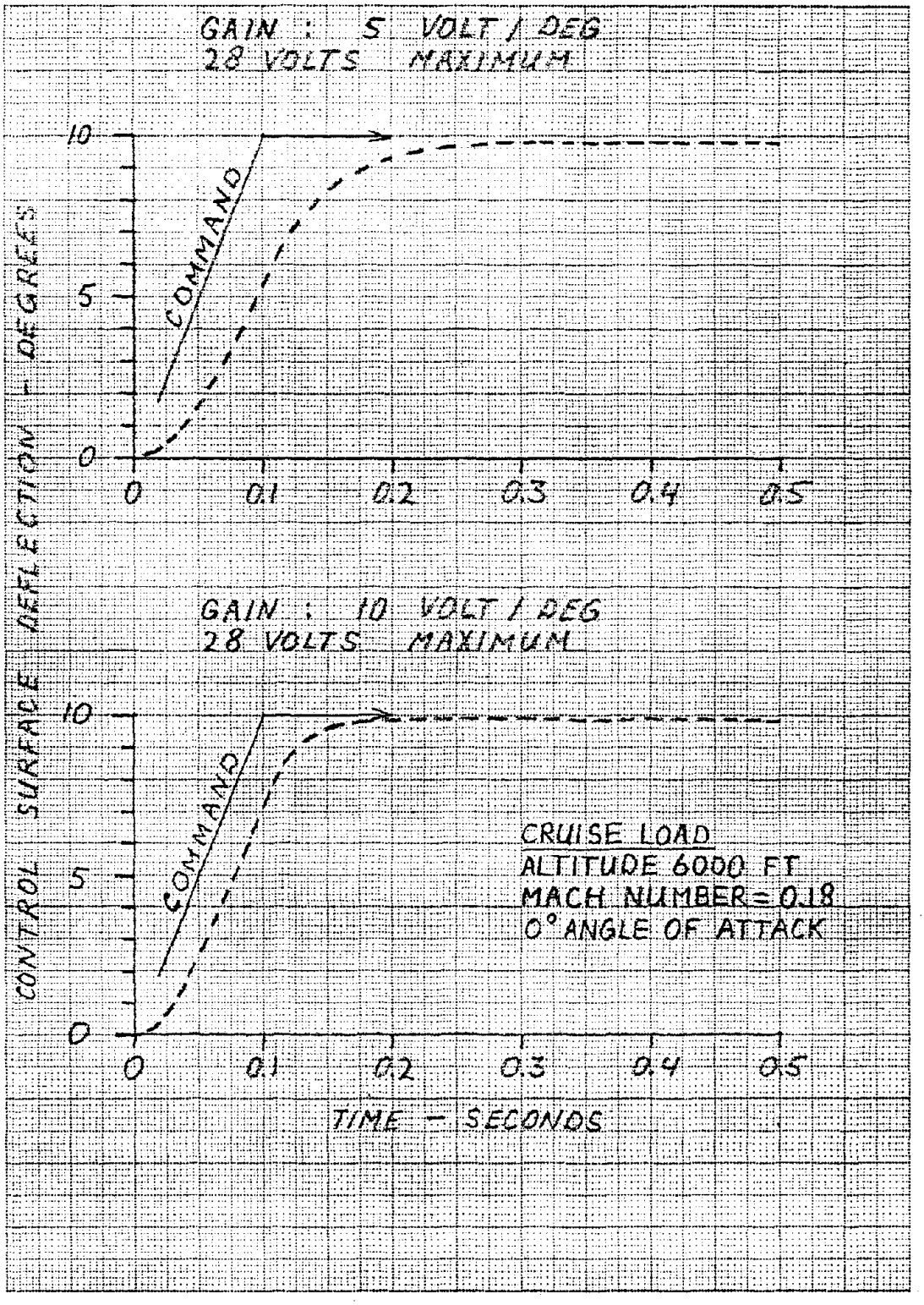


| CALC | HE | | REVISED | DATE |
|---|---|---|---|---|
| CHECK | | | | |
| APPD | | | | |
| APPD | | | | |
| | | | | |

Figure 3.13: Sm-Co Actuator - Cruise Load at 10° Different Gains

UNIVERSITY OF KANSAS

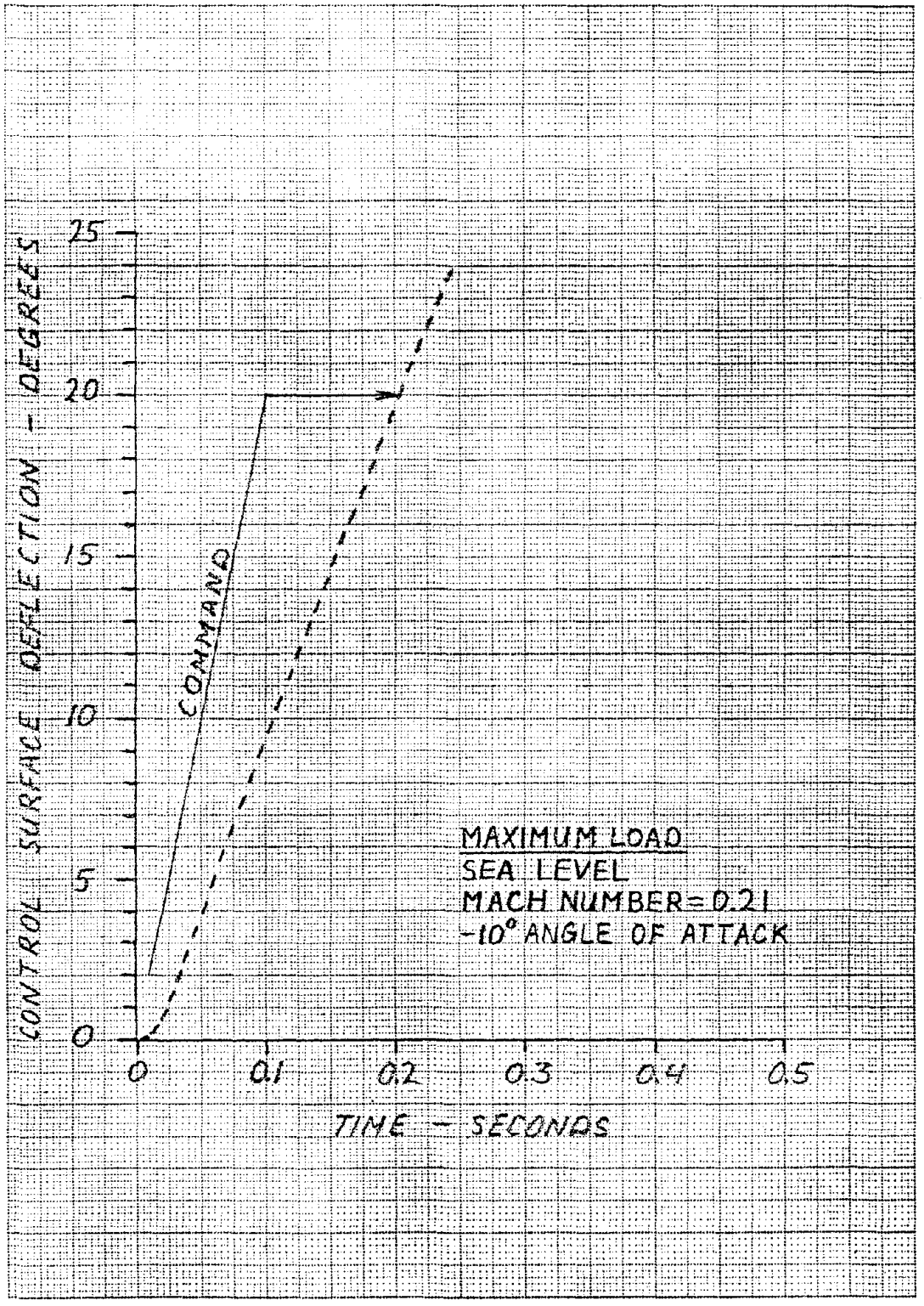


| | | | | | |
|---|---|---|---|---|---|
| CALC | HE | | REVISED | DATE | Figure 3.14: Sm-Co Actuator - Maximum Load, Open Loop |
| CHECK | | | | | |
| APPD | | | | | |
| APPD | | | | | |
| | | | | | UNIVERSITY OF KANSAS |

actuator. Both stabilator and aileron are equipped with hingeline actuators. Because of the larger hingemoments for the stabilator, a slightly bigger actuator has been used (motor length 4.2 in) with a different current limit ($I_{max}$ = 45.8 Amp). The hingemoments for cruise and approach conditions can be found in Section 2.3.

Stabilator time histories are shown in Figure 3.15 and aileron time histories in Figure 3.16. These figures also show linear approximations according to:

$$\delta(t) = \delta_c(t) \{ 1 - e^{-\frac{t}{\tau_a}} \} \tag{3.44}$$

In this equation, $\tau_a$ is referred to as the actuator time constant. In Section 6.3 an actuator transfer function will be used according to (3.44). In the frequency domain, this is expressed as:

$$H(s) = \frac{\delta(s)}{\delta_c(s)} = \frac{1}{1 + \tau_a s} \tag{3.45}$$

Table 3.2 gives values of actuator time constants for use in Section 6.3.

Table 3.2 - Airplane B Actuator Time Constants

| Flight Condition | Control Surface | Time Constant |
|---|---|---|
| Cruise | Aileron | 0.06 sec |
| | Stabilator | 0.06 sec |
| Approach | Aileron | 0.06 sec |
| | Stabilator | 0.06 sec |

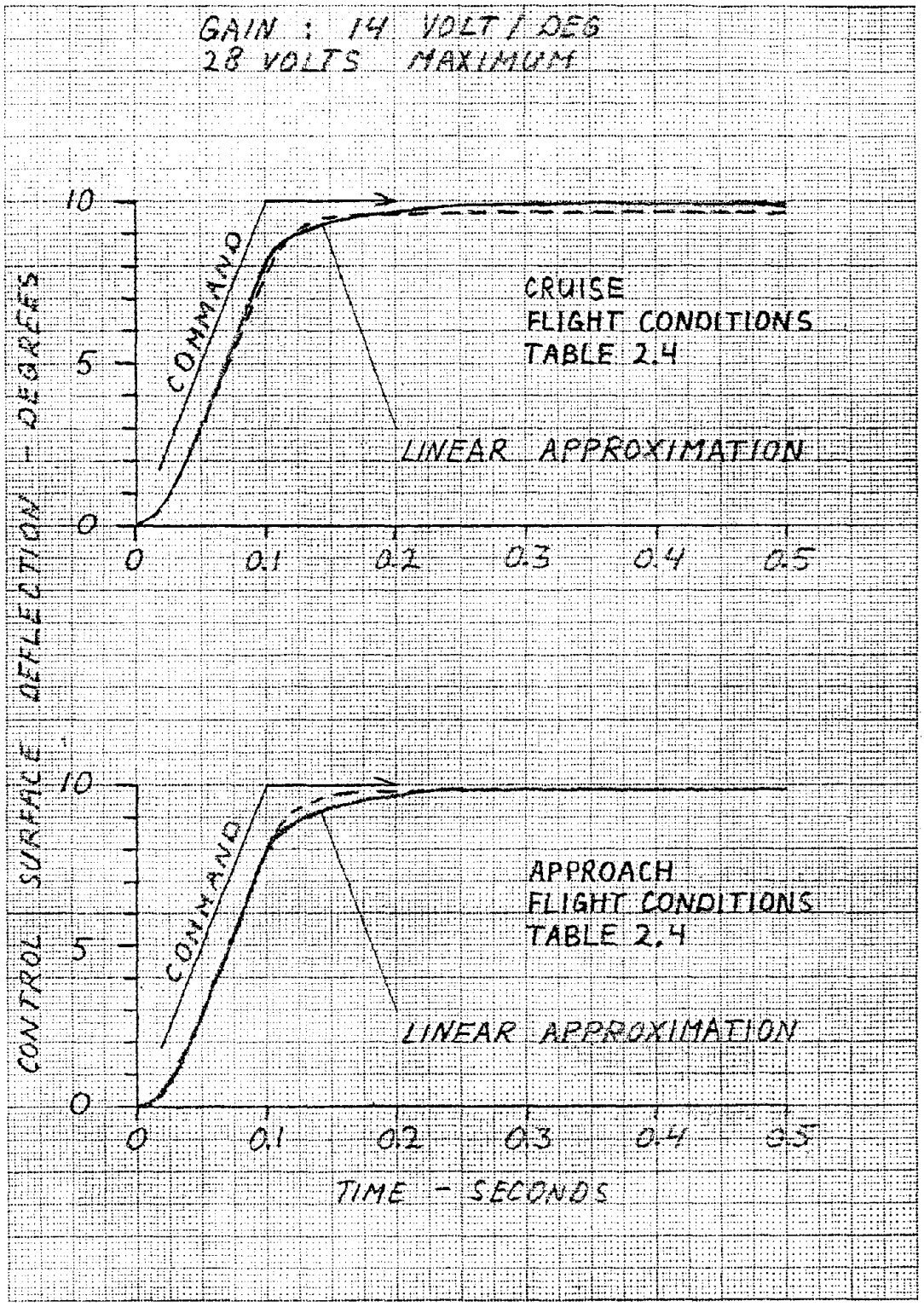


| | | | | |
|---|---|---|---|---|
| CALC | HE | | REVISED | DATE |
| CHECK | | | | |
| APPD | | | | |
| APPD | | | | |
| | | | | |

Figure 3.15: Airplane B, Stabilator Time Histories

UNIVERSITY OF KANSAS

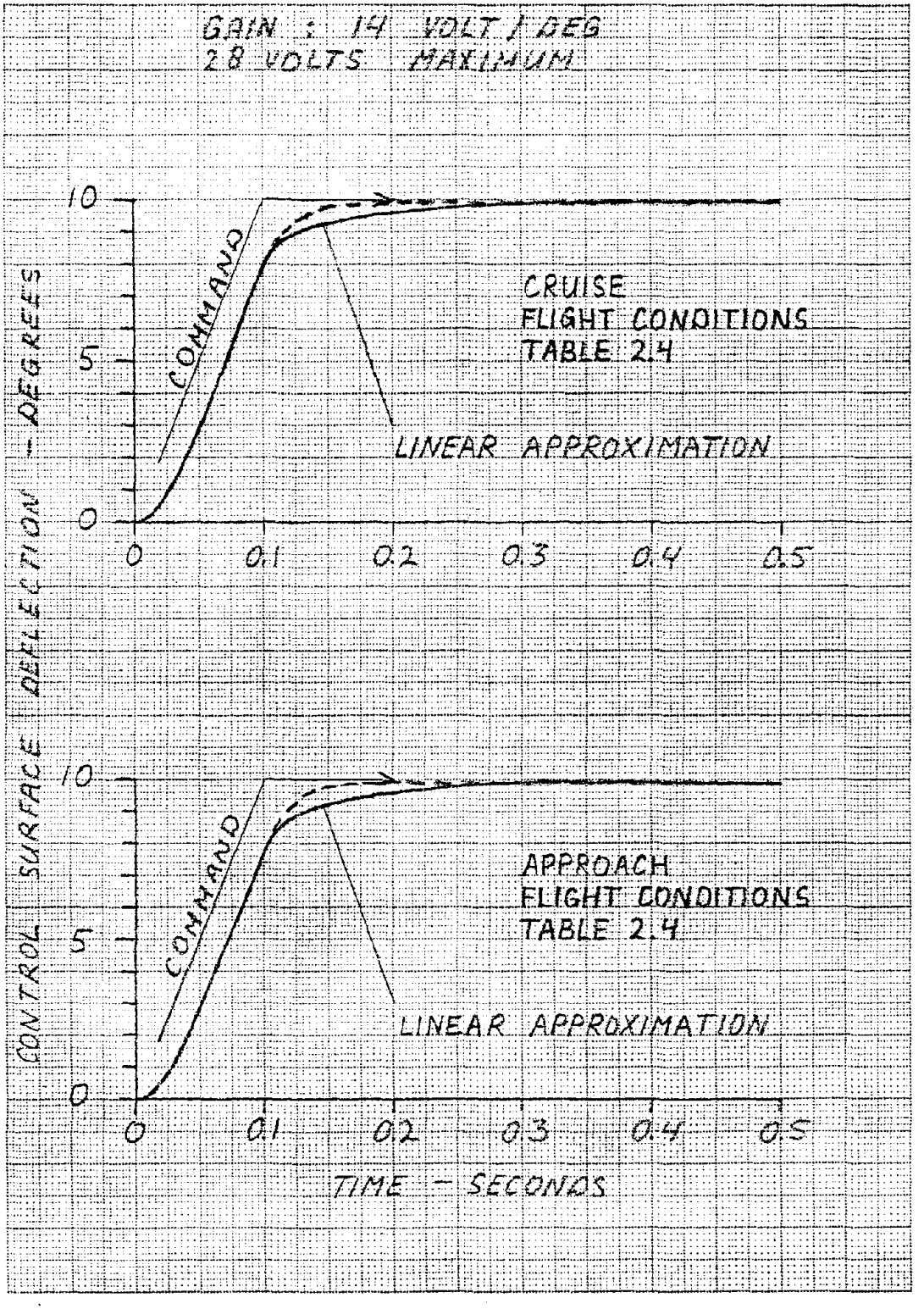


| | | | | | |
|---|---|---|---|---|---|
| CALC | HE | | REVISED | DATE | Figure 3.16: Airplane B, Aileron Time Histories |
| CHECK | | | | | |
| APPD | | | | | |
| APPD | | | | | UNIVERSITY OF KANSAS |
| | | | | | PAGE 60 |

References for Chapter 3

1. Parker, R. J., "Rare Earth Permanent Magnets and Energy Conversion Processes," Hitachi Magnetics Corporation, Edmore, Michigan 48829.

2. Wood, N. E., Echols, E. F. and Ashmore, J. H., "Electromechanical Actuation Feasibility Study," AFFDL-TR-76-42, May 1976.

3. Voigt, A. A., "Electric Flight Contol Systems - Applicable Now!" General Dynamics Corporation, Pomona, California.

4. Canfield, E. B., "Electromechanical Control Systems and Devices," Robert E. Krieger Publishing Company, Huntington, New York, 1977.

5. Wuertz, K. L., "Rare Earth Cobalt Motors," Airesearch Manufacturing Company of California, 1977.

# CHAPTER 4

## ELECTRO-PNEUMATIC ACTUATORS

Pneumatic systems have been used widely in aircraft and spacecraft systems. Because of their simplicity and reliability, pneumatic and vacuum components are used on engine control valves, cabin pressurization controls and autopilot controls. Applications for pneumatic actuators are generally the two position on-off system. For a variable position system, such as a control surface, more attention needs to be paid to system dynamics and stability than for the two position system.

Section 4.1 deals with components necessary for a pneumatic control system. Section 4.2 then outlines the mathematical model used in the evaluation. Section 4.3 then applies this model to the control surface described in Section 2.1 to find the time response characteristics. Aircraft A has been used for evaluating the closed loop response characteristics for the pneumatic actuator, and the time responses for the elevator and aileron are shown in Section 4.3. These response characteristics are then used in Section 6.2 to determine the dynamic response characteristics of Aircraft A.

### 4.1 CHARACTERISTICS

A pneumatic actuation system for positioning an aircraft control surface is shown in Figure 4.1. A compressor pump pressurizes a supply tank which provides a constant supply pressure to the actuator through the pressure regulator. Movement of the piston is controlled by supply and exhaust valves at each end of the actuator housing.

Compressor pumps for pneumatic systems are normally of the rotating vane or reciprocating piston type. Air cooling is normally sufficient for compressors operating in the range of several horseposer. Ratings

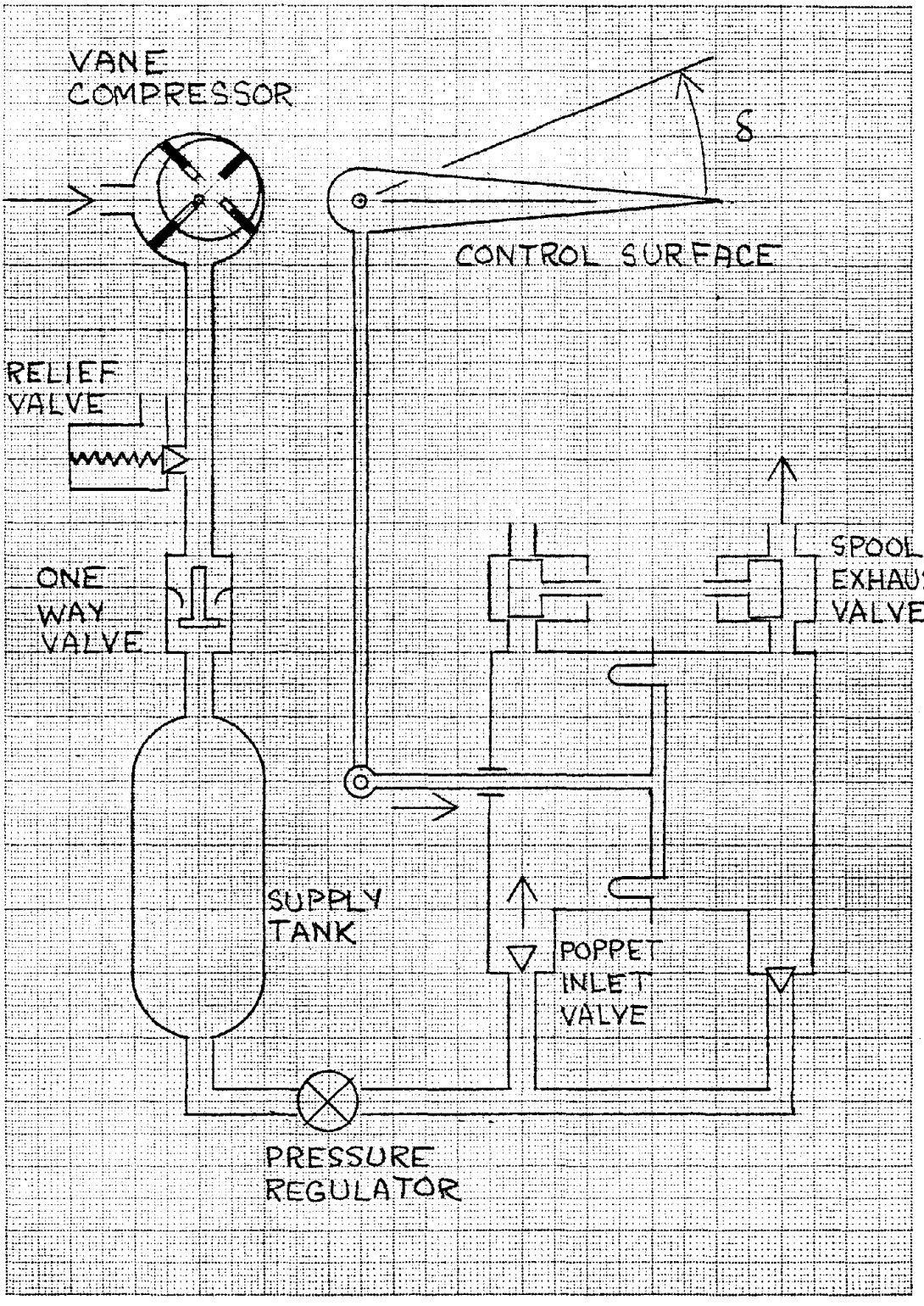


| | | | | | |
|---|---|---|---|---|---|
| CALC | | | REVISED | DATE | Figure 4.1: Electro-Pneumatic Actuation System |
| CHECK | | | MSR | | |
| APPD | | | | | |
| APPD | | | | | |
| | | | | | UNIVERSITY OF KANSAS |

for pumps are normally in terms of volumetric flow rate q, at atmospheric pressure, the following equation being used:

$$q = \left( \frac{P_s + 14.7 \text{ psi}}{14.7 \text{ psi}} \right) q_s \qquad (4.1)$$

where $q_s$ is the flow rate at supply pressure $P_s$ in $lbs/in^2$.

Filters are needed to remove particulate matter and water. Water should be removed from the air before reaching the pump with precautions such as heating elements used in case of icing conditions. A 40-micron filter for particulate matter can be used ahead of the pressure regulator and actuator valves. Because air has poor lubricating properties, a lubrication unit should also be used in the system.

The supply tank is used to handle peak loads and allows the compressor to run at a constant speed. It also provides a reserve in case of a compressor failure. Reference 2 states that the energy storage capability of a compressed gas tank is greater than that for electric storage batteries on a weight basis. A one way valve is used to allow the supply tank to remain pressurized when the compressor is off and a relief valve to prevent excessive supply pressures. The pressure regulator supplies constant pressure to the actuator at some level lower than that of the supply tank.

Several types of valves are used in pneumatic systems. Spool valves are shown for the exhaust ports and are the most widely used for servomechanisims. For a closed loop electro-pneumatic system the spool in the valve is controlled by a coil and magnet assembly in which the current is varied by a feedback loop made of position transducers on the control wheel and control surface. Poppet valves are shown for the supply ports and are used as a two position control for the supply pressure to the actuator.

Pneumatic actuators fall into three categories: piston, diaphragm and bellows, as shown in Figure 4.2. Piston actuators require rings or seals to keep leakage to a minimum, require higher tolerances than the other types and are more subject to wear. Diaphragm actuators use a flexible seal to stop leakage but are more limited in displacement than the piston type. The diaphragm material also is more limited in operating temperature ranges than the piston type. The bellows type can be made of metal and used in high temperature applications such as actuation using rocket exhaust gases. Making the bellows of metal gives it a high stiffness requiring high supply pressures, and long term usage can result in metal fatigue.

Using air instead of hydraulic fluid in the system results in poor damping characteristics because of the low viscosity and compressibility of air. Also the compressibility of the gas makes the system equations very non-linear and analysis more complex than for the hydraulic system. Pressure changes involve a greater time delay in the pneumatic system than in the hydraulic system where pressure rises to the supply level almost immediately after opening the control valve. The pneumatic system, however, is not subject to cavitation and pressure surges that can be encountered in the hydraulic actuator.

Another problem in pneumatic systems is leakage. This can be reduced by using a low supply pressure. Lowering the supply pressure, however, requires a larger piston area making the minimum supply pressure dependent on volumetric and weight limitations of the actuator.

## 4.2 MATHEMATICAL MODEL

A meter-out control system method has been used for the pneumatic

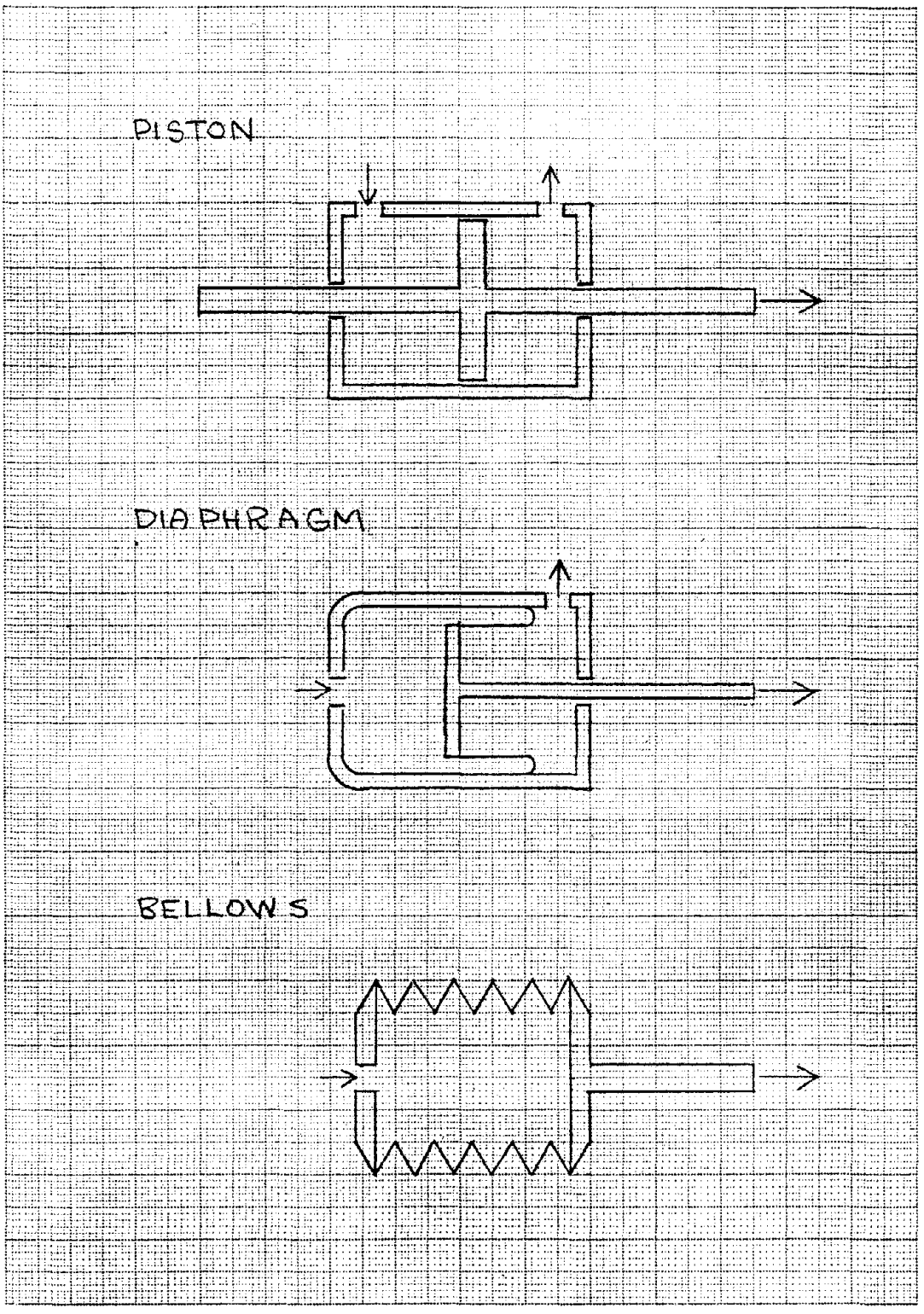


| | | | | | |
|---|---|---|---|---|---|
| CALC | | | REVISED | DATE | Figure 4.2: Pneumatic Actuator Types |
| CHECK | | | MSR | | |
| APPD | | | | | |
| APPD | | | | | |
| | | | | | UNIVERSITY OF KANSAS |

control system where the exhaust valve is used for the positional control. Initially both the exhaust and supply sides of the piston are at supply pressure; and upon receiving an input command, the supply valve on the exhaust side closes and the exhaust valve opens as shown in Figure 4.1. The exhaust valve is then shut using a feedback loop connected to the control wheel. Meter out control for fluid systems is described in detail in Reference 1.

In determining the equations governing the motion of the piston, the following assumptions will be made:

1. The mass flow out of the exhaust is assumed to be adiabatic, isothermal and obeys the perfect gas law.
2. Flow will be choked in the exhaust valve ($P_2/P_e > 1.89$), which is normally the case unless excessive valve openings (feedback gains) are used.
3. Supply pressure is constant (infinite capacity).
4. The external load is only a function of piston (control surface) position.
5. The exhaust valve behaves linearly (valve area for input signal).

Using these assumptions, the equation of motion for the piston can be expressed as:

$$[\, P_s - P_2(t)]\, A_p = m_e \ddot{x}\,(t) + F_L\,(x) \tag{4.2}$$

For an isothermal process the following relationship holds:

$$\frac{\dot{M}_2(t)}{M_2(t)} = \frac{\dot{V}_2(t)}{V_2(t)} + \frac{\dot{P}_2(t)}{P_2(t)} \tag{4.3}$$

Using the perfect gas law for an isothermal process ($T_2$ constant):

$$M_2(t) = \frac{P_2(t)\ V_2(t)}{RT_2} \tag{4.4}$$

Mass flow out of the choked exhaust valve can be expressed as:

$$\dot{M}_2(t) = - \frac{\partial \dot{M}_2}{\partial P_2} P_2(t)\ A_v(t) \tag{4.5}$$

where

$$\frac{\partial \dot{M}_2}{\partial P_2} = \frac{C_q}{\sqrt{T_2}} \left[ \frac{\gamma}{R} \left(\frac{2}{\gamma + 1}\right)^{\frac{\gamma+1}{\gamma-1}} \right]^{1/2} \tag{4.6}$$

Combining the above expressions to obtain an expression for change in pressure:

$$\dot{P}_2(t) = P_2(t) \left[ \frac{1}{M_2(t)} \dot{M}_2(t) + \frac{1}{V_2(t)} \dot{V}_2(t) \right] \tag{4.7}$$

$$\dot{P}_2(t) = P_2(t) \left[ \frac{-RT_2}{P_2(t)\ V_2(t)} \frac{\partial \dot{M}_2}{\partial P_2} A_v(t) P_2(t) + \frac{A_p \dot{x}(t)}{V_2(t)} \right] \tag{4.8}$$

$$\dot{P}_2(t) = - \frac{P_2(t)}{V_2(t)} \left[ RT_2 \frac{\partial \dot{M}_2}{\partial P_2} A_v(t) - A_p \dot{x}(t) \right] \tag{4.9}$$

The valve will be treated as a pure gain, since the dynamics of the valve are normally an order of magnitude smaller than the dynamics of the actuator (Reference 3). For a position feedback loop:

$$A_v(t) = K_v\ [x_c(t) - x(t)] \tag{4.10}$$

A block diagram combining the above equations is shown in Figure 4.3. A Fortran computer program for computing the time histories is outlined in the Appendix.

## 4.3 DESIGN EXAMPLES

The electro-pneumatic actuator has been evaluated with the control surface model described in Section 2.1 and also in a small single-engine general aviation aircraft (Aircraft A) described in Section 2.2.

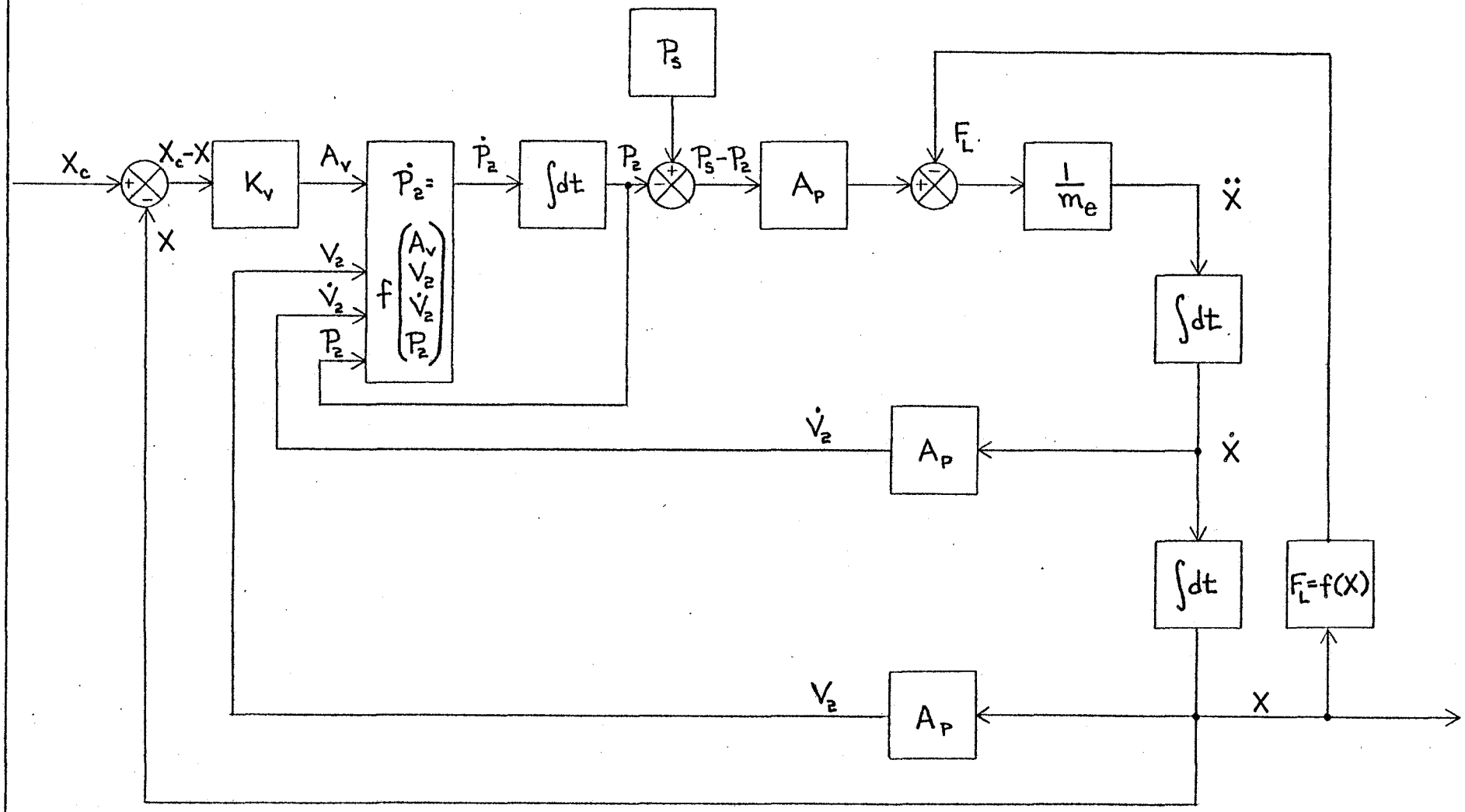


| | | | | | |
|---|---|---|---|---|---|
| CALC | | | REVISED | DATE | Figure 4.3: Pneumatic Actuator Control System Block Diagram |
| CHECK | | | | | |
| APPD | | | | | |
| APPD | | | | | UNIVERSITY OF KANSAS |
| | | | | | PAGE |

The control surface model has been used as a means of comparison to the other actuators, and the aircraft evaluation has been used for the closed loop analysis done in Chapter 6.

### 4.3.1 CONTROL SURFACE MODEL

The pneumatic actuator used for this evaluation is a commercially available actuator shown in Figure 7.1. A piston area of 16 square inches was used to provide sufficient force for a 50 psi pressure differential for the control surface model described in Section 2.1. A 100 psi pressure was also used to observe change in response characteristics due to an increase in supply pressure. Since static pressure varies with altitude (14.70 psi at sea level and 11.78 psi at 6000 ft), the supply pressure will decrease with altitude.

Three loading conditions have been used in evaluating the pneumatic actuation system and are described in Section 2.1.2. The inertia loading closed loop response is shown in Figure 4.4 and shows little change in time response but an increased oscillatory amplitude for an increase in supply pressure. Figure 4.5 shows the closed loop response for the cruise loading, and Figure 4.6 shows the same response at the maximum load condition. These two figures show the effect of an increased loading on the response characteristics. The time response for a reduced control surface deflection of 10° is shown in Figure 4.7, and the change in response for a variation in valve gain is shown in Figure 4.8. Open loop response of the pneumatic actuator at maximum load condition is shown in Figure 4.9. These time histories can be compared to responses for the electro-mechanical and hydraulic actuators in Sections 3.3 and 4.3, respectively.

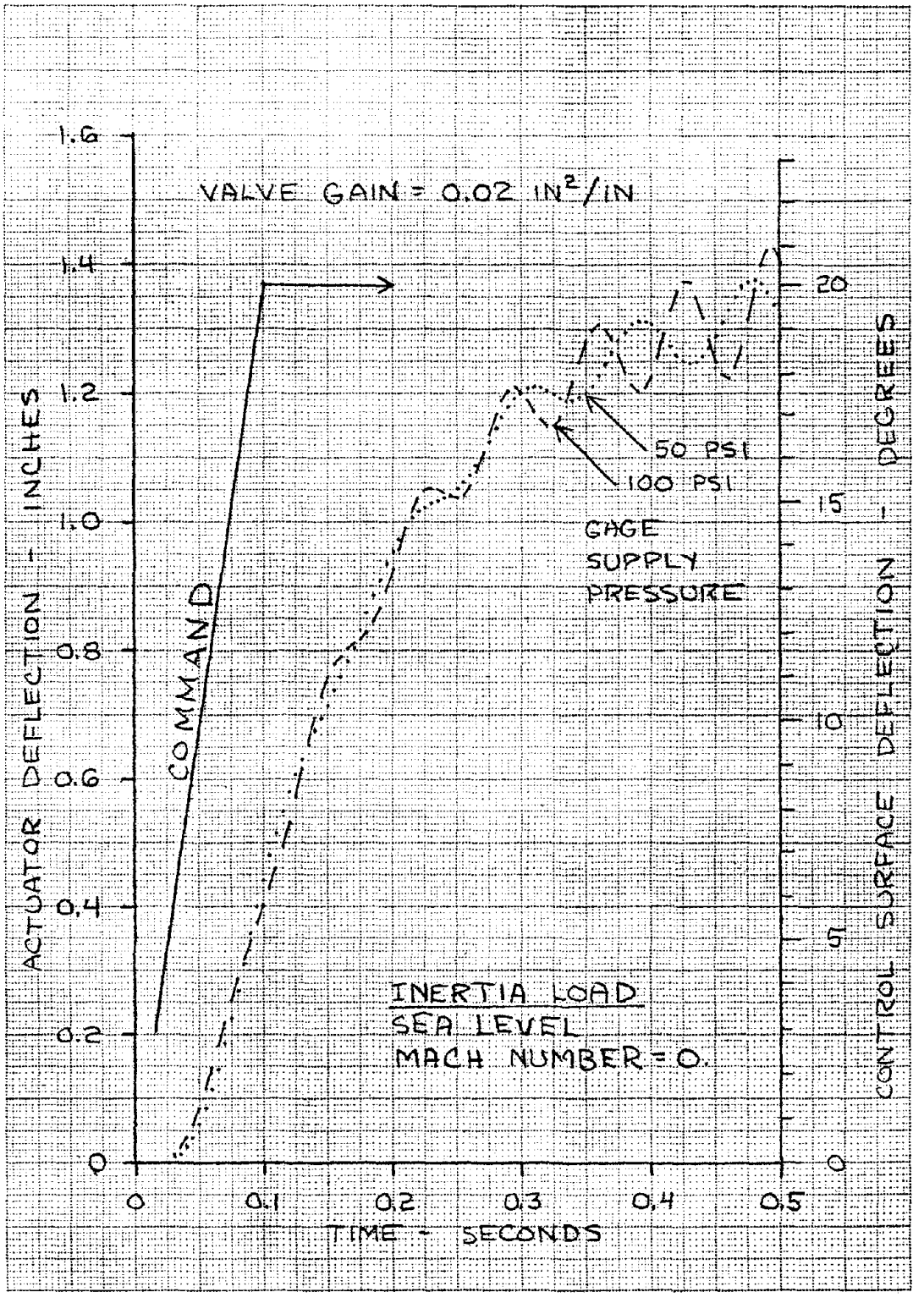


| | | | | | |
|---|---|---|---|---|---|
| CALC | | | REVISED | DATE | Figure 4.4: Pneumatic Actuator-Inertia Load, Closed Loop |
| CHECK | | | | | |
| APPD | | | | | |
| APPD | | | | | |
| | | | | | UNIVERSITY OF KANSAS |

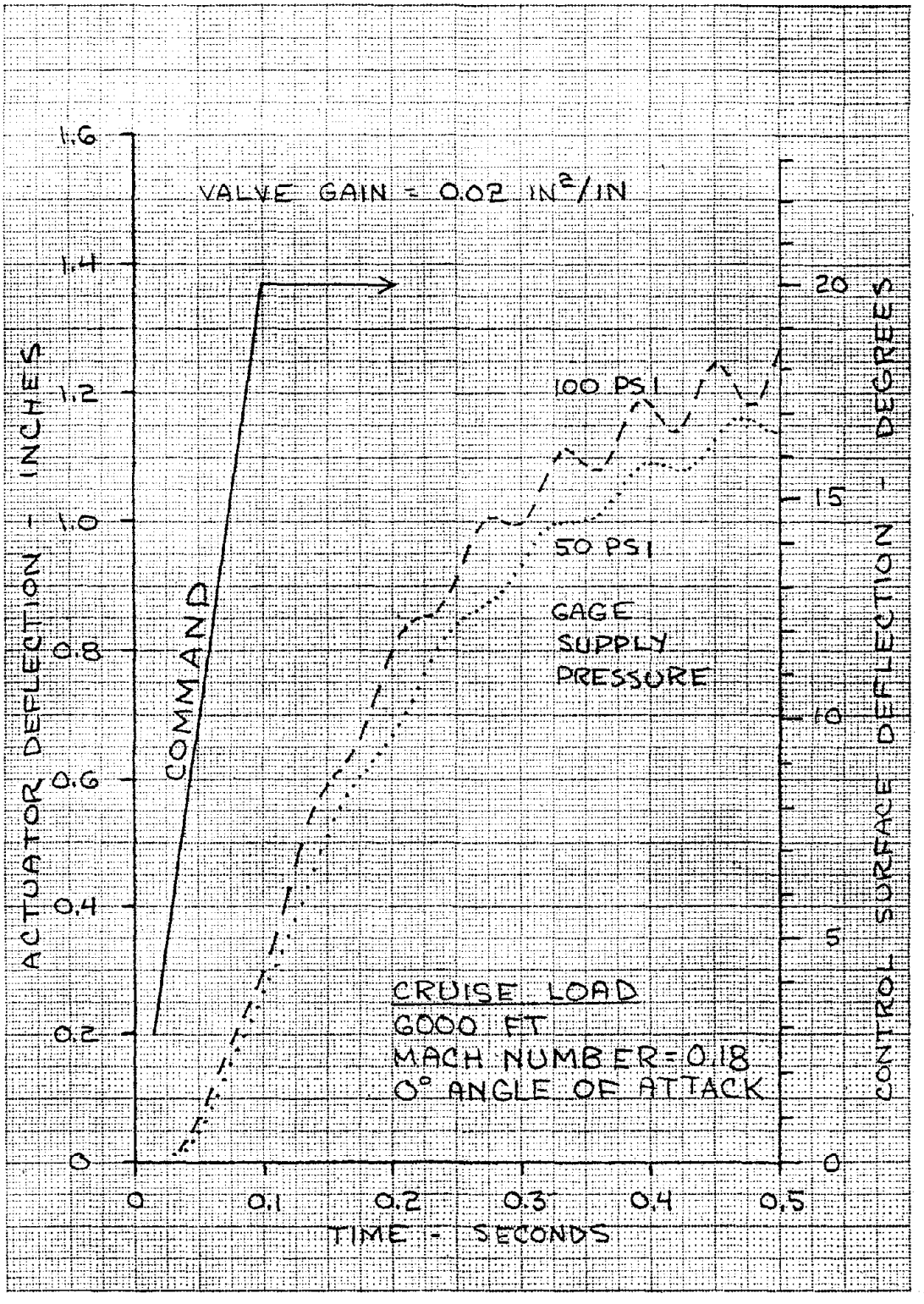


| | | | | | |
|---|---|---|---|---|---|
| CALC | | | REVISED | DATE | Figure 4.5: Pneumatic Actuator-Cruise Load, Closed Loop |
| CHECK | | | | | |
| APPD | | | | | |
| APPD | | | | | |
| | | | UNIVERSITY OF KANSAS | | PAGE 72 |

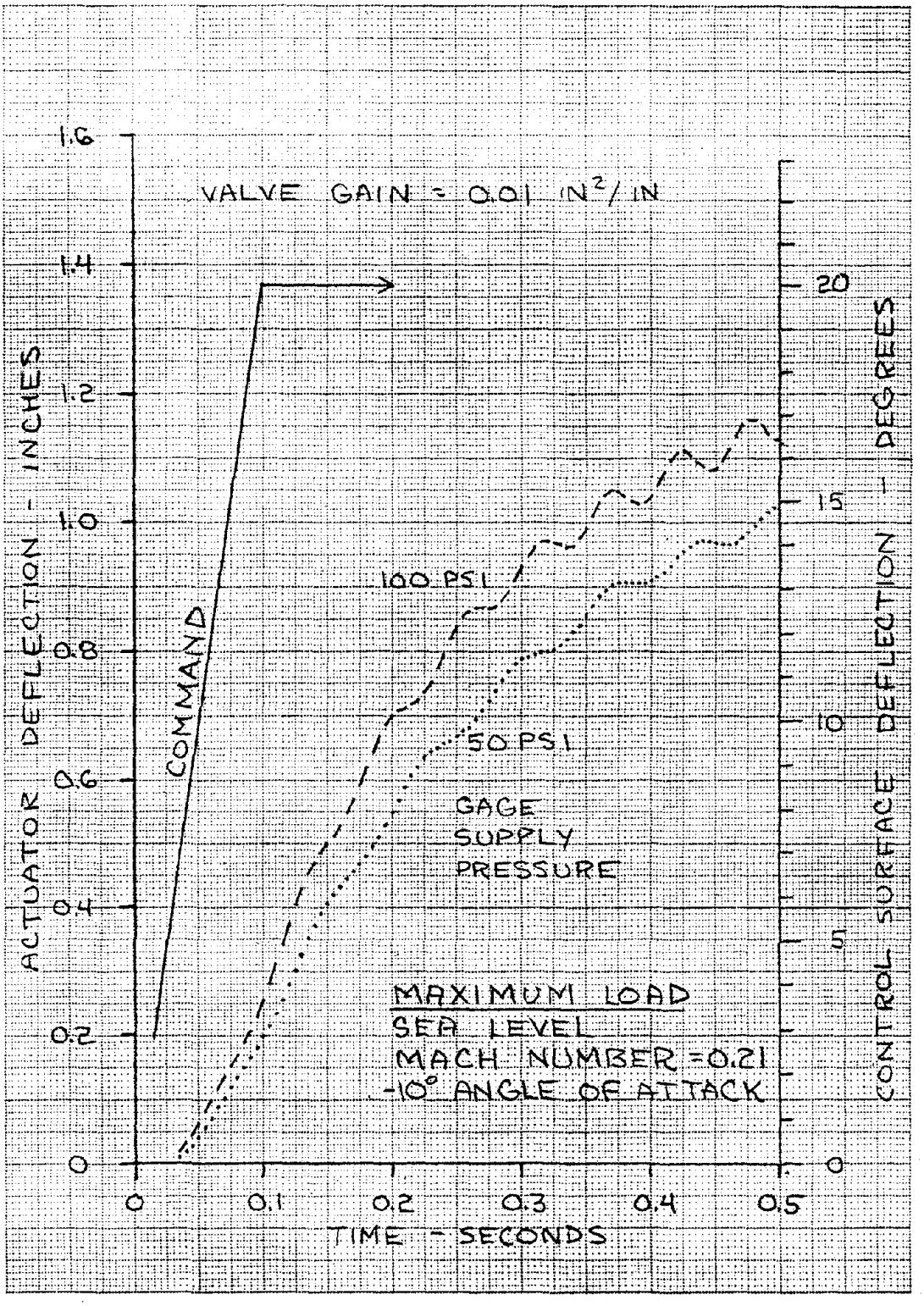


| CALC | | | REVISED | DATE | Figure 4.6: Pneumatic Actuator-Maximum Load, Closed Loop | |
|---|---|---|---|---|---|---|
| CHECK | | | | | | |
| APPD | | | | | | |
| APPD | | | | | | |
| | | | | | UNIVERSITY OF KANSAS | PAGE 73 |

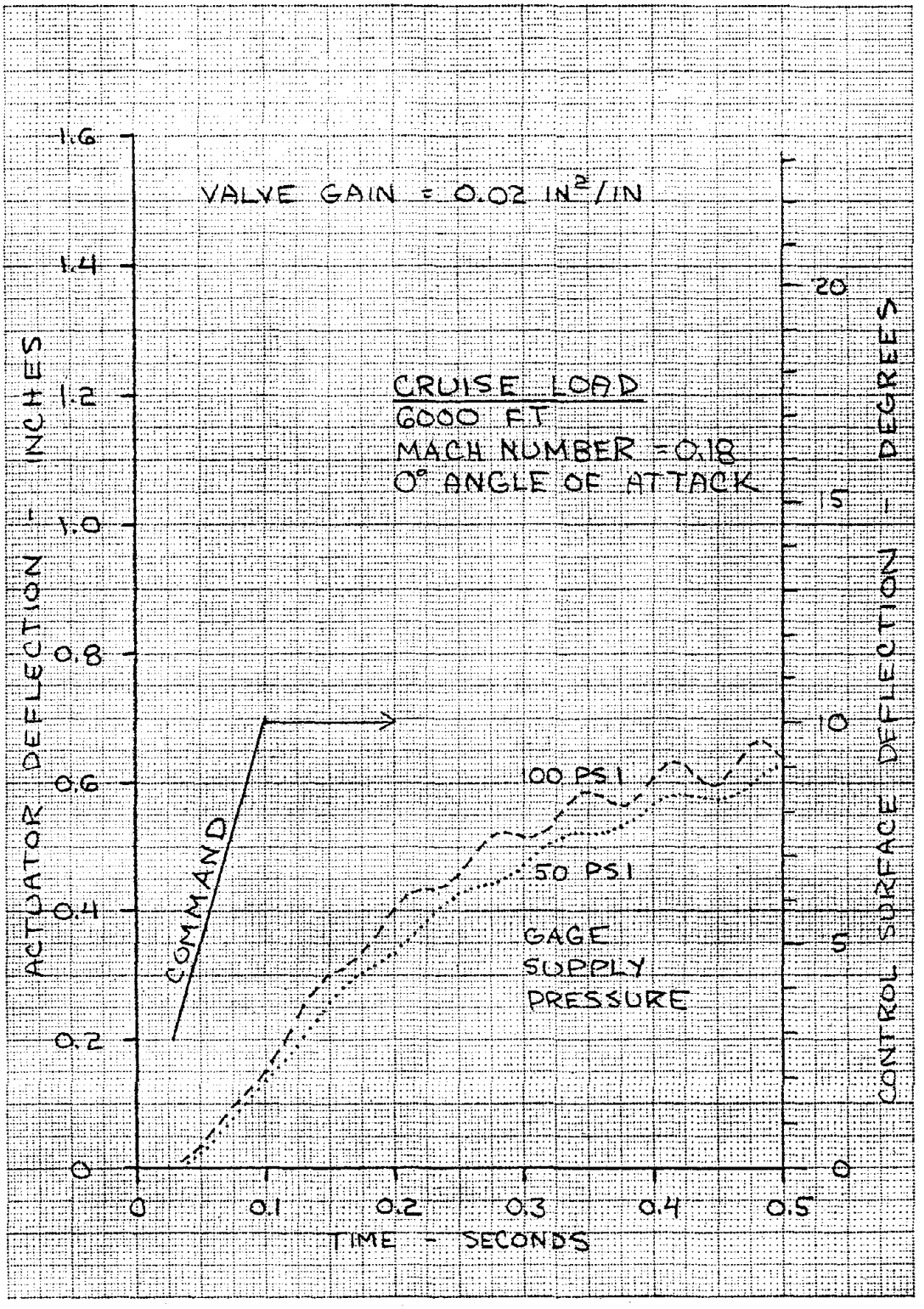


| CALC | | | REVISED | DATE |
|---|---|---|---|---|
| CHECK | | | | |
| APPD | | | | |
| APPD | | | | |
| | | | | |

Figure 4.7: Pneumatic Actuator-Cruise Load at 10°, Closed Loop

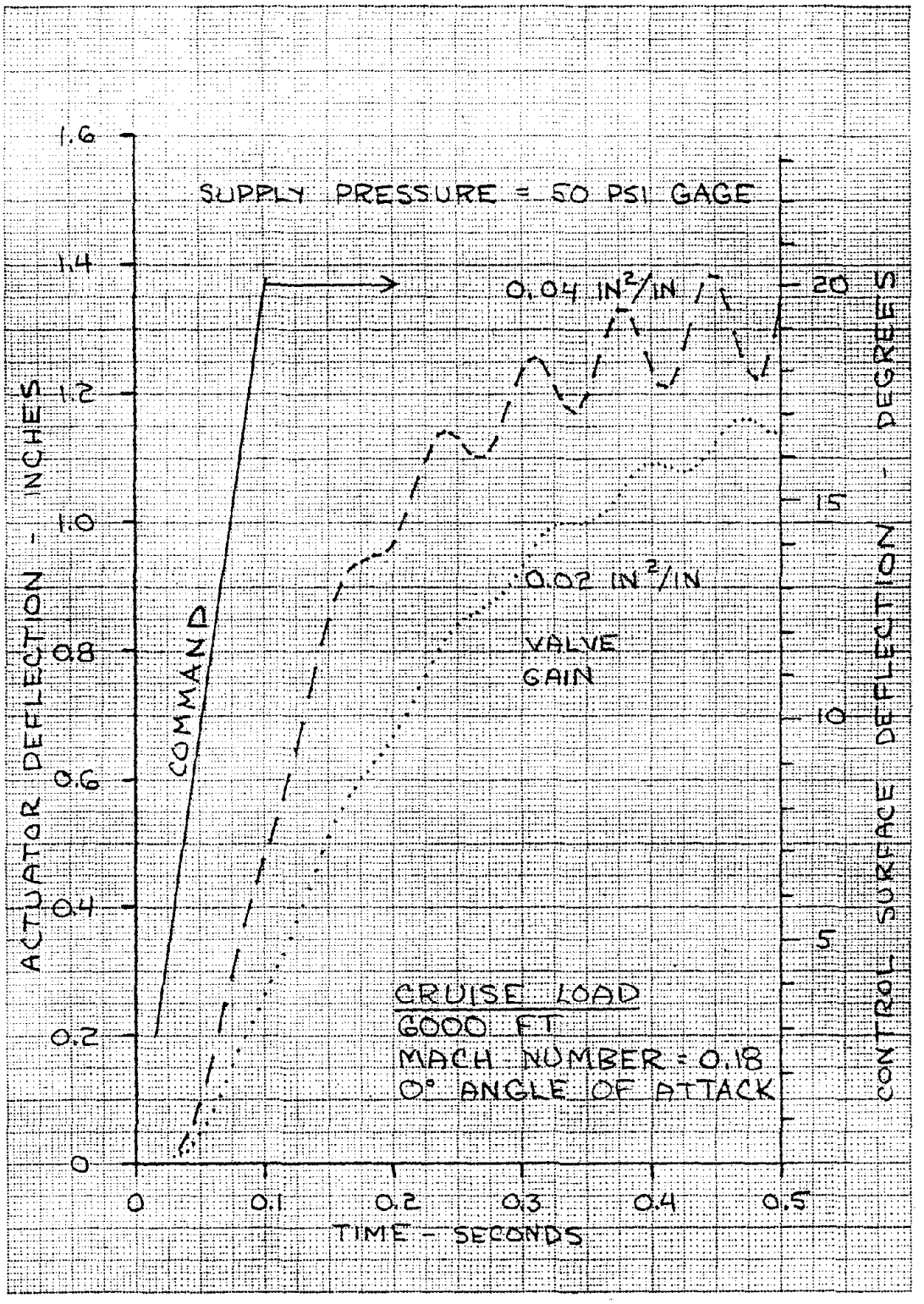


| CALC | | | REVISED | DATE |
|---|---|---|---|---|
| CHECK | | | | |
| APPD | | | | |
| APPD | | | | |
| | | | | |

Figure 4.8: Pneumatic Actuator - Cruise Load, Variable Closed Loop Gain

UNIVERSITY OF KANSAS

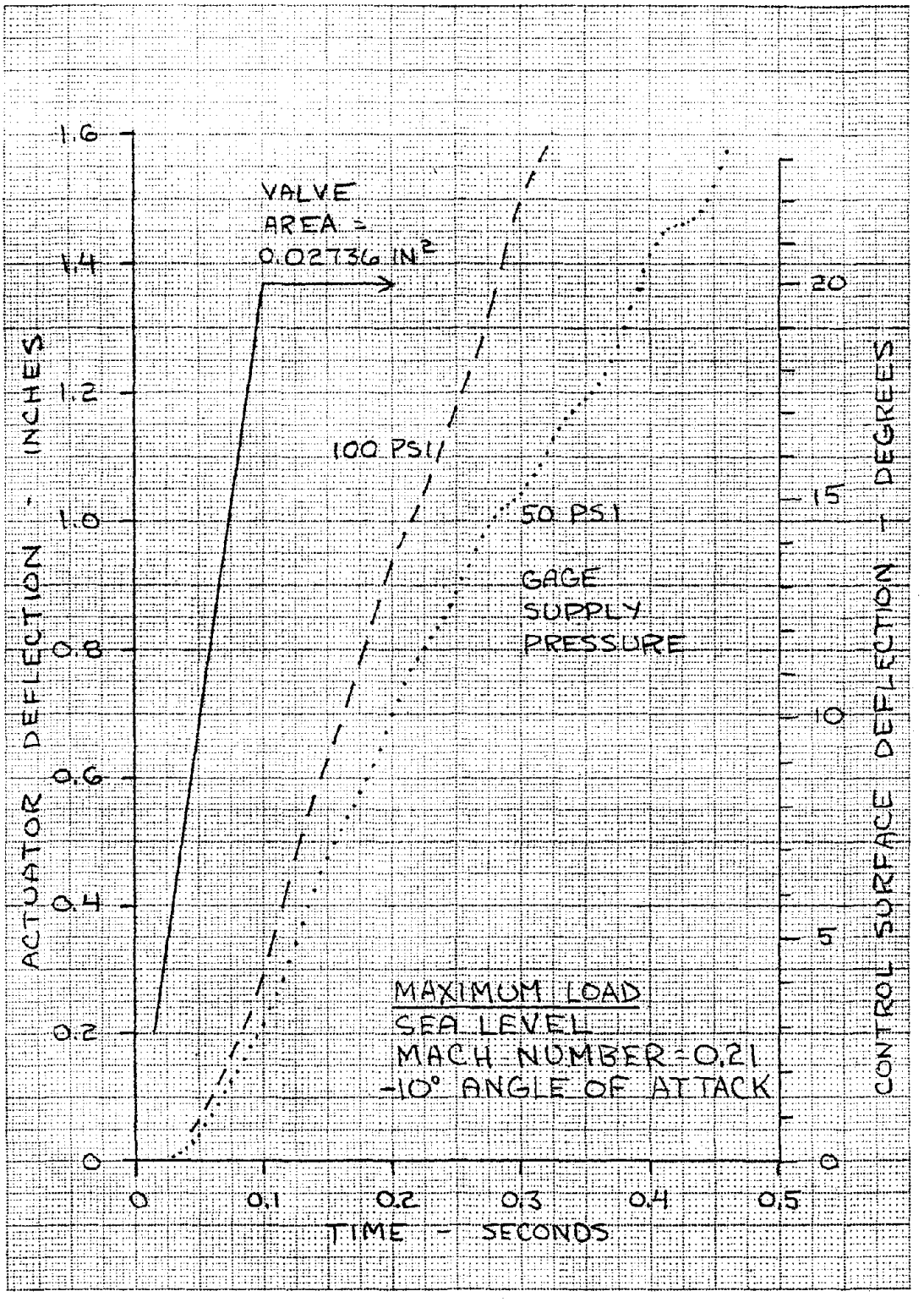


| CALC | | | REVISED | DATE |
|---|---|---|---|---|
| CHECK | | | | |
| APPD | | | | |
| APPD | | | | |
| | | | | |

Figure 4.9: Pneumatic Actuator-Maximum Load, Open Loop

UNIVERSITY OF KANSAS

### 4.3.2 AIRCRAFT MODEL

The single engine light aircraft (Aircraft A) has been used for the pneumatic actuator to find aircraft response characteristics. A four inch moment arm will be used for the elevator and a two inch moment arm for the aileron. The same size actuator and a supply pressure of 50 psi gauge has been used. The hinge moments for cruise and approach configurations are found in Section 2.2.

Time histories for the elevator are shown in Figure 4.10 and for the ailerons in Figure 4.11. The closed loop response characteristics for the aircraft will be determined using Laplace transforms, and the actuator response can be represented as:

$$H(s) = \frac{1}{1 + \tau_a s} \tag{4.11}$$

In this equation $\tau_a$ is referred to as the time constant of the actuator. This function in the time domain can be written in the form:

$$x(t) = x_c(t) \left[ 1 - e^{-\frac{t}{\tau_a}} \right] \tag{4.12}$$

The time histories in Figure 4.10 and 4.11 show the linear approximations, and the time constants for the flight conditions are shown in the following table:

Table 4.1 - Aircraft A Actuator Time Constants

| Configuration | Control Surface | Time Constant |
|---|---|---|
| CRUISE | Aileron | 0.45 sec |
| | Elevator | 0.40 sec |
| APPROACH | Aileron | 0.25 sec |
| | Elevator | 0.22 sec |

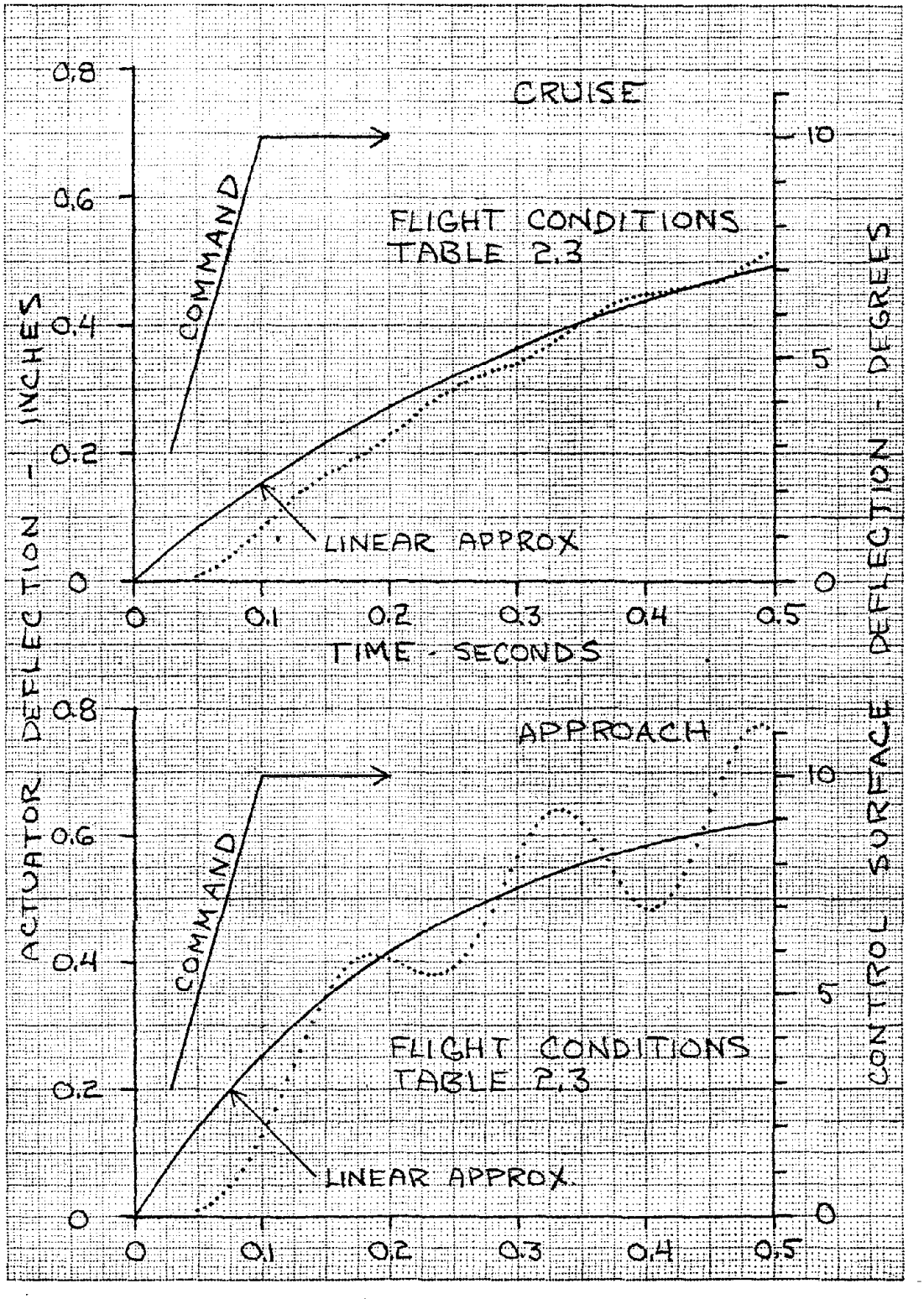


| | | | | | |
|---|---|---|---|---|---|
| CALC | | | REVISED | DATE | Figure 4.10: Airplane A, Elevator Time Histories |
| CHECK | | | MSR | | |
| APPD | | | | | |
| APPD | | | | | UNIVERSITY OF KANSAS |
| | | | | | PAGE 78 |

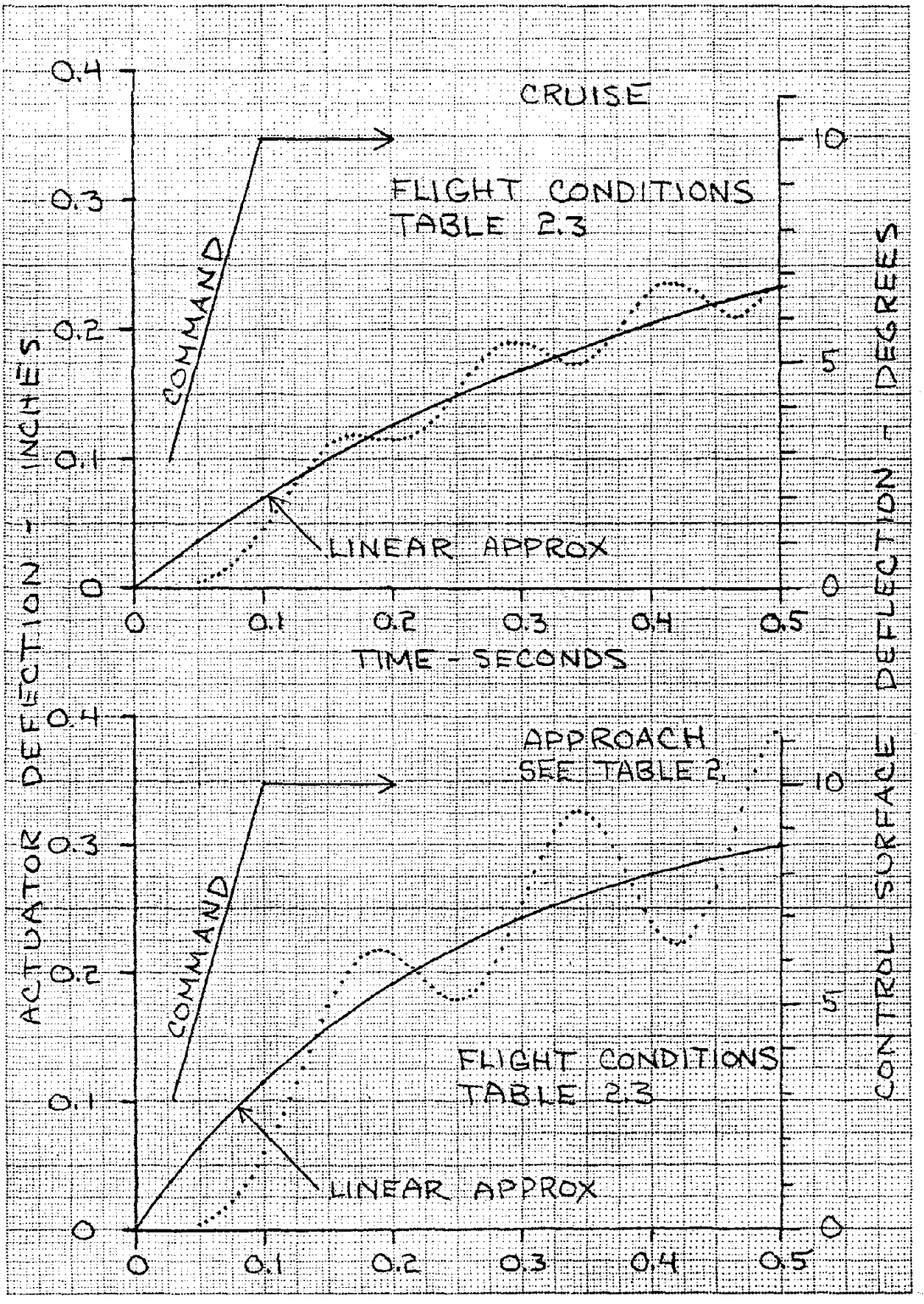


| | | | | | |
|---|---|---|---|---|---|
| CALC | | | REVISED | DATE | Figure 4.11: Airplane A, Aileron Time Histories |
| CHECK | | | | | |
| APPD | | | | | |
| APPD | | | | | |
| | | | | | UNIVERSITY OF KANSAS |

References for Chapter 4

1. McCloy, D. and Martin, H. R., "The Control of Fluid Power," John Wiley & Sons, 1973.

2. Andersen, Blaine W., "The Analysis and Design of Pneumatic Systems," John Wiley & Sons, 1967.

3. Stringer, John, "Hydraulic Systems Analysis," John Wiley & Sons, 1976.

4. Roskam, Jan, "Fight Dynamics of Rigid and Elastic Airplanes," Volumes 1 and 2, published by Roskam Aviation and Engineering Corporation, 519 Boulder, Lawrence, Kansas, 1972.

5. Reethof, G., "Analysis and Design of a Servomotor Operating on High-Pressure Compressed Gas," Transactions of the ASME, May 1957.

6. Shearer, J. L., "Study of Pneumatic Processes in the Continuous Control of Motion with Compressed Air," Transactions of the ASME, February 1956.

# CHAPTER 5

## ELECTRO-HYDRAULIC ACTUATORS

Hydraulic actuation is currently the industry standard for large commercial and military aircraft. Because of the incompressibility of the hydraulic fluid, the hydraulic actuator is a stiffer system with a faster time response than the pneumatic actuator. Motion of the hydraulic actuator is generally governed by the flow rate, as opposed to the pneumatic actuator where motion depends primarily on pressure differential across the piston. By directly controlling flow rate with the control valve, accurate positional control is more easily obtainable with hydraulic actuation.

Section 5.1 outlines hydraulic control systems and the components that make up the systems. Section 5.2 outlines the mathematical model used for the hydraulic actuator. Section 5.3 then applies this model to the control surface described in Section 2.1 to find the time response characteristics. Aircraft C has been used for evaluating the closed loop response characteristics for the hydraulic actuator, and the time responses for the aileron and elevator are shown in Section 5.3. These response characteristics are then used in Section 6.4 to determine the dynamic response characteristics of Aircraft C.

### 5.1 CHARACTERISTICS

Two hydraulic systems applicable for an aircraft control system are shown in Fig. 5.1 and 5.2. The first system is the simplest and uses a fixed displacement pump and a relief valve. The second, more complex system uses an accumulator with an off-loading valve. Both systems provide a relatively constant supply pressure to the actuation system.

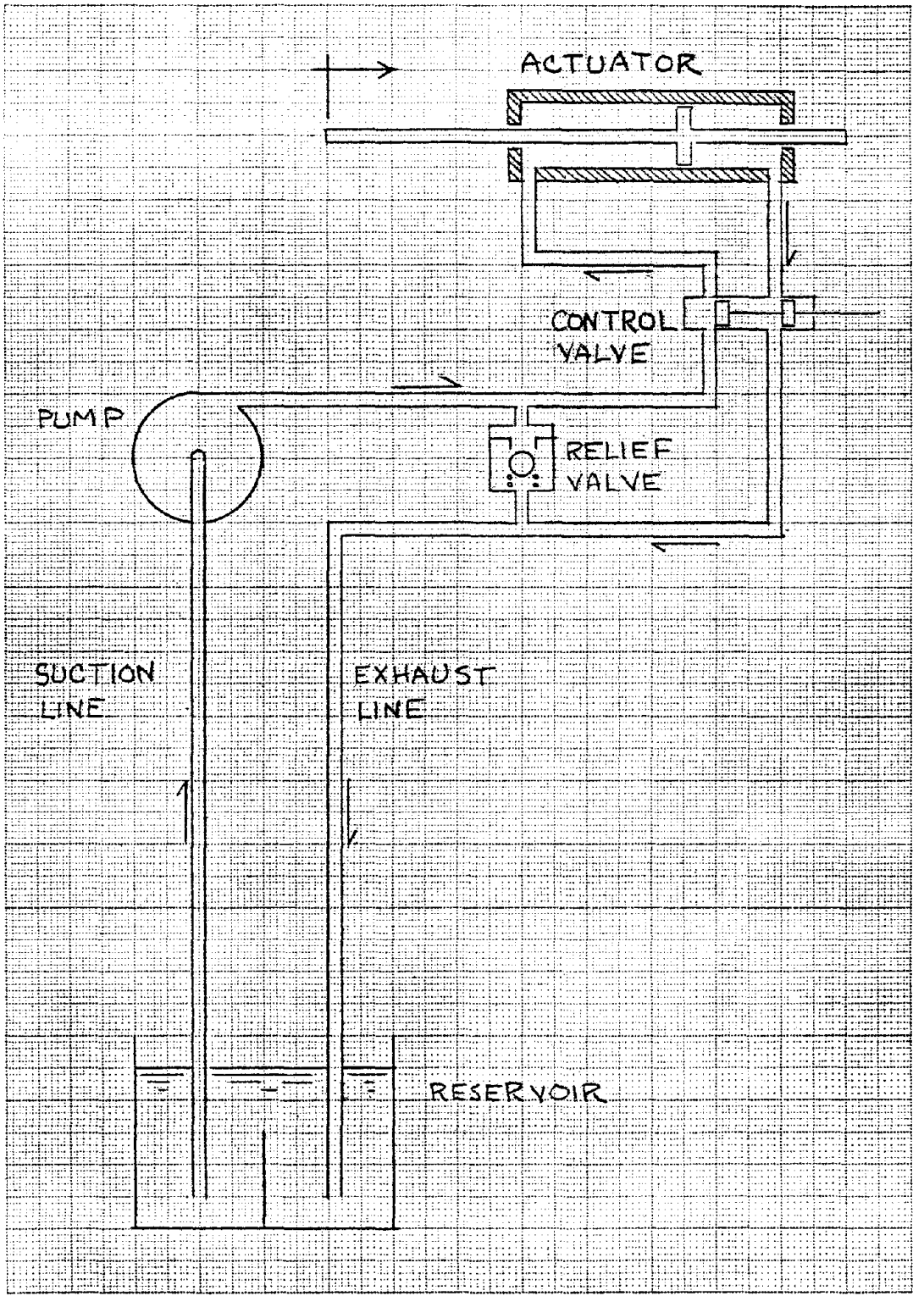


| | | | | |
|---|---|---|---|---|
| CALC | | | REVISED | DATE |
| CHECK | | | MSR | |
| APPD | | | | |
| APPD | | | | |
| | | | | |

Figure 5.1: Relief Valve Hydraulic System

UNIVERSITY OF KANSAS

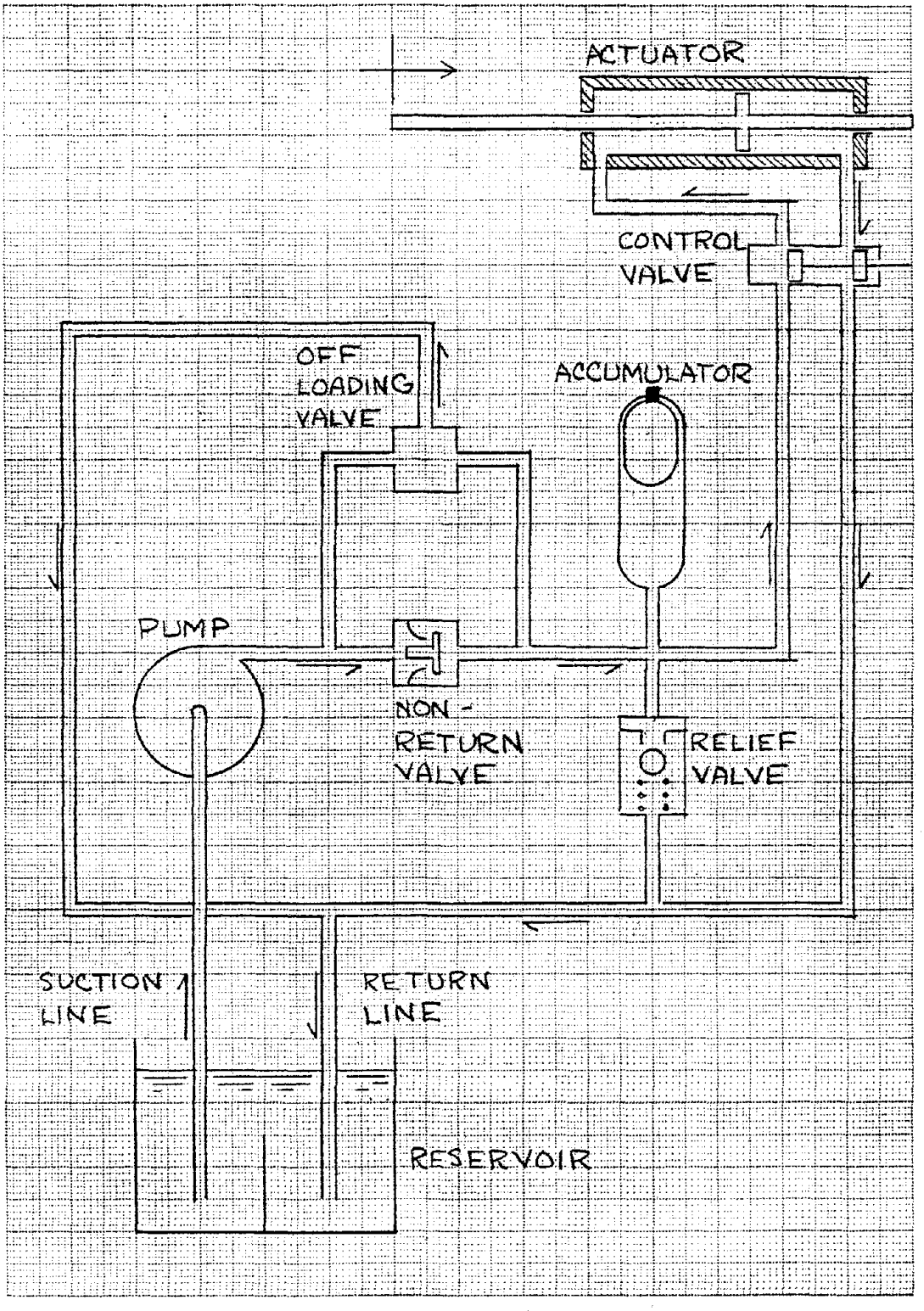


| | | | | | |
|---|---|---|---|---|---|
| CALC | | | REVISED | DATE | Figure 5.2: Off Loading Valve Hydraulic System |
| CHECK | | | MSR | | |
| APPD | | | | | |
| APPD | | | | | |
| | | | | | UNIVERSITY OF KANSAS |

The first system uses a fixed displacement pump with the relief valve maintaining a maximum system pressure. Flow in excess of system demand is sent back to the reservoir through the relief valve. Flow through the relief valve heats up the fluid, and a cooling tank may be necessary to keep system temperatures below a maximum of 120° F. This system uses fewer components than the next system described and is less expensive, but the lost cost advantage may be offset by the weight and volume penalties if a cooling tank is necessary.

An accumulator and off-loading valve system is more suitable for the varying flow requirements that will be present in an aircraft control system. Initially the off-loading valve is closed and the fixed displacement pump charges the accumulator. When the system rises to the supply pressure, the off-loading valve opens and off-loads the pump. The accumulator then maintains the system pressure with the non-return valve closed. As the accumulator discharges, pressure will drop to the low level setting of the off-loading valve, which will then close. The pump will then supply the system and recharge the accumulator repeating the cycle.

A good reservoir design is needed to prevent air from getting into the system. Fig. 5.3 shows a typical arrangement. The suction line needs to be well below the surface to prevent a vortex from forming, which would draw air into the system. The return line should also be well submerged so it does not agitate the surface forming air bubbles. Baffles between the suction and return line prevent particular matter from recirculating. A layer of gauze with 60 strands per inch can be placed between the return and suction lines to stop air bubbles. The reservoir should have a capacity of three to five minutes at the rated flow rate of the pump.

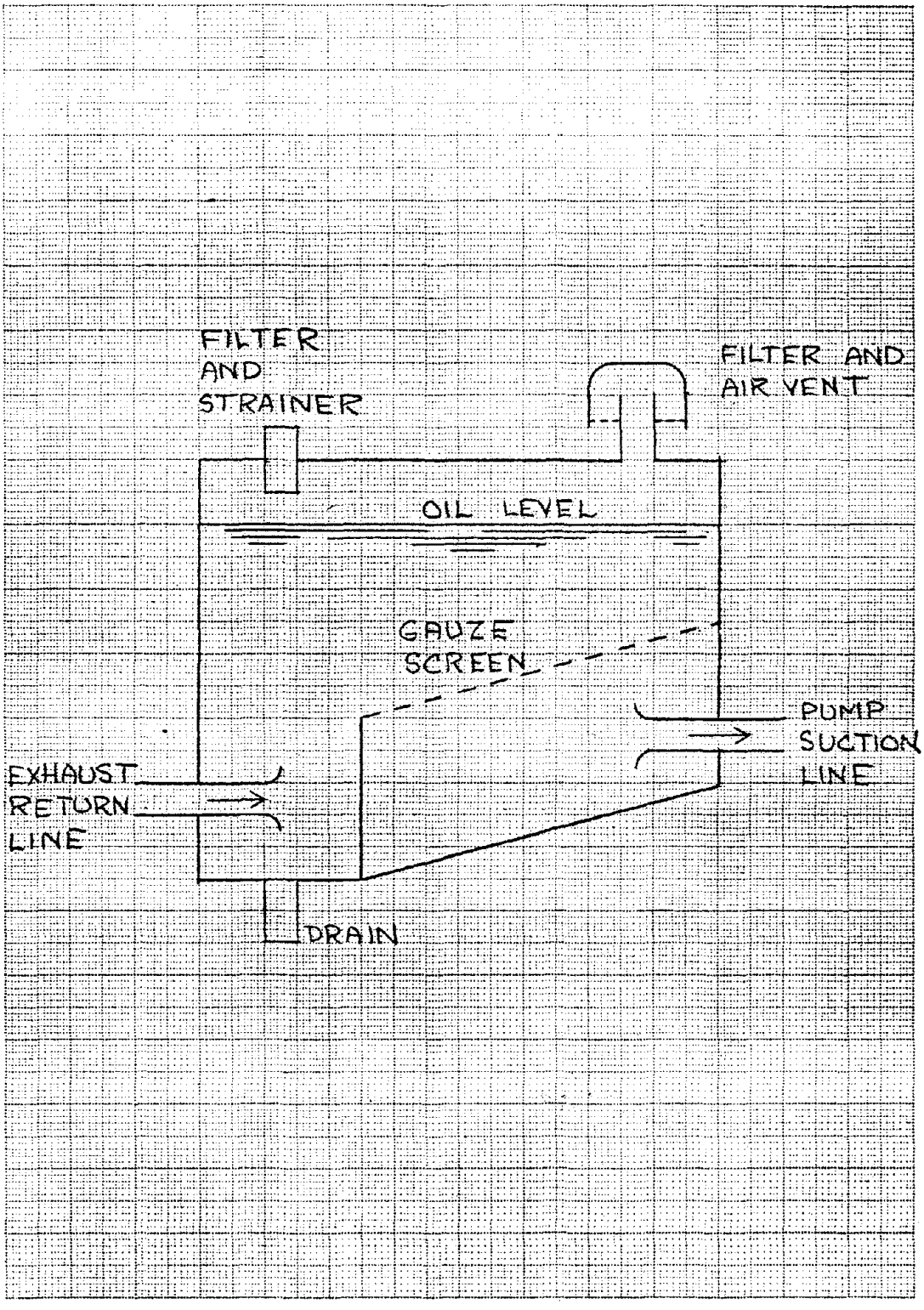


| | | | | | | |
|---|---|---|---|---|---|---|
| CALC | | | REVISED | DATE | Figure 5.3: Hydraulic Reservoir | |
| CHECK | | | MJR | | | |
| APPD | | | | | | |
| APPD | | | | | | |
| | | | | | UNIVERSITY OF KANSAS | PAGE 85 |

Pumps commonly used in hydraulic systems are shown in Fig. 5.4. Power for the pump is supplied by an electric motor or, more probably in the case of an aircraft, an accessory gearbox on the engine. Geared pumps are the cheapest to manufacture and can be used to system pressures of 2500 psi but are very inefficient at low speeds. The vane pump uses an eccentric rotor and spring loaded vanes which vary the volume in the housing and force liquid through using the created vacuum and can be used to a system pressure of 1000 psi. Both vane and geared pumps have overall efficiencies (flow rate for input work) of 80 to 85%. The swash plate pump is used for high pressure applications (up to 5000 psi). The swash plate pump is frequently used when the pump is in a closed loop system, since the flow rate can be easily varied by changing the swash plate angle.

The accumulator is an energy storage unit which uses a compressed gas, usually nitrogen. It is a high pressure cylinder with a rubber bag inside that is at some pressure below the supply pressure. As fluid is forced in, the gas bag is compressed raising the pressure. The accumulator helps smooth out pressure fluctuations due to pump action and acts as a reserve for short duration, high flow demand periods.

Filters are needed to protect the components from erosion due to particulate matter, especially the valves. Servo valves require filtration levels of 5 to 10 microns, and filters for this contamination level tend to be expensive. They should be placed just upstream of the valve and replaced regularly to avoid excessive pressure drop across the filter.

In most hydraulic servo mechanisms requiring positive and negative displacements, a four-way valve is normally used. The basic types available are illustrated in Fig. 5.4. It is called a four-way valve because

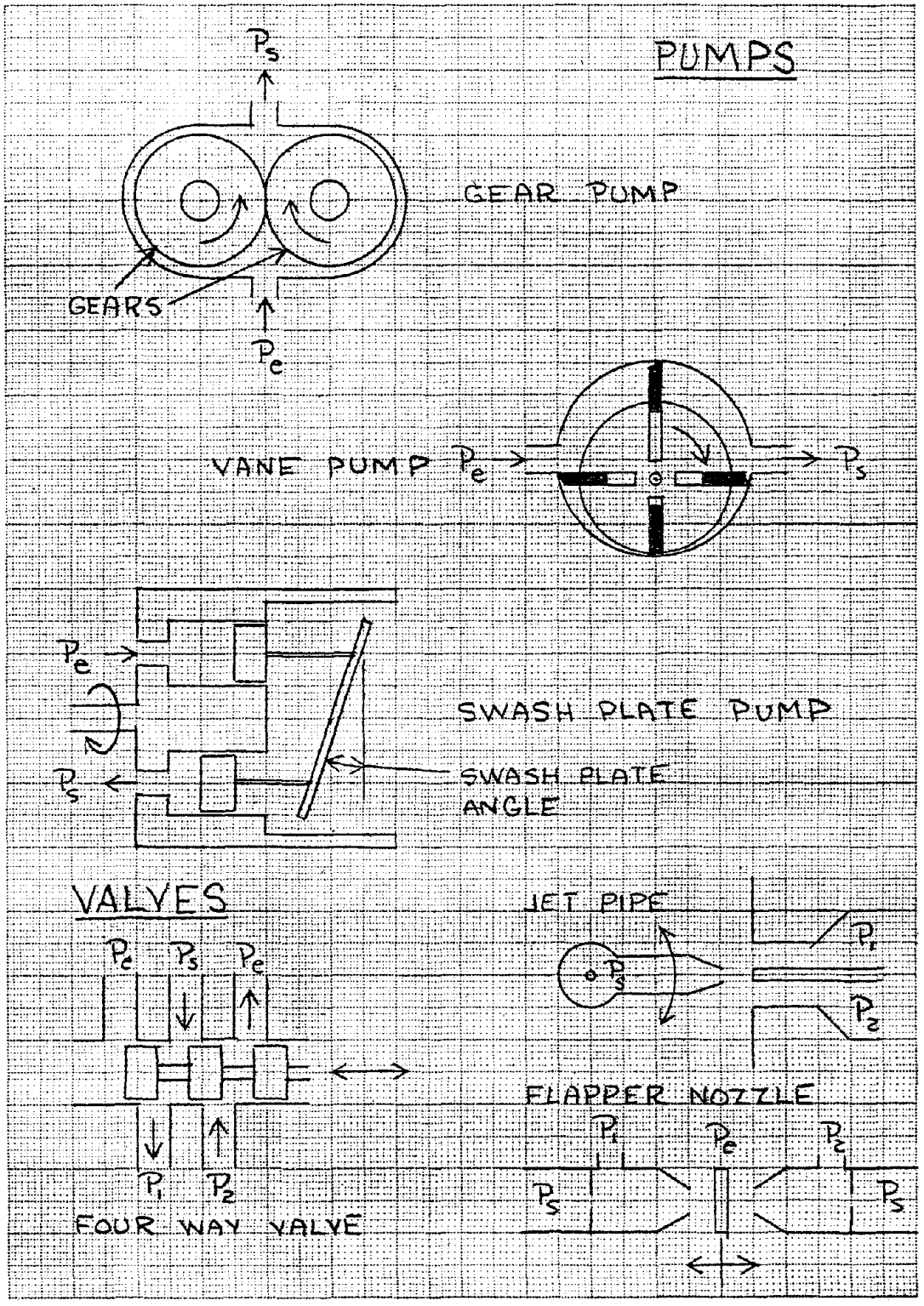


| | | | | | |
|---|---|---|---|---|---|
| CALC | | | REVISED | DATE | Figure 5.4: Hydraulic Pumps & Valves |
| CHECK | | | MSR | | |
| APPD | | | | | |
| APPD | | | | | |
| | | | | | UNIVERSITY OF KANSAS |

there are two control ports and at least one supply and exhaust port. The spool valve is the most popular for servo-mechanisms with a normal error of $\pm$ 5% (flow rate to valve opening). The spool valve is also the most expensive to manufacture, requiring machining tolerances of as low as a few microns. It is normally powered by an electronic valve drive amplifier requiring typically 2 to 10 watts of power. Jet pipe and flapper nozzle valves are less sensitive to contamination but have a high quiescent power loss and are only used for low power applications.

Two categories of hydraulic actuators are rotary and linear. Rotary have the advantage for large angular displacements over 30° but have the disadvantage of a fixed moment arm which is built in the actuator. Gearing the actuator can help alleviate this problem if the actuator has a greater maximum angular displacement than is required.

## 5.2 MATHEMATICAL MODEL

The equations of motion for a hydraulic actuator are normally based on the flow rate through the actuator. A linear and rotary hydraulic actuation system is shown in Fig. 5.5. In formulating the mathematical model, the following assumptions will be made:

1. The hydraulic fluid is incompressible, and there is no cavitation of the fluid.
2. The supply pressure is constant, and the exhaust pressure is negligible.
3. Flow rate into the supply side of the actuator equals flow rate out of the exhaust side.
4. No flow reversal or negative valve displacements are permitted.

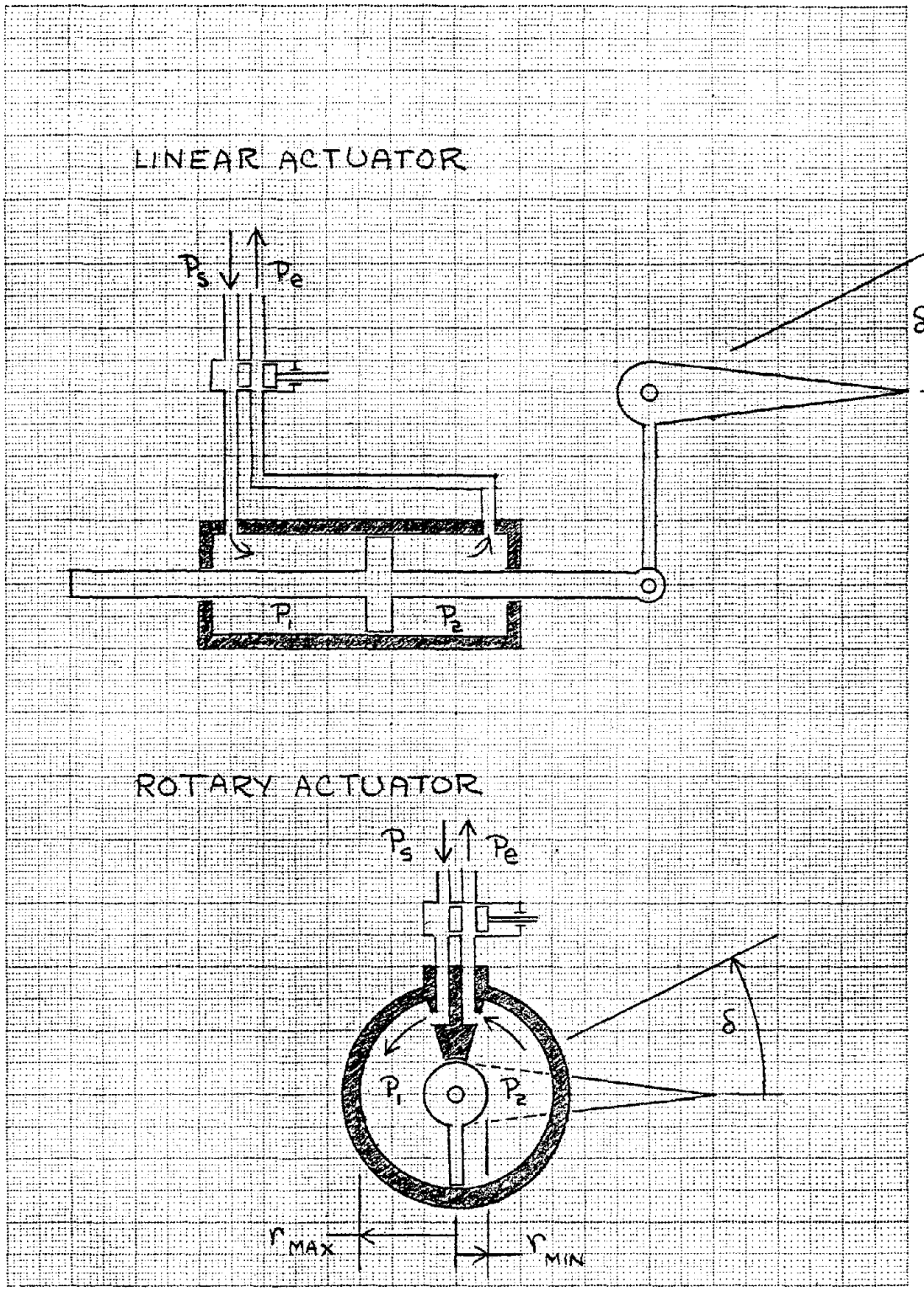


| | | | | | | |
|---|---|---|---|---|---|---|
| CALC | | | REVISED | DATE | Figure 5.5: Linear and Rotary Hydraulic Actuators | |
| CHECK | | | MSR | | | |
| APPD | | | | | | |
| APPD | | | | | | |
| | | | | | UNIVERSITY OF KANSAS | PAGE 89 |

5. Exhaust valve area equals inlet valve area.

The equations of flow for the supply and exhaust valve openings can be expressed as follows, with $C_d$ the coefficient of discharge which is dependent on valve geometry (typically $C_d = 0.625$).

$$q_1(t) = C_d A_v(t) \sqrt{\frac{2}{\rho} [P_s - P_1(t)]} \tag{5.1}$$

$$q_2(t) = C_d A_v(t) \sqrt{\frac{2}{\rho} [P_2(t) - P_e]} \tag{5.2}$$

$$q_1(t) = q_2(t) = q(t) \tag{5.3}$$

Assuming exhaust pressure ($P_e$) is small in comparison to supply pressure, it can be regarded as zero. Load pressure will be difined as follows:

$$P_L(t) = P_1(t) - P_2(t) \tag{5.4}$$

Using load pressure in the equations for flow rates $q_1(t)$ and $q_2(t)$ and having $P_e = .0$ results in:

$$P_1(t) = \frac{P_s + P_L(t)}{2} \tag{5.5}$$

$$P_2(t) = \frac{P_s - P_L(t)}{2} \tag{5.6}$$

$$q(t) = C_d A_v(t) \sqrt{\frac{P_s - P_L(t)}{\rho}} \tag{5.7}$$

It is noted that flow rate varies with load pressure $P_L(t)$ and valve opening $A_v(t)$. For small perturbations the following equations can be used:

$$q(t) = \frac{\partial q}{\partial A_v} A_v(t) + \frac{\partial q}{\partial P_L} P_L(t) \tag{5.8}$$

$$\frac{\partial q}{\partial A_v} = C_d \sqrt{\frac{P_s - P_L(t)}{\rho}} \tag{5.9}$$

$$\frac{\partial q}{\partial P_L} = - \frac{C_d A_v(t)}{2\sqrt{\rho[P_s - P_L(t)]}} \tag{5.10}$$

The equation of motion for the linear hydraulic actuator can be expressed as:

$$P_L(t)A_p = m_e \ddot{x}(t) + F_L(x) \tag{5.11}$$

For the rotary hydraulic actuator, assuming no gearbox is used, the equation of motion is:

$$P_L(t)A_p r_p = I\ddot{\delta}(t) + M_L(\delta) \tag{5.12}$$

where:

$$r_p = \frac{r_{max} + r_{min}}{2} \tag{5.13}$$

The response time of the valve is short enough in comparison to that of the actuator that it can be treated as a pure gain.

$$\text{linear} \quad A_v(t) = K_v[x_c(t) - x(t)] \tag{5.14}$$

$$\text{rotary} \quad A_v(t) = K_v[\delta_c(t) - \delta(t)] \tag{5.15}$$

In the linear actuator flow rate is equated to the piston velocity (assuming no leakage) by the following equation:

$$\dot{x}(t) = \frac{q(t)}{A_p} \tag{5.16}$$

Conversion of flow rate to displacement is more complex for the rotary actuator than for the linear; referring to Fig. 5.5, the rotational velocity is found from the flow rate by:

$$\dot{\delta}(t) = \frac{2(r_{max} - r_{min})}{A_p(r_{max}^2 - r_{min}^2)} q(t) \tag{5.17}$$

A block diagram showing the interaction of the above variables for a linear hydraulic actuator is shown in Fig. 5.6. A Fortran computer program to compute the time history of a linear hydraulic actuator is found in Appendix A.

## 5.3 DESIGN EXAMPLES

The control surface model described in Section 2.1 has been used with the electro-hydraulic actuator in the same manner as the two other actuator types in Sections 3.3 and 4.3. Aircraft C is described in Section 2.4, and the time responses for the aileron and elevator found in this section are used in the closed loop analysis in Section 6.4.

### 5.3.1 CONTROL SURFACE MODEL

The hydraulic actuator used for the control surface model is a commercially available linear actuator shown in Fig. 7.2. A linear actuator is chosen because it is more commonly used on aircraft control systems. An effective piston area of 1.46 square inches is used to provide sufficient force for a 500 psi supply pressure for the control surface model described in Section 2.1. To find the change in response due to an increase in supply pressure, a 1000 psi supply pressure was also used. The specific gravity for the hydraulic fluid is 0.867, being based on a commercially available aircraft hydraulic fluid.

The three loading conditions used in evaluating the control surface model are described in Section 2.1.2. The inertia loading is shown in Fig. 5.7 and shows the increase in amplitude due to an increased supply pressure. Closed loop response for the cruise loading in Fig. 5.8 and for the maximum load in Fig. 5.9 show how

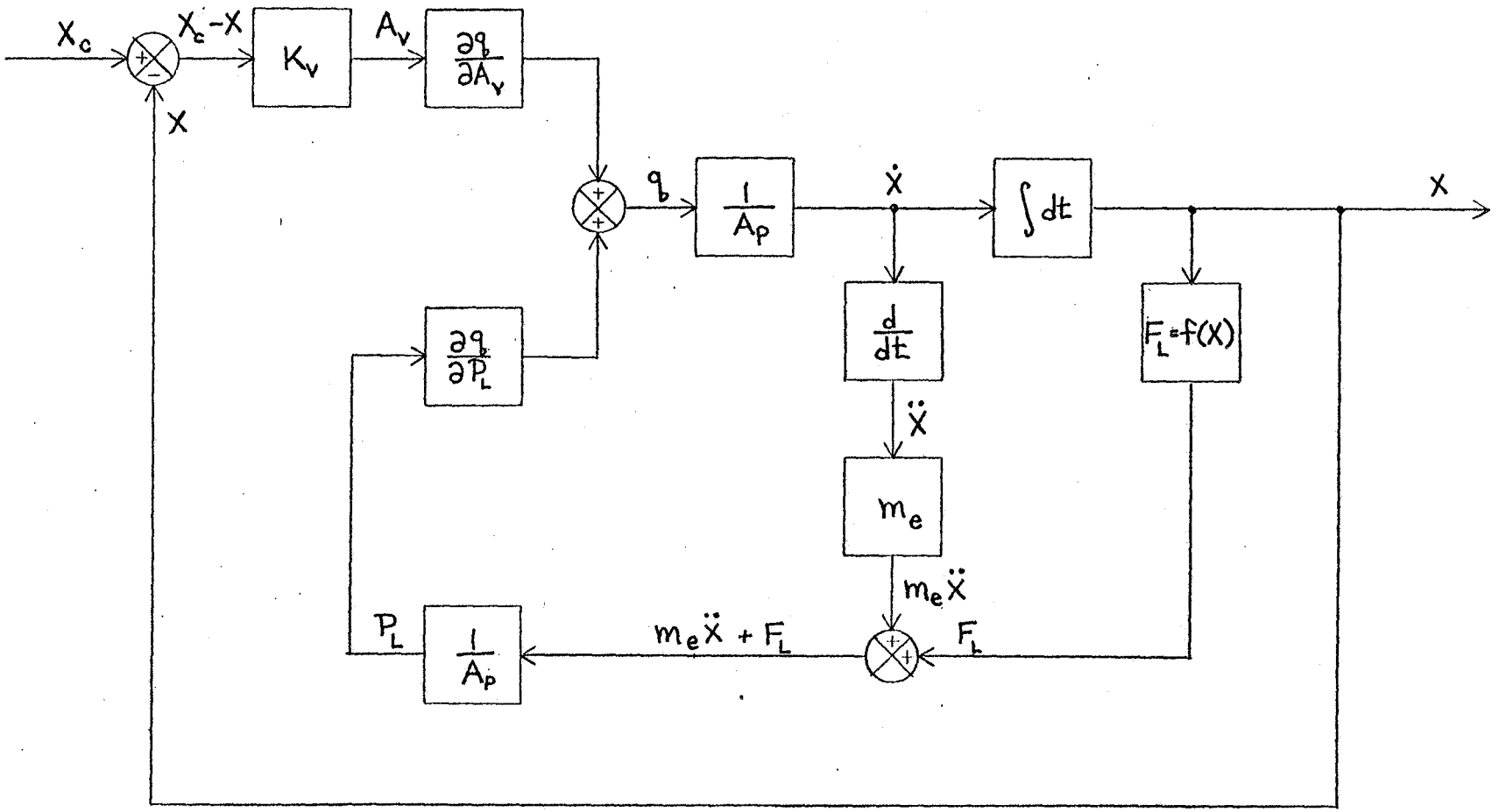


| | | | | |
|---|---|---|---|---|
| CALC | | | REVISED | DATE |
| CHECK | | | | |
| APPD | | | | |
| APPD | | | | |
| | | | | |

Figure 5.6: Hydraulic Actuator Control System Block Diagram

UNIVERSITY OF KANSAS

PAGE

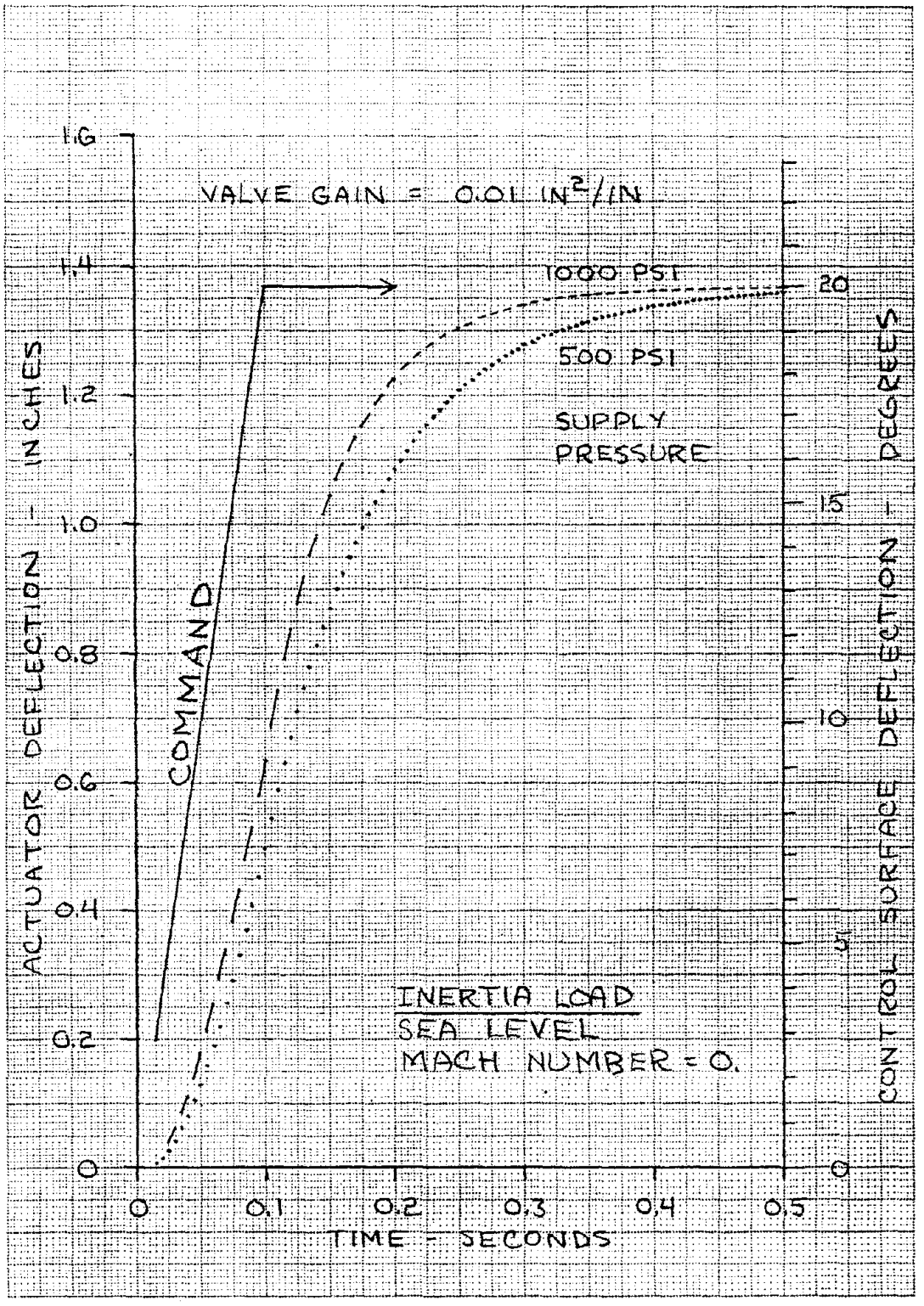


| | | | | |
|---|---|---|---|---|
| CALC | | | REVISED | DATE |
| CHECK | | | | |
| APPD | | | | |
| APPD | | | | |
| | | | | |

Figure 5.7: Hydraulic Actuator-Inertia Load, Closed Loop

UNIVERSITY OF KANSAS

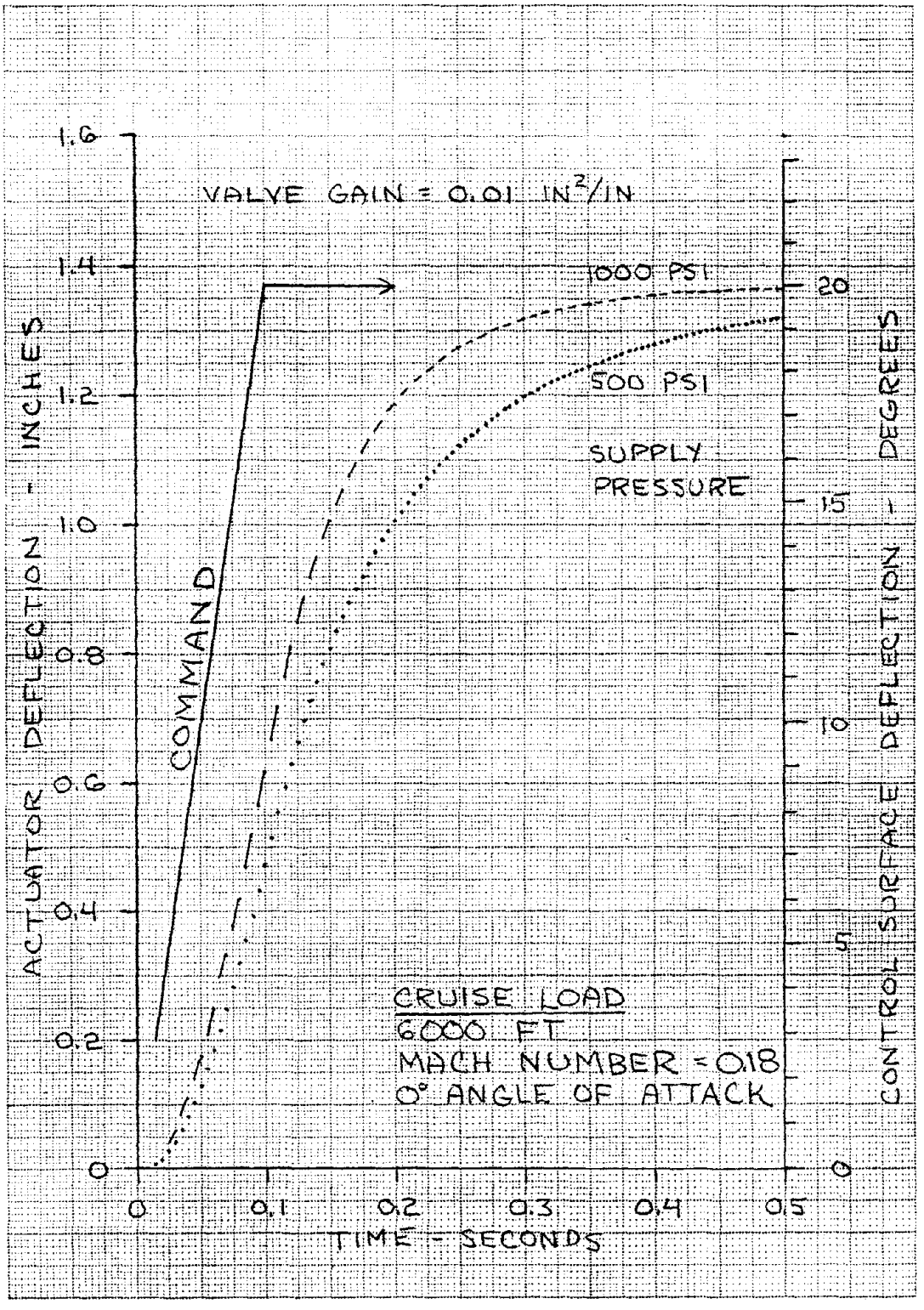


| | | | | | |
|---|---|---|---|---|---|
| CALC | | | REVISED | DATE | Figure 5.8: Hydraulic Actuator- Cruise Load, Closed Loop |
| CHECK | | | | | |
| APPD | | | | | |
| APPD | | | | | |
| | | | | | UNIVERSITY OF KANSAS |

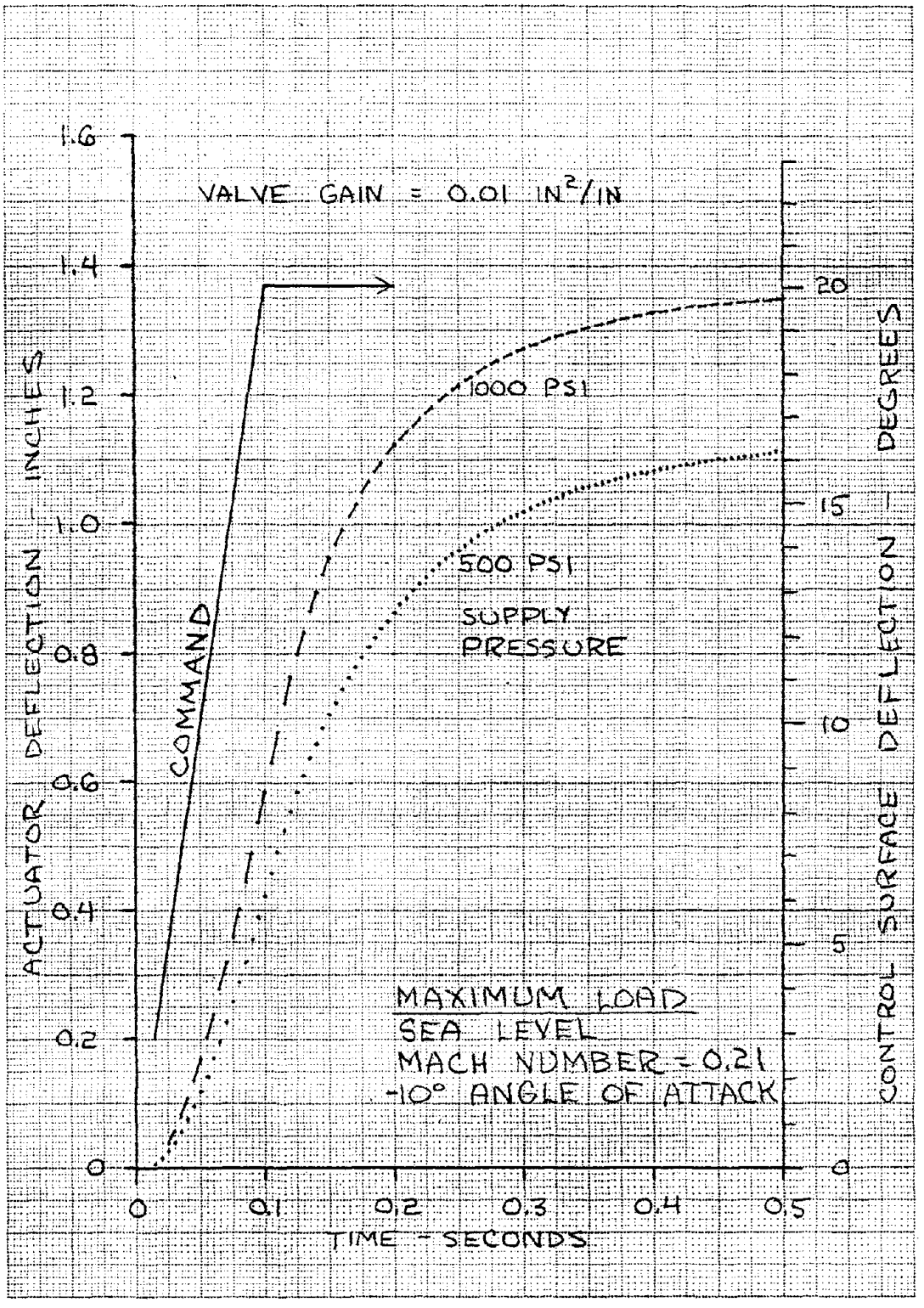


| | | | | | |
|---|---|---|---|---|---|
| CALC | | | REVISED | DATE | Figure 5.9: Hydraulic Actuator- Maximum Load, Closed Loop |
| CHECK | | | | | |
| APPD | | | | | |
| APPD | | | | | |
| | | | | | UNIVERSITY OF KANSAS |

a change in loading affects the response characteristics. Time response for a reduced control surface deflection of 10° is shown in Fig. 5.10, and the change in response for a higher valve gain is shown in Fig. 5.11. It should be noted that doubling the valve gain essentially doubles the required flow rate, requiring an increased pumping capacity. Open loop response of the hydraulic actuator at maximum load is shown in Fig. 5.12. A comparison can be made between the time histories in this section and the same responses in Section 3.3 for electro-mechanical and 4.3 for pneumatic.

5.3.2 AIRCRAFT MODEL

The twin engine turboprop aircraft (Aircraft C) has been used for the hydraulic actuator to find aircraft response characteristics. A moment arm of four inches for the elevator and two inches for the aileron has been used. The same size actuator as for the control surface model of Section 5.3.1 has been used with a supply pressure of 1500 psi. The hinge moments for cruise and approach configurations are found in Section 2.4. Linear approximations for the time histories are the same as for the pneumatic actuator and are described in Section 4.3.2. The time histories are shown for the elevator in Fig. 5.13 and for the aileron in Fig. 5.14. The time constants for the hydraulic actuators are summarized in the following table:

Table 5.1 - Aircraft C Actuator Time Constants

| Configuration | Control Surface | Time Constant |
|---|---|---|
| CRUISE | Aileron | 0.12 sec |
| | Elevator | 0.13 sec |
| APPROACH | Aileron | 0.12 sec |
| | Elevator | 0.13 sec |

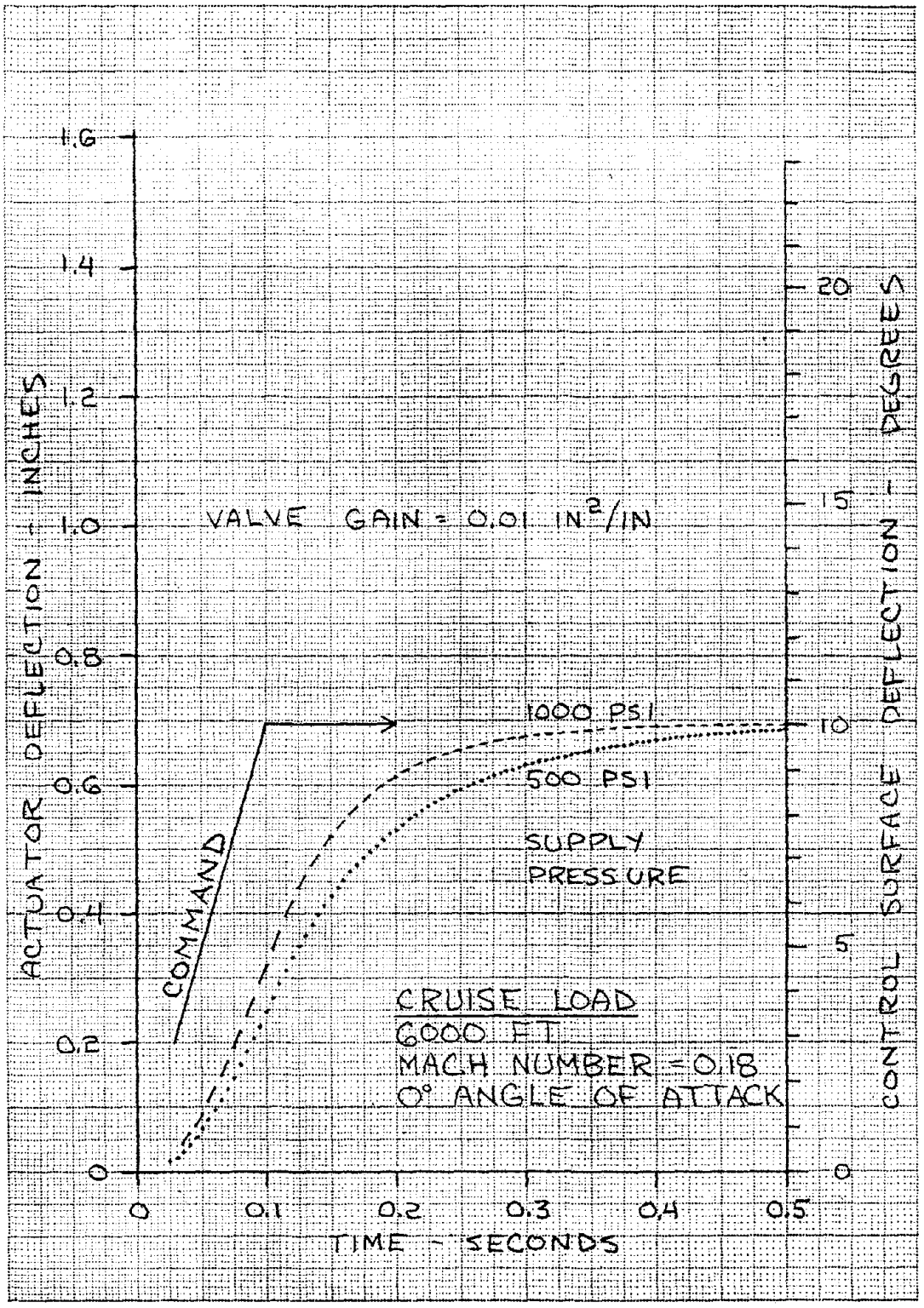


| | | | | |
|---|---|---|---|---|
| CALC | | | REVISED | DATE |
| CHECK | | | | |
| APPD | | | | |
| APPD | | | | |
| | | | | |

Figure 5.10: Hydraulic Actuator-Cruise Load at 10°, Closed Loop

UNIVERSITY OF KANSAS

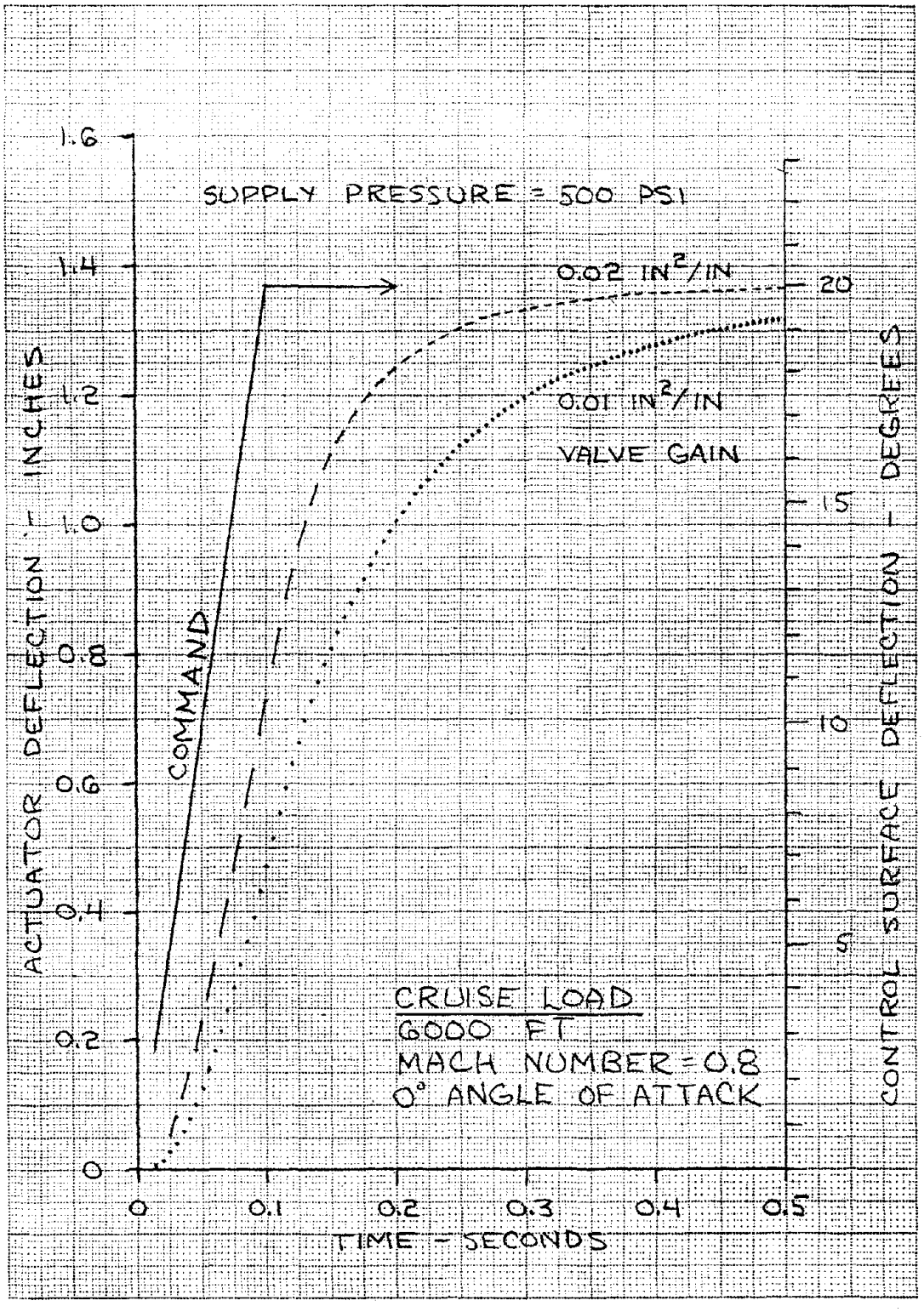


| | | | | | |
|---|---|---|---|---|---|
| CALC | | | REVISED | DATE | Figure 5.11: Hydraulic Actuator- Cruise Load, Variable Closed Loop Gain |
| CHECK | | | | | |
| APPD | | | | | |
| APPD | | | | | |
| | | | | | UNIVERSITY OF KANSAS |

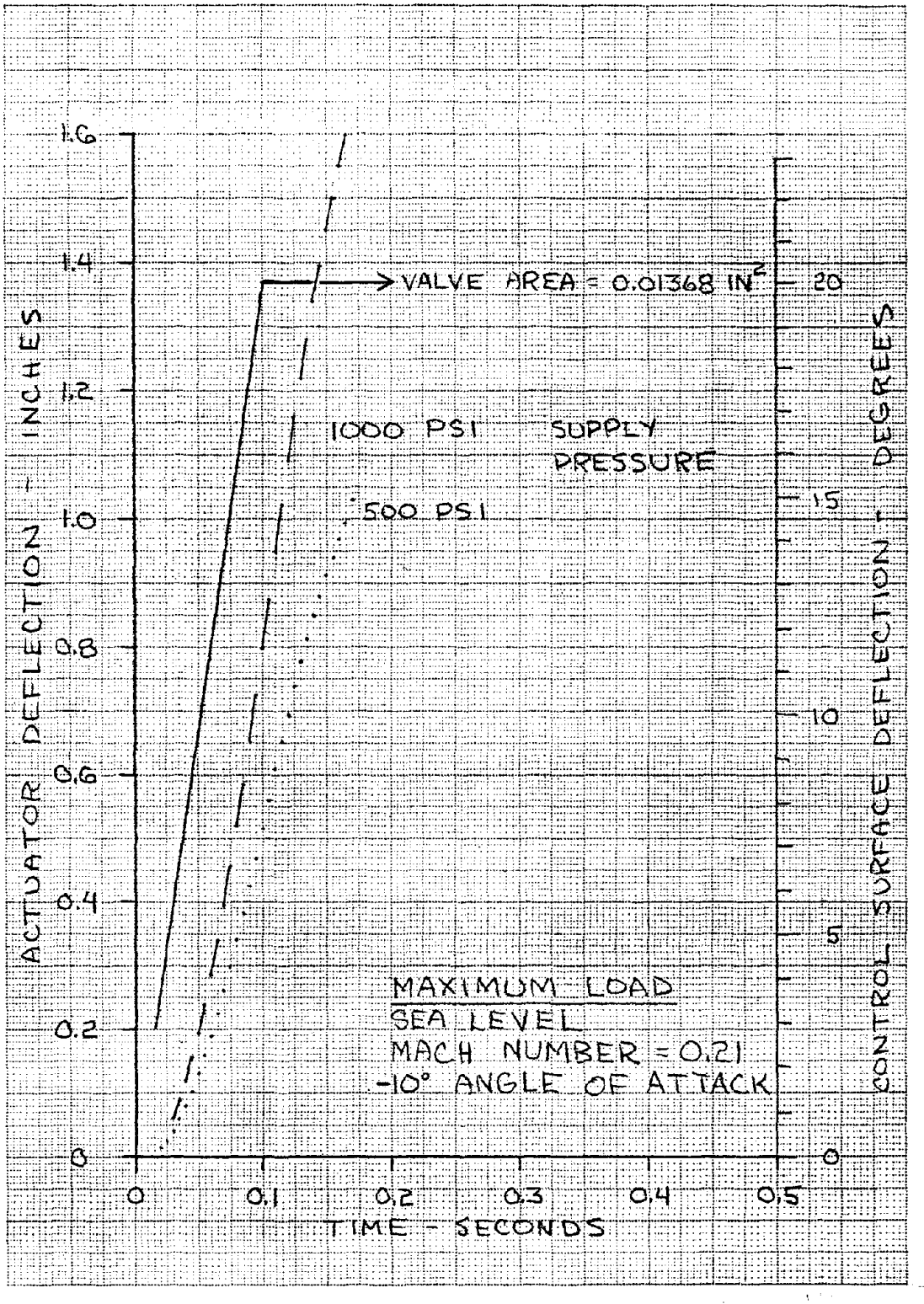


| CALC | | | REVISED | DATE |
|---|---|---|---|---|
| CHECK | | | | |
| APPD | | | | |
| APPD | | | | |
| | | | | |

Figure 5.12: Hydraulic Actuator - Maximum Load, Open Loop

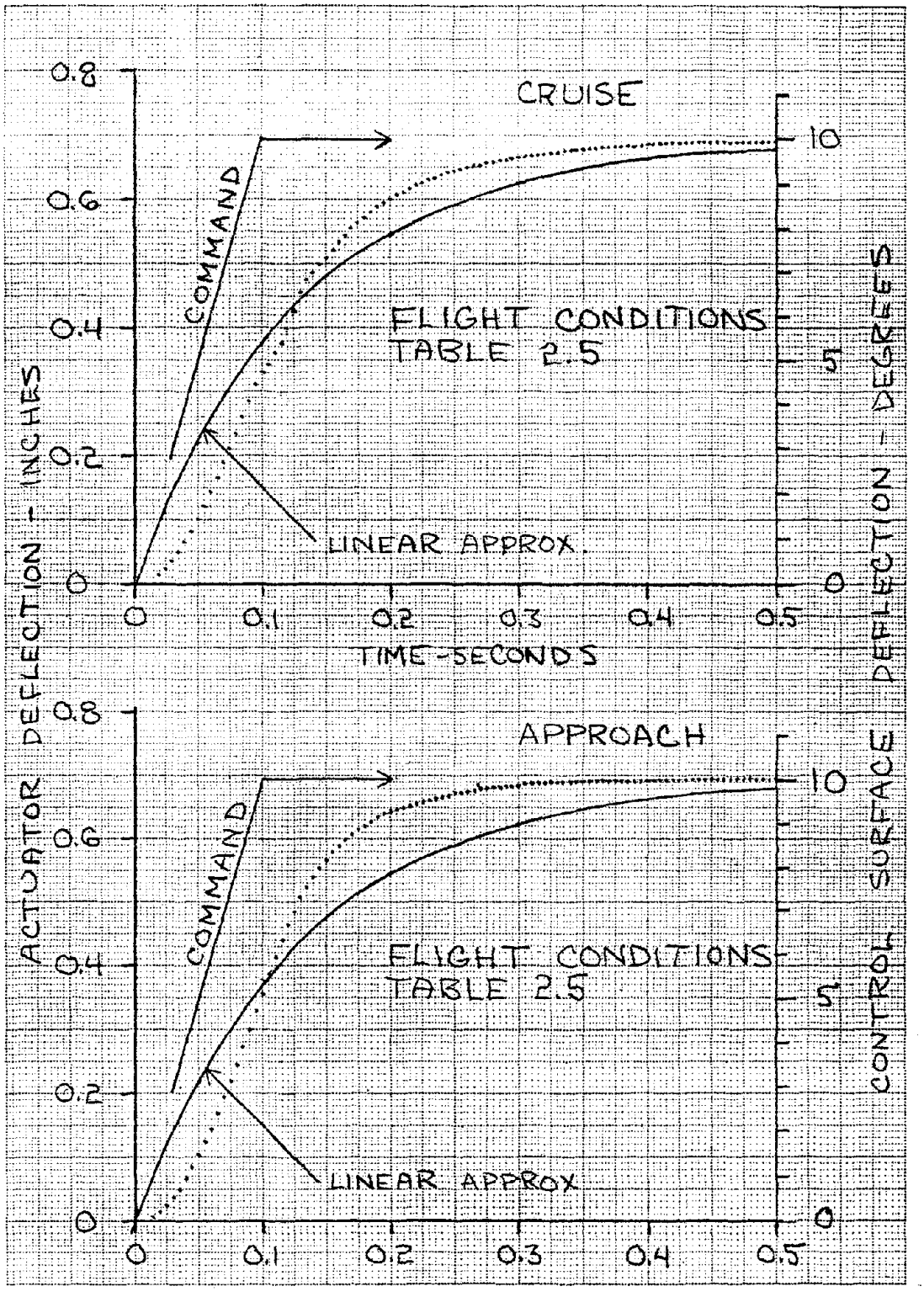


| | | | | | |
|---|---|---|---|---|---|
| CALC | | | REVISED | DATE | Figure 5.13: Airplane C, Elevator Time Histories |
| CHECK | | | MSR | | |
| APPD | | | | | |
| APPD | | | | | |
| | | | | | UNIVERSITY OF KANSAS |

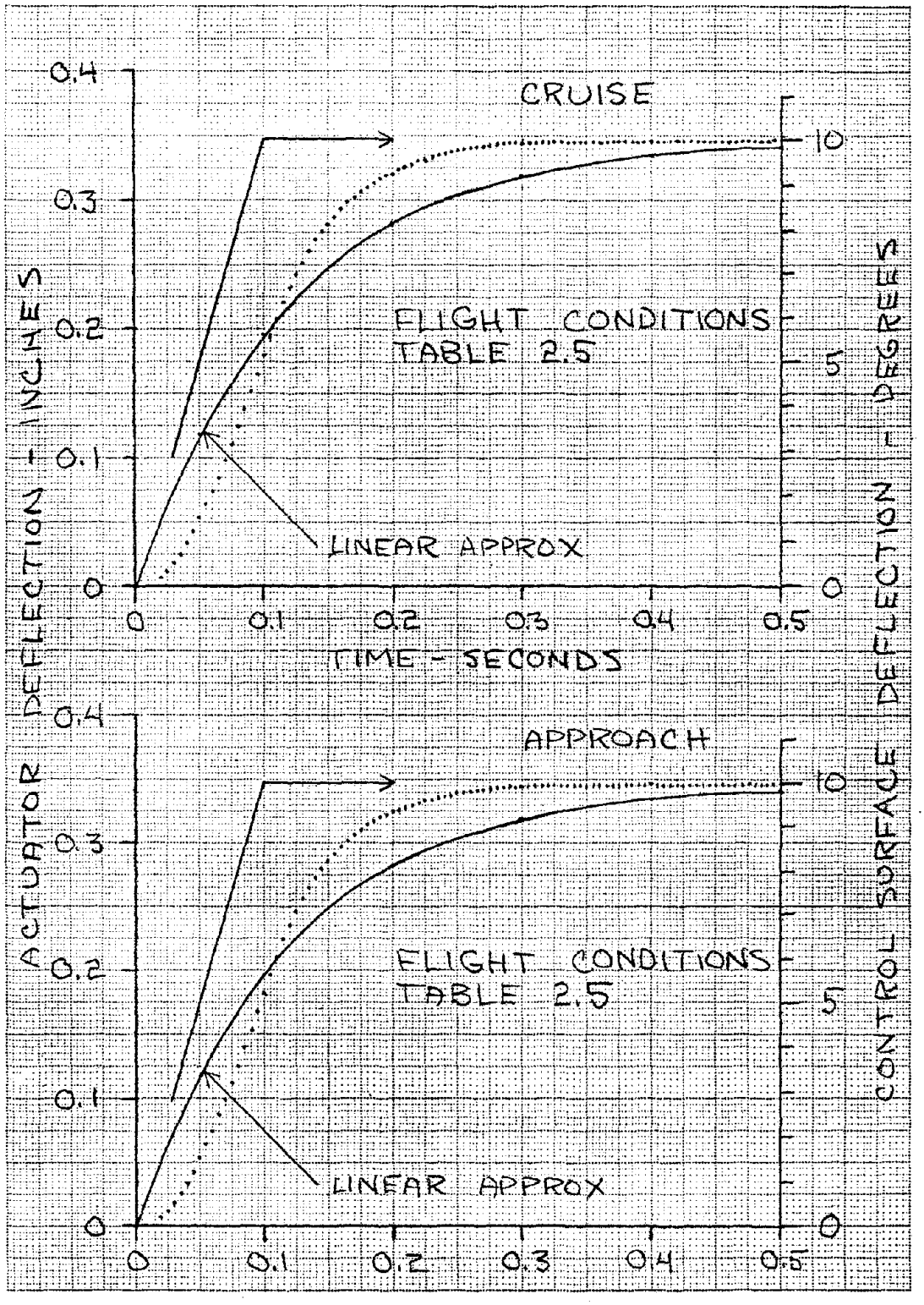


| | | | | |
|---|---|---|---|---|
| CALC | | | REVISED | DATE |
| CHECK | | | | |
| APPD | | | | |
| APPD | | | | |
| | | | | |

Figure 5.14: Airplane C, Aileron Time Histories

UNIVERSITY OF KANSAS

References for Chapter 5

1. McCloy, D. and Martin, H. R., "The Control of Fluid Power," John Wiley & Sons, 1973.

2. Stringer, John, "Hydraulic Systems Analysis," John Wiley & Sons, 1976.

3. Walters, R, "Hydraulic and Electro-Hydraulic Servo Systems," Iliffe Books Ltd., 1967.

4. Roskam, Jan, "Flight Dynamics of Rigid and Elastic Airplanes," Volumes 1 and 2, published by Roskam Aviation and Engineering Corporation, 519 Boulder, Lawrence, Kansas, 1972.

# CHAPTER 6

## CLOSED LOOP CONTROL SYSTEM ANALYSIS

In this chapter some closed loop control system analyses will be done on three different airplanes. These airplanes have been described to some extent in Chapter 2, and more information will be presented in this chapter. The flight control system modes that will be examined are pitch attitude hold and bank angle hold. Simplified airplane transfer functions will be used because the reason for this analysis is not the design of an automatic flight control system but to have a look at the performance of the different types of actuators.

Since all actuator types are compared with each other on the standard control surface described in Section 2.1, it is not necessary to examine each type of actuator for each airplane. The following distribution has been made: the electro-pneumatic actuator will be used on airplane A, the electro-mechanical actuator on airplane B and the electro-hydraulic actuator on airplane C. The actuators have been sized for these airplanes in Sections 4.3.2 , 3.3.2, and 5.3.2, respectively. Approximate actuator-plus-control surface transfer functions, which have been derived also in these sections, will be used here.

Two flight conditions will be examined for each control system mode: cruise and approach. For each airplane, these flight conditions have been defined in Chapter 2.

All cases will be studied with pilot-in-the-loop operation. To do this, a pilot transfer function has been adopted from Ref. 1.

Computation of closed loop stability will be done by a computer program described in Reference 2. Root loci can be drawn based on

the output of this computer program and will be presented in the following sections.

## 6.1 FLIGHT CONTROL SYSTEM MODES, PILOT MODEL AND ACTUATOR TRANSFER FUNCTIONS

The following flight control system modes will be examined: pitch attitude hold and bank angle hold. To simplify the calculations, the short period approximation and the roll approximation are used. These approximations are, respectively (Ref. 6.1):

$$\frac{\theta}{\delta_E} = \frac{\left(U_1 M_{\delta_E} + Z_{\delta_E} M_{\dot{\alpha}}\right) s + \left(M_\alpha Z_{\delta_E} - Z_\alpha M_{\delta_E}\right)}{sU_1 \left\{ s^2 - \left(M_q + \frac{Z_\alpha}{U_1} + M_{\dot{\alpha}}\right) s + \left(\frac{Z_\alpha M_q}{U_1} - M_\alpha\right)\right\}} \tag{6.1}$$

and:

$$\frac{\phi}{\delta_A} = \frac{L_{\delta_A}}{s\,(s - L_p)} \tag{6.2}$$

The meaning of these symbols is shown in further detail in Table 6.1.

Table 6.1 - Dimensional Stability Derivatives

$$M_{\delta_E} = \frac{\bar{q}_1 S \bar{c} C_{m_{\delta_E}}}{I_{yy}} \quad (\sec^{-2}) \qquad M_\alpha = \frac{\bar{q}_1 S \bar{c} C_{m_\alpha}}{I_{yy}} \quad (\sec^{-2})$$

$$M_{\dot{\alpha}} = \frac{\bar{q}_1 S \bar{c}^2 C_{m_{\dot{\alpha}}}}{2 I_{yy} U_1} \quad (\sec^{-1}) \qquad Z_\alpha = -\frac{\bar{q}_1 S \left(C_{L_\alpha} + C_{D_1}\right)}{m} \quad (\text{ft sec}^{-2})$$

$$M_q = \frac{\bar{q}_1 S \bar{c}^2 C_{m_q}}{2 I_{yy} U_1} \quad (\sec^{-1}) \qquad Z_{\delta_E} = -\frac{\bar{q}_1 S\, C_{L_{\delta_E}}}{m} \quad (\text{ft sec}^{-2})$$

$$L_{\delta_A} = \frac{\bar{q}_1 S b C_{\ell_{\delta_A}}}{I_{xx}} \quad (\sec^{-2}) \qquad L_p = \frac{\bar{q}_1 S b^2 C_{\ell_p}}{2 I_{xx} U_1} \quad (\sec^{-1})$$

Because all flight modes will be studied with the pilot in the loop, a pilot transfer function must be known; the following transfer function

is taken from Ref. 1:

$$H_p(s) = K_p \left[ \frac{1 - \frac{\tau}{2} s}{1 + \frac{\tau}{2} s} \right] (T_L s + 1) \qquad (6.3)$$

The term between brackets is the Padé approximation of $e^{-\tau s}$, in which $\tau$ is the pilot reaction time constant. $\tau$ can range from 0.12 sec to 0.2 sec for a normal, healthy pilot (Ref. 1) and will be taken as 0.16 sec here. $K_p$ is the pilot gain (variable) and $T_L$ the lead time constant. A pilot has the ability to generate lead (foreseeing what is going to happen); but the more lead he generates, the sooner he gets tired. $T_L$ will be taken as 0.1 sec here (pilots like to have a little bit of lead), but it must be kept in mind that $T_L$ is variable.

The hinge moment curves presented in Chapter 2 have been used in Chapters 3, 4 and 5 to calculate time responses of the different actuator-airplane combinations. The transfer functions associated with the first-order linear approximations of these time responses will be used here; they have the following form:

$$H(s) = \frac{1}{\tau_a s + 1} \qquad (6.4)$$

in which $\tau_a$ is the time constant of the actuator-plus-control surface closed loop system. Estimated time constants of actuator-airplane combinations can also be found in Chapters 3, 4 and 5.

## 6.2 FLIGHT CONTROL SYSTEM ANALYSIS, AIRPLANE A

Basic data on airplane A and on its cruise and approach flight condition have been presented in Section 2.2. Time constants for the electro-pneumatic actuator, which will be used in this airplane, can be found in Section 4.3.2. Data necessary for computation of the transfer functions (6.1) and (6.2) are presented in Tables 6.2 (cruise)

and 6.4 (approach). The actual transfer functions are presented in Tables 6.3 and 6.5 for cruise and approach, respectively. Stability derivative data have been obtained from References 3, 4, 5 and 6.

Table 6.2 - Dynamic Characteristics of Airplane A (Cruise)

$M_{\delta_E} = -36.73 \text{ sec}^{-2}$ $\quad M_{\alpha} = -29.13 \text{ sec}^{-2}$

$M_{\dot{\alpha}} = -1.309 \text{ sec}^{-1}$ $\quad Z_{\alpha} = -480.4 \text{ ft sec}^{-2}$

$M_{q} = -5.694 \text{ sec}^{-1}$ $\quad Z_{\delta_E} = -39.37 \text{ ft sec}^{-2}$

$L_{\delta_A} = 79.02 \text{ sec}^{-2}$ $\quad L_{p} = -13.95 \text{ sec}^{-1}$

Table 6.3 - Transfer Functions for Airplane A (Cruise)

$$\frac{\theta}{\delta_E} = \frac{-1.800\ (\frac{s}{2.05} + 1)}{s(\frac{s^2}{(6,45)^2} + \frac{2(0.71)}{6.45} s + 1)}$$

poles: $s_1 = 0$ $\quad \omega_{n_{S.P.}} = 6.45$ rad/sec

$s_{2,3} = -4.60 \pm 4.52j$ $\quad \zeta_{S.P.} = 0.71$

zeroes: $s_1 = -2.05$

$$\frac{\phi}{\delta_A} = \frac{5.665}{s(\frac{s}{13.95} + 1)}$$

poles: $s_1 = 0$

$s_2 = -13.95$

Table 6.4 - Dynamic Characteristics of Airplane A (Approach)

$M_{\delta_E} = -9.27\ \text{sec}^{-2}$ $\quad M_{\alpha} = -8.02\ \text{sec}^{-2}$

$M_{\dot{\alpha}} = -0.97\ \text{sec}^{-2}$ $\quad Z_{\alpha} = -135.2\ \text{ft sec}^{-2}$

$M_{q} = -3.22\ \text{sec}^{-1}$ $\quad Z_{\delta_E} = -9.14\ \text{ft sec}^{-2}$

$L_{\delta_A} = -21.75\ \text{sec}^{-2}$ $\quad L_{p} = -8.057\ \text{sec}^{-1}$

Table 6.5 - Transfer Functions for Airplane A (Approach)

$$\frac{\theta}{\delta_E} = \frac{-0.678\ (\frac{s}{1.20} + 1)}{s\ (\frac{s^2}{(4.03)^2} + \frac{2(0.68)}{4.03}\ s + 1)}$$

poles: $s_1 = 0$ $\quad \omega_{n_{S.P.}} = 4.03$ rad/sec

$s_{2,3} = -2.73 \pm 2.97j$ $\quad \zeta_{S.P.} = 0.68$

zeroes: $s_1 = -1.20$

$$\frac{\phi}{\delta_A} = \frac{2.699}{s(\frac{s}{8.057} + 1)}$$

poles: $s_1 = 0$

$s_2 = -8.057$

Root loci for airplane A are shown in Figures 6.1-6.4. $K_p$ is the variable pilot gain. In cruise, the actuator-plus-control surface pole lies at about s = -2.5, while in approach it lies approximately at s = -4 [see Section 4.3.2 for $\tau_a$-values in (6.4)]. This is because the aerodynamic loads are higher in cruise than in approach and the

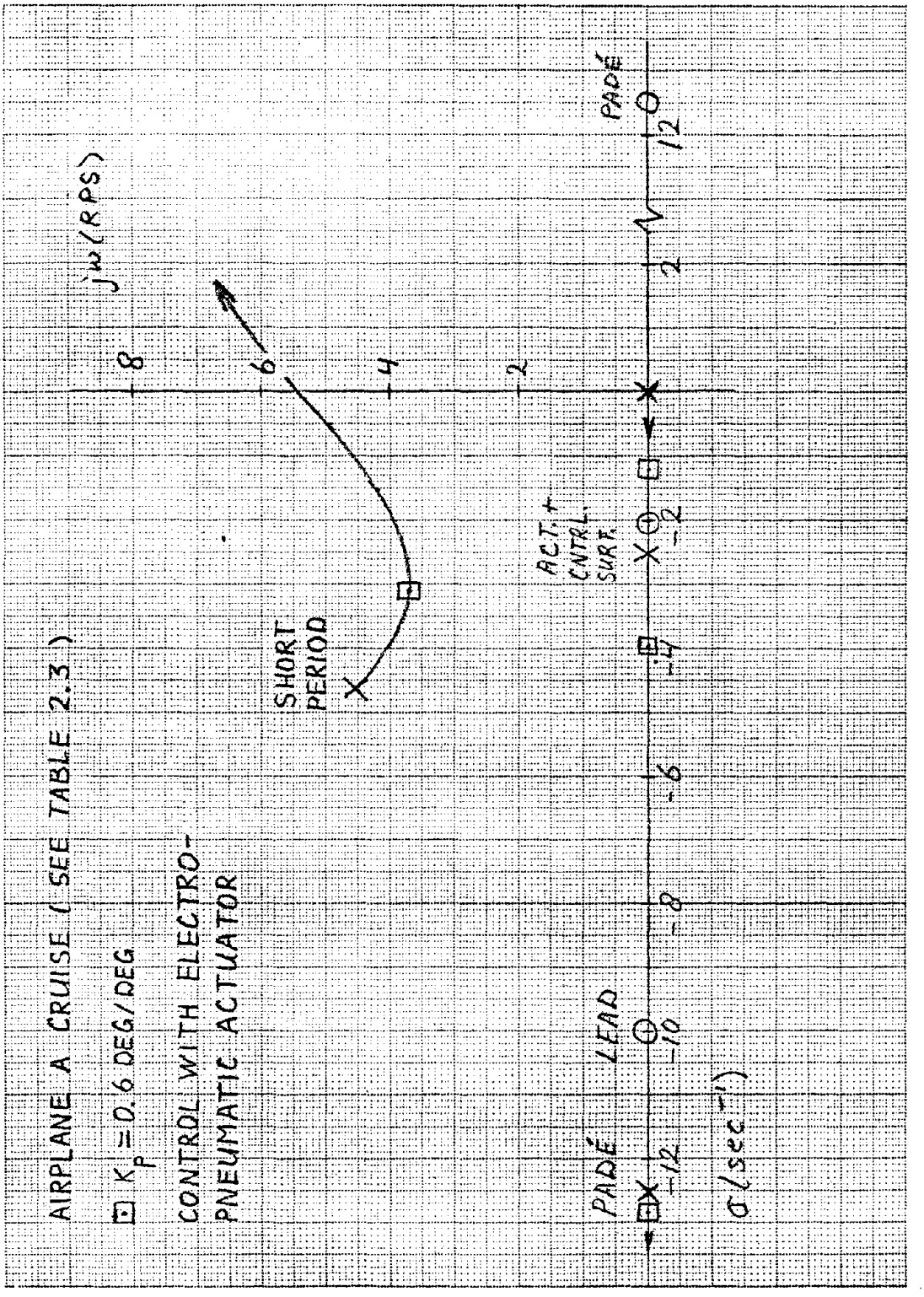


| | | | | |
|---|---|---|---|---|
| CALC | HE | 78/2/26 | REVISED | DATE |
| CHECK | | | | |
| APPD | | | | |
| APPD | | | | |
| | | | | |

Figure 6.1: Theta Hold Airplane A, Cruise
Electro-Pneumatic Actuator

UNIVERSITY OF KANSAS

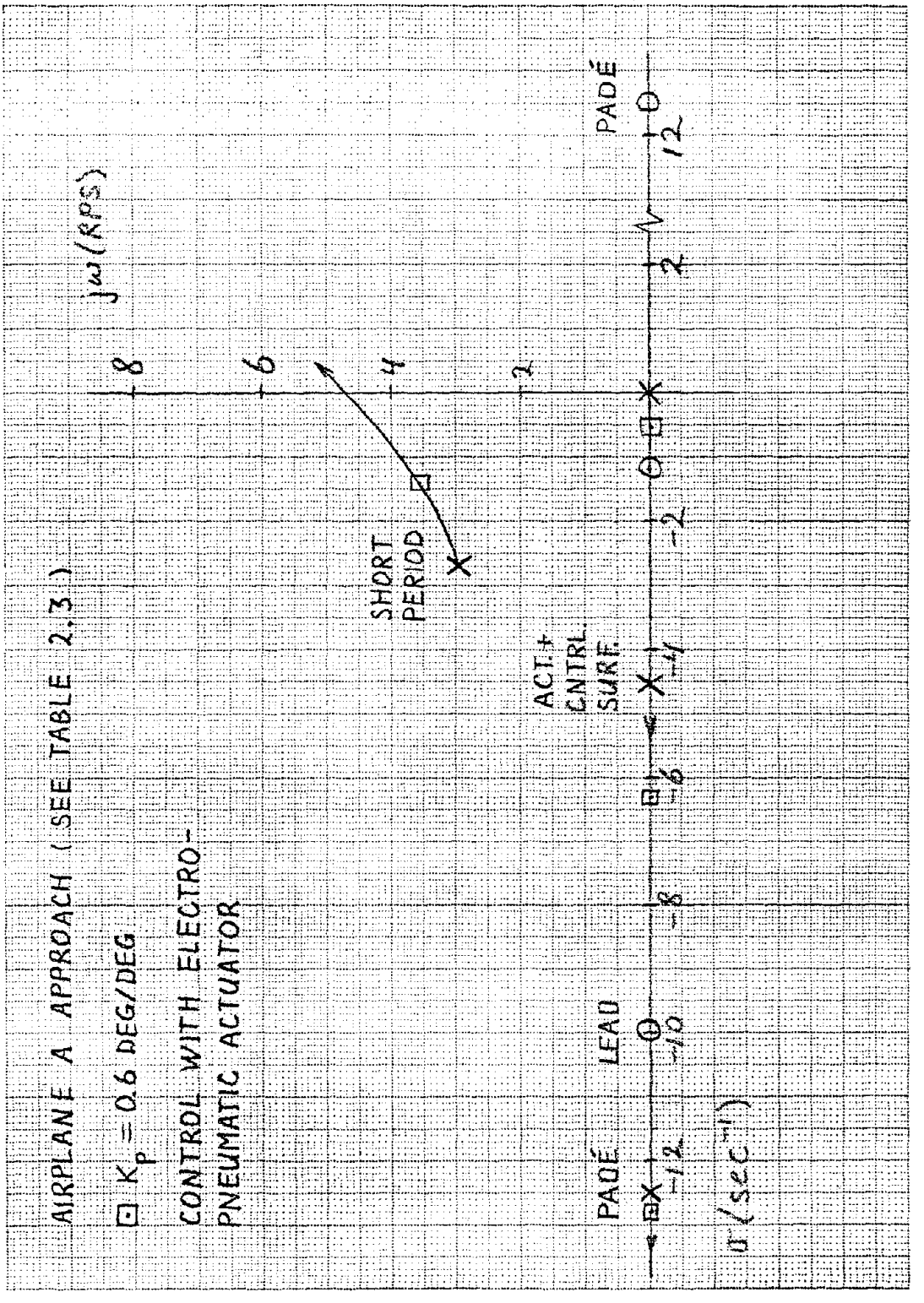


| | | | | |
|---|---|---|---|---|
| CALC | HE | 78/2/27 | REVISED | DATE |
| CHECK | | | | |
| APPD | | | | |
| APPD | | | | |
| | | | | |

Figure 6.2: Theta Hold Airplane A, Approach
Electro-Pneumatic Actuator

UNIVERSITY OF KANSAS

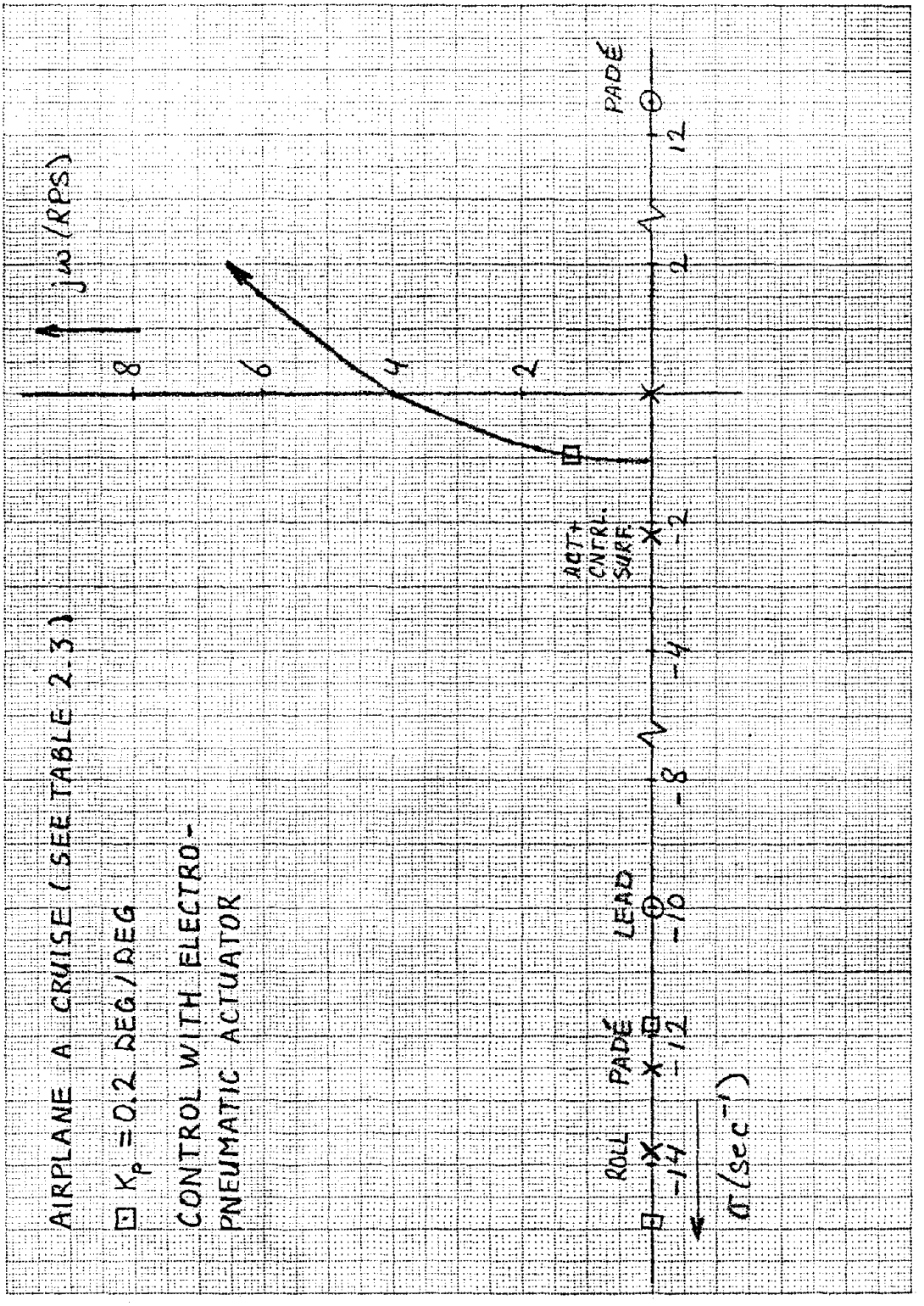


| | | | | | | |
|---|---|---|---|---|---|---|
| CALC | HE | | REVISED | DATE | Figure 6.3: Phi Hold Airplane A, Cruise Electro-Pneumatic Actuator | |
| CHECK | | | | | | |
| APPD | | | | | | |
| APPD | | | | | UNIVERSITY OF KANSAS | PAGE 111 |

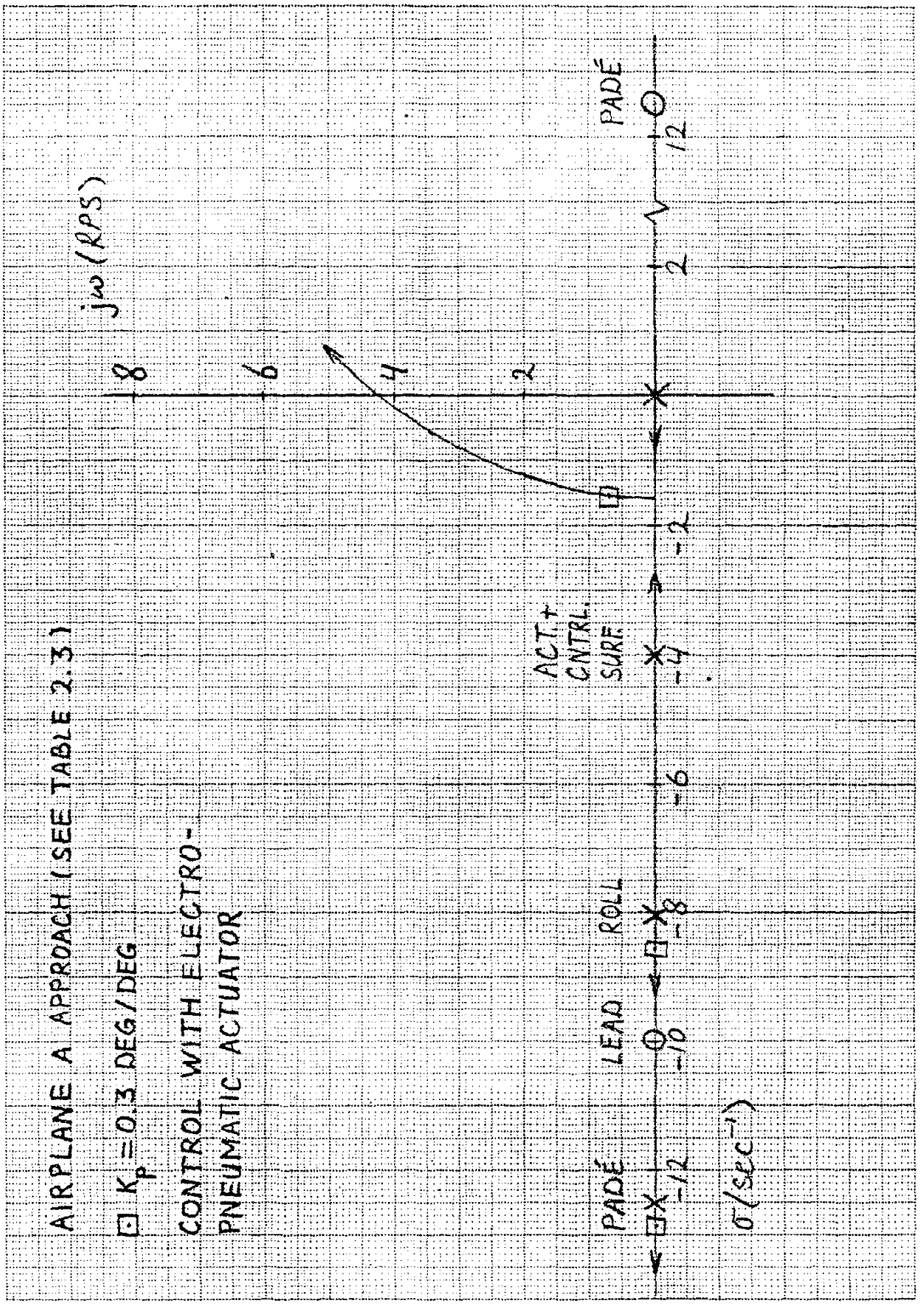


| | | | | |
|---|---|---|---|---|
| CALC | HE | 78/3/1 | REVISED | DATE |
| CHECK | | | | |
| APPD | | | | |
| APPD | | | | |
| | | | | |

Figure 6.4: Phi Hold Airplane A, Approach Electro-Pneumatic Actuator

UNIVERSITY OF KANSAS

pneumatic actuator is very sensitive to this. One might wonder why the actuator poles are situated in almost the same spot for elevator and aileron, because the hinge moments for these control surfaces differ very much in both cruise and approach. However, the actuator moment arm for the elevator is twice as big as it is for the aileron, so that the aerodynamic loads as seen by the actuator are not very much different for elevator and aileron.

The pitch attitude hold performs reasonably well for both cruise and approach (Fig. 6.1 and 6.2). The pole in the origin that indicates neutral stability for pitch angles, moves to the left towards a zero. For $K_p = 0.6$ the closed loop system is well damped and the response fast enough. The system is unstable for $K_p > 2.8$ in cruise and for $K_p > 3.6$ in approach, so as long as the pilot doesn't overreact to the responses of his airplane everything goes well. It is not necessary for him to generate more lead.

Performance of the bank angle hold is not so good as that of the pitch attitude hold, but it is still acceptable (Fig. 6.3 and 6.4). In this case there is no zero between the pole in the origin (neutral stability for bank angles) and the actuator pole, so they come together for increasing $K_p$ and form a complex conjugate pair (which means oscillatory behavior). For $K_p = 0.2$ in cruise and $K_p = 0.3$ in approach, closed loop response is reasonable; but the low $K_p$ values indicate that the pilot has to be very careful with his stick to avoid pilot-induced oscillations. The system is unstable for $K_p > 1.4$ in cruise and for $K_p > 2.5$ in approach.

What the pilot could do here is to generate more lead so that the lead zero comes to the right of the actuator pole. In cruise

$T_L$ would have to have a value of 0.5 sec; it is not very probable that the pilot will do this because he wants to be relaxed during cruise and this is not compatible with such a high $T_L$. In approach, however, $T_L$ should be about 0.3 sec; and this is very well possible because it would only be needed for a short time, and the pilot is already much more alert than in cruise. This $T_L$ value would not harm the pitch attitude hold, either. Another possibility is to build in a lead-lag circuit in the feedback loop to improve actuator behavior.

Though these are only simple examples, they show that the electro-pneumatic actuator will do its work in this environment, though the airplane closed loop response would be better with a faster actuator, especially for the bank angle hold mode.

## 6.3 FLIGHT CONTROL SYSTEM ANALYSIS, AIRPLANE B

This is the light twin, and data on its dimensions and flight conditions have been presented in Section 2.3. Time constants for the electro-mechanical actuator, which will be used in this airplane, can be found in Section 3.3.2. The necessary data for computation of the airplane transfer functions are presented in Tables 6.6 (cruise) and 6.8 (approach). The transfer functions themselves are presented in Tables 6.7 (cruise) and 6.9 (approach). Stability derivative data have been obtained from References 5, 7 and 8.

Table 6.6 - Dynamic Characteristics of Airplane B (Cruise)

$M_{\delta_E} = -87.72 \text{ sec}^{-2}$ $\quad M_{\alpha} = -22.71 \text{ sec}^{-2}$

$M_{\dot{\alpha}} = -1.90 \text{ sec}^{-1}$ $\quad Z_{\alpha} = -472.7 \text{ ft sec}^{-2}$

$M_{q} = -3.79 \text{ sec}^{-1}$ $\quad Z_{\delta_E} = -116.5 \text{ ft sec}^{-2}$

$L_{\delta_A} = 18.05 \text{ sec}^{-2}$ $\quad L_{p} = -6.67 \text{ sec}^{-1}$

Table 6.7 - Airplane B Transfer Functions (Cruise)

$$\frac{\theta}{\delta_E} = \frac{-5.267\ (\frac{s}{1.82} + 1)}{s(\frac{s^2}{(5.48)^2} + \frac{2(0.69)}{5.48}\, s + 1)}$$

poles: $s_1 = 0$ $\quad \omega_{n_{S.P.}} = 5.48$ rad/sec

$s_{2,3} = -3.81 \pm 3.94j$ $\quad \zeta_{S.P.} = 0.69$

zeroes: $s_1 = -1.82$

$$\frac{\phi}{\delta_A} = s(\frac{s}{6.67} + 1)$$

poles: $s_1 = 0$

$s_2 = -6.67$

Compared to the $\frac{\theta}{\delta_E}$ transfer function of airplane A in cruise, airplane B has a much higher gain. This is caused by the fact that airplane B has a stabilator instead of a stabilizer-elevator combination as is the case with airplane A.

Table 6.8 - Dynamic Characteristics of Airplane B (Approach)

$M_{\delta_E} = -21.41 \text{ sec}^{-2}$ $\quad M_{\alpha} = -6.48 \text{ sec}^{-2}$

$M_{\dot{\alpha}} = -1.21 \text{ sec}^{-1}$ $\quad Z_{\alpha} = -136.3 \text{ ft sec}^{-2}$

$M_{q} = -2.21 \text{ sec}^{-1}$ $\quad Z_{\delta_E} = -28.31 \text{ ft sec}^{-2}$

$L_{\delta_A} = 4.604 \text{ sec}^{-2}$ $\quad L_{p} = -3.666 \text{ sec}^{-1}$

Table 6.9 - Airplane B Transfer Functions (Approach)

$$\frac{\theta}{\delta_E} = \frac{-2.573\ (\frac{s}{1.10} + 1)}{s\ (\frac{s^2}{(3.00)^2} + \frac{2(0.76)}{3.00}\ s + 1\ )}$$

poles: $s_1 = 0$ $\quad \omega_{n_{S.P.}} = 3.0$ rad/sec

$s_{2,3} = -2.79 \pm 1.95j$ $\quad \zeta_{S.P.} = 0.76$

zeroes: $s_1 = -1.10$

$$\frac{\phi}{\delta_A} = \frac{1.256}{s\ (\frac{s}{3.666} + 1)}$$

poles: $s_1 = 0$

$s_2 = -3.666$

Root loci for airplane B are shown in Figures 6.5-6.8. $K_p$ is the variable pilot gain. The actuator-plus-control surface pole is situated

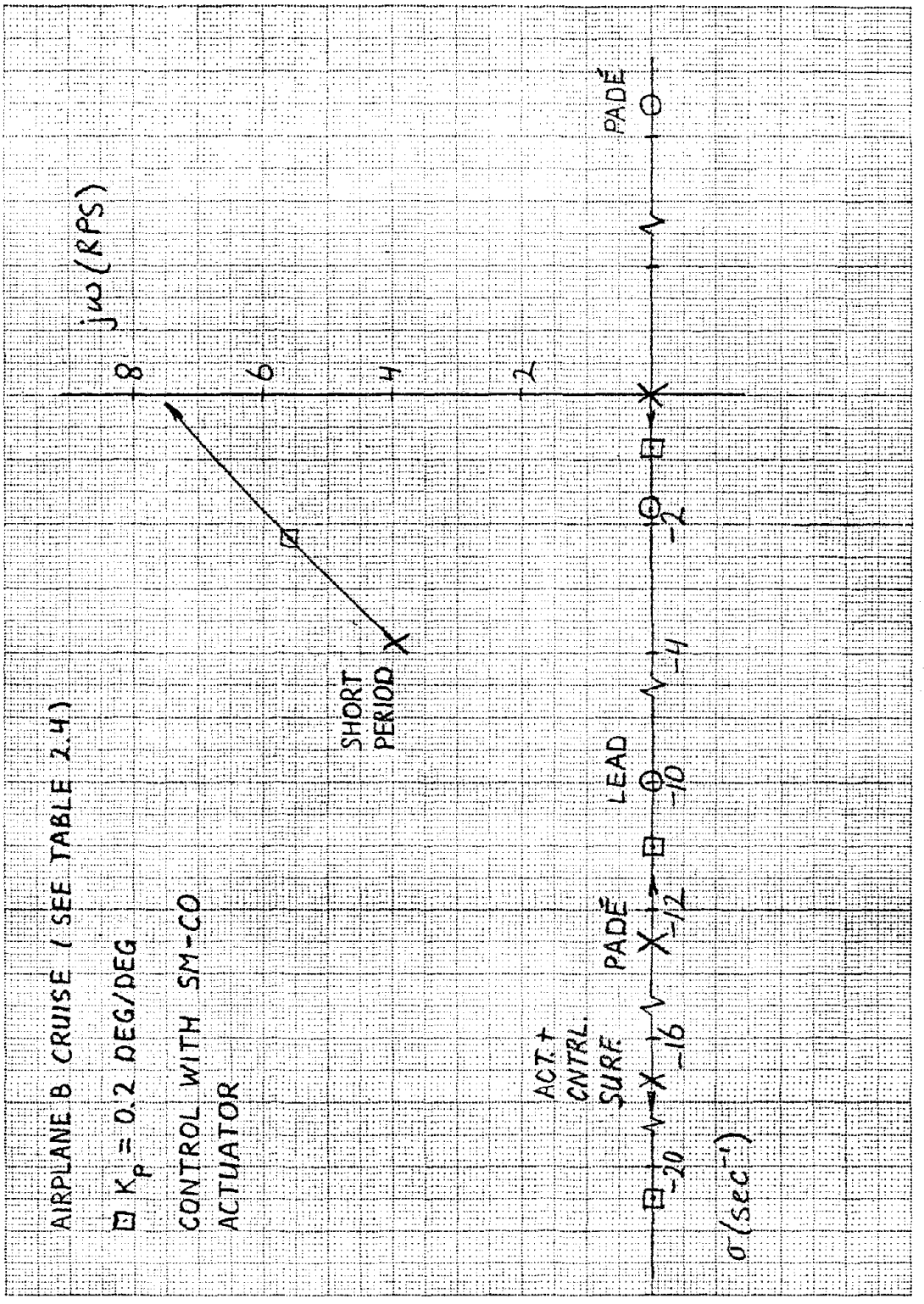


| | | | | | | |
|---|---|---|---|---|---|---|
| CALC | HE | | REVISED | DATE | Figure 6.5: Theta Hold Airplane B, Cruise Sm-Co Actuator | |
| CHECK | | | | | | |
| APPD | | | | | | |
| APPD | | | | | | |
| | | | | | UNIVERSITY OF KANSAS | PAGE 117 |

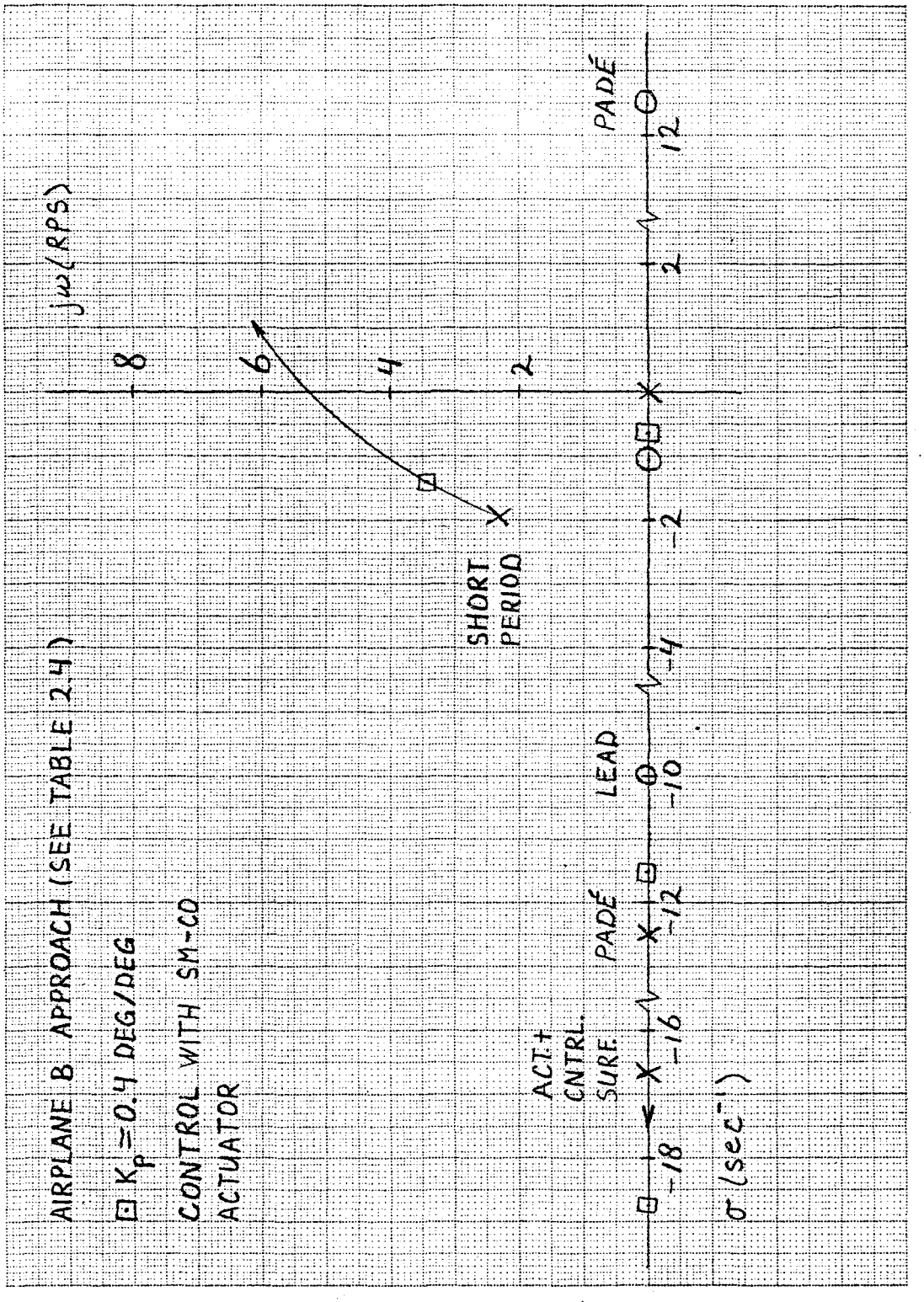


| | | | | |
|---|---|---|---|---|
| CALC | HE | | REVISED | DATE |
| CHECK | | | | |
| APPD | | | | |
| APPD | | | | |
| | | | | |

Figure 6.6: Theta Hold Airplane B, Approach Sm-Co Actuator

UNIVERSITY OF KANSAS

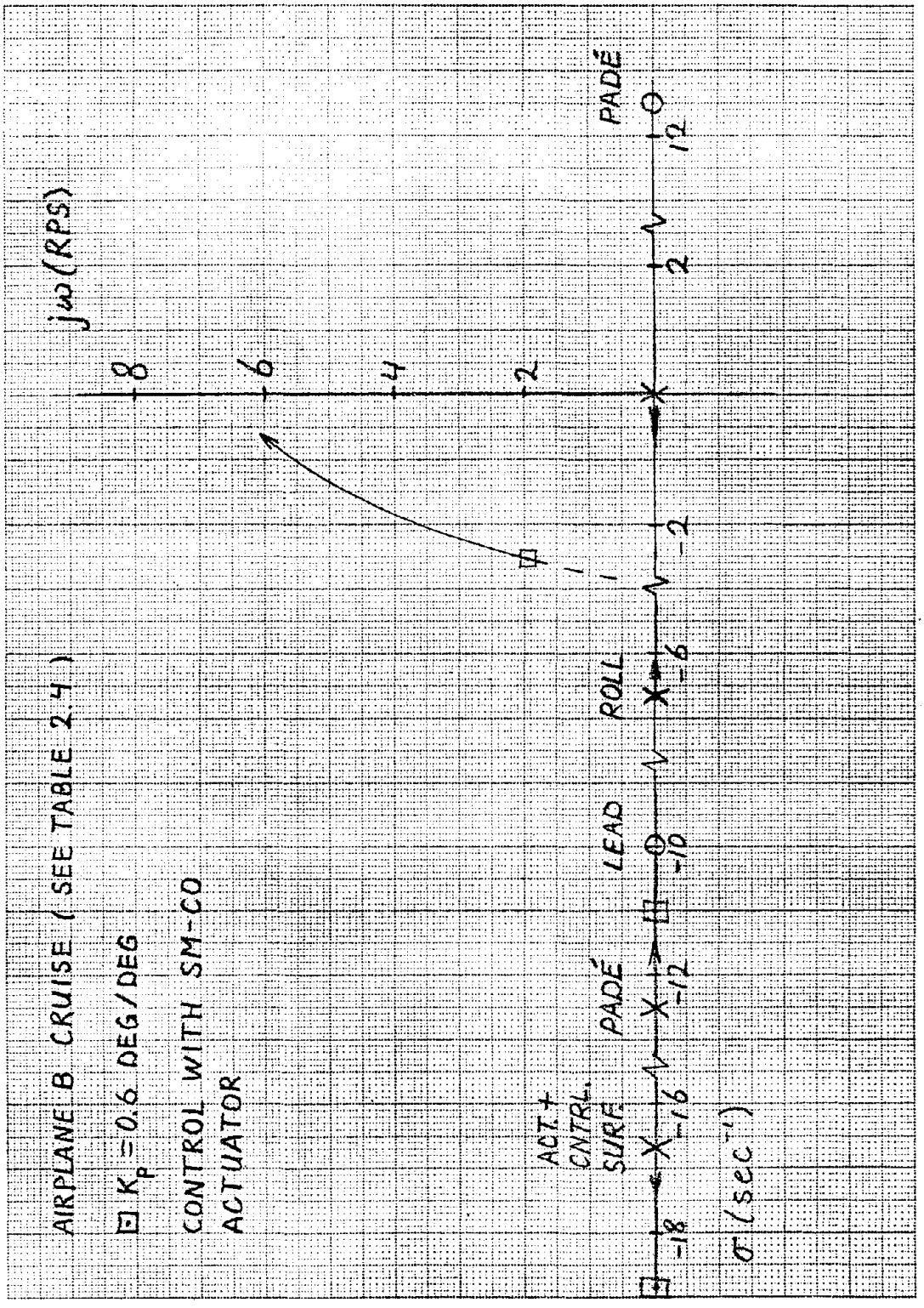


| | | | | | |
|---|---|---|---|---|---|
| CALC | HE | | REVISED | DATE | Figure 6.7: Phi Hold Airplane B, Cruise Sm-Co Actuator |
| CHECK | | | | | |
| APPD | | | | | |
| APPD | | | | | |
| | | | | | UNIVERSITY OF KANSAS |

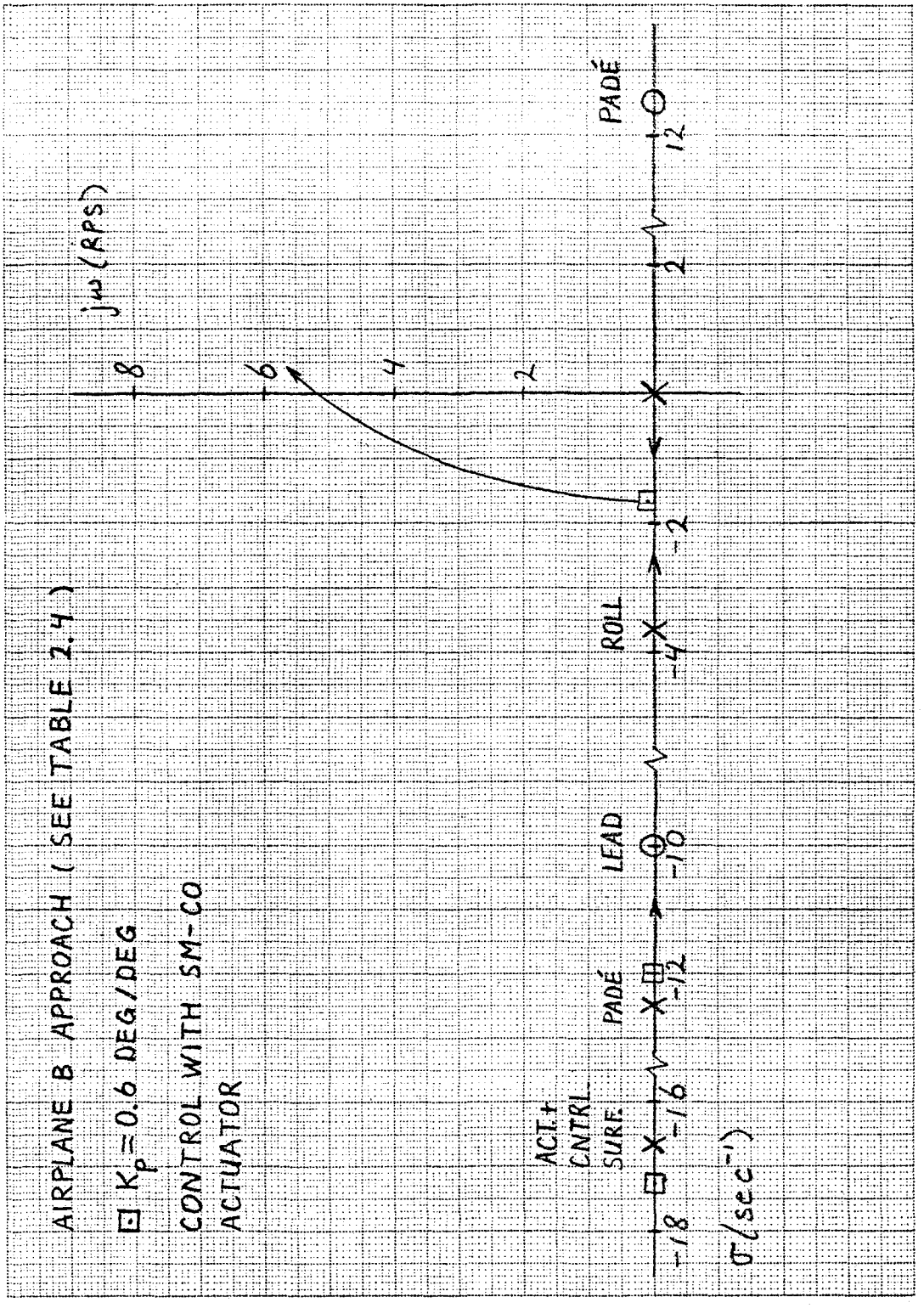


| | | | | | |
|---|---|---|---|---|---|
| CALC | HE | | REVISED | DATE | Figure 6.8: Phi Hold Airplane B, Approach Sm-Co Actuator |
| CHECK | | | | | |
| APPD | | | | | |
| APPD | | | | | |
| | | | | | UNIVERSITY OF KANSAS |

in the same spot for both flight modes and both flight conditions. This is because this type of actuator is designed in such a way that the aerodynamic load has very little influence on the actuator time constants [see Section 3.3.2 for $\tau_a$ values in (6.4)].

For small $K_p$ values the pitch attitude hold mode is well damped (see Fig. 6.5 and 6.6), but it is unstable for $K_p>0.7$ in cruise and for $K_p>1.4$ in approach. This behavior is not caused by the actuator, as is the case with the bank angle hold mode on airplane A, but by the high stabilator effectiveness. The pilot has to be very careful with control stick deflections. This is not a very desirable situation, but it could be solved easily with a pitch rate inner feedback loop which brings the short period pole down and to the left in the s-plane. However, doing this falls outside the scope of this analysis.

The position of the lead zero is not very critical here; the pilot may generate a little more or a little less lead without causing a very different closed loop behavior.

Performance of the bank angle hold mode is good: well damped without being very slow for both cruise and approach. Again the actuator pole does not interfere with the poles of the airplane. The system goes unstable for $K_p>3.2$ in cruise and does not go unstable for the range of examined $K_p$ values ($0<K_p<5$) in approach, so there is hardly any chance of pilot induced oscillations here. If the pilot would generate a little more lead in cruise, for example a $T_L$ of 0.16 sec so that his lead zero would be just to the right of the roll pole, the airplane response would even be better. This also holds for the approach condition if $T_L=0.3$ sec.

The electro-mechanical samarium-cobalt actuator performs well under the conditions considered because its response is fast enough to avoid interference with the overall airplane and can be made to do so for many different airplanes, which will make it a good choice for actuation requirements.

## 6.4 FLIGHT CONTROL SYSTEM ANALYSIS, AIRPLANE C

Geometric and flight condition data on this airplane, the twin-engine turboprop, can be found in Section 2.4. A linear electro-hydraulic actuator will be used in this airplane, and its closed loop time constants for aileron and elevator are presented in Section 5.3.2. The dimensional stability derivatives necessary for computation of the transfer functions (6.1) and 6.2) are shown in Tables 6.10 (cruise) and 6.12 (approach). The actual cruise and approach transfer functions can be seen in Tables 6.11 and 6.13, respectively. Stability derivative data have been taken from Ref. 4.

Table 6.10 - Dynamic Characteristics of Airplane C (Cruise)

| | |
|---|---|
| $M_{\delta_E} = -23.08\ sec^{-2}$ | $M_{\alpha} = -21.81\ sec^{-2}$ |
| $M_{\dot{\alpha}} = -0.758\ sec^{-2}$ | $Z_{\alpha} = -579.3\ ft\ sec^{-2}$ |
| $M_{q} = -2.833\ sec^{-1}$ | $Z_{\delta_E} = -63.09\ ft\ sec^{-2}$ |
| $L_{\delta_A} = 16.98\ sec^{-2}$ | $L_{p} = -2.782\ sec^{-1}$ |

Table 6.11 - Transfer Functions of Airplane C (Cruise)

$$\frac{\theta}{\delta_E} = \frac{-1.045\ (\frac{s}{1.33} + 1)}{s\ (\frac{s^2}{(5.05)^2}) + \frac{2(0.48)}{5.05}\ s + 1)}$$

poles: $s_1 = 0$ $\qquad \omega_{n_{S.P.}} = 5.05$ rad/sec

$s_{2,3} = -2.44 \pm 4.42j$ $\qquad \zeta_{S.P.} = 0.48$

zeroes: $s_1 = -1.33$

$$\frac{\phi}{\delta_A} = \frac{6.104}{s\ (\frac{s}{2.782} + 1)}$$

poles: $s_1 = 0$

$s_2 = -2.782$

Table 6.12 - Dynamic Characteristics of Airplane C (Approach)

$M_{\delta_E} = -5868\ \text{sec}^{-2}$ $\qquad M_\alpha = -6.424\ \text{sec}^{-2}$

$M_{\dot{\alpha}} = -0.537\ \text{sec}^{-1}$ $\qquad Z_\alpha = -180.2\ \text{ft sec}^{-2}$

$M_q = -2.01\ \text{sec}^{-1}$ $\qquad Z_{\delta_E} = -16.32\ \text{ft sec}^{-2}$

$L_{\delta_A} = 4.456\ \text{sec}^{-2}$ $\qquad L_p = -1.971\ \text{sec}^{-1}$

Table 6.13 - Transfer Functions of Airplane C (Approach)

$$\frac{\theta}{\delta_E} = \frac{-0.653\left(\frac{s}{0.96} + 1\right)}{s\left(\frac{s^2}{(2.92)^2} + \frac{2(0.62)}{2.92}s + 1\right)}$$

poles: $s_1 = 0$ $\qquad \omega_{n_{S.P.}} = 2.92$ rad/sec

$s_{2,3} = -1.81 \pm 2.30j$ $\qquad \zeta_{S.P.} = 0.62$

zeroes: $s_1 = -0.96$

$$\frac{\phi}{\delta_A} = \frac{2.306}{s\left(\frac{s}{1.971} + 1\right)}$$

poles: $s_1 = 0$

$s_2 = -1.971$

Root loci for airplane C are presented in Figures 6.9-6.12. $K_p$ is again the variable pilot gain. The actuator-plus-control surface pole lies a little bit to the right of s = -8 for the elevator and a little bit to the left of s = -8 for the aileron, independent of flight condition [see Section 5.3.2 for the actuator time constants in (6.4)].

For $K_p$ values smaller than one the pitch attitude hold is reasonably well damped, a bit better in approach than in cruise; see Fig. 6.9 and 6.10. It goes unstable for $K_p > 1.6$ in cruise and for $K_p > 3.4$ in approach. The actuator pole moves to the left toward the lead zero and does not cause any problems. There is no necessity for the pilot to generate more lead.

Performance of the bank angle hold mode is reasonable for small pilot gains. It goes unstable for $K_p > 1.0$ in cruise and for $K_p > 2.7$

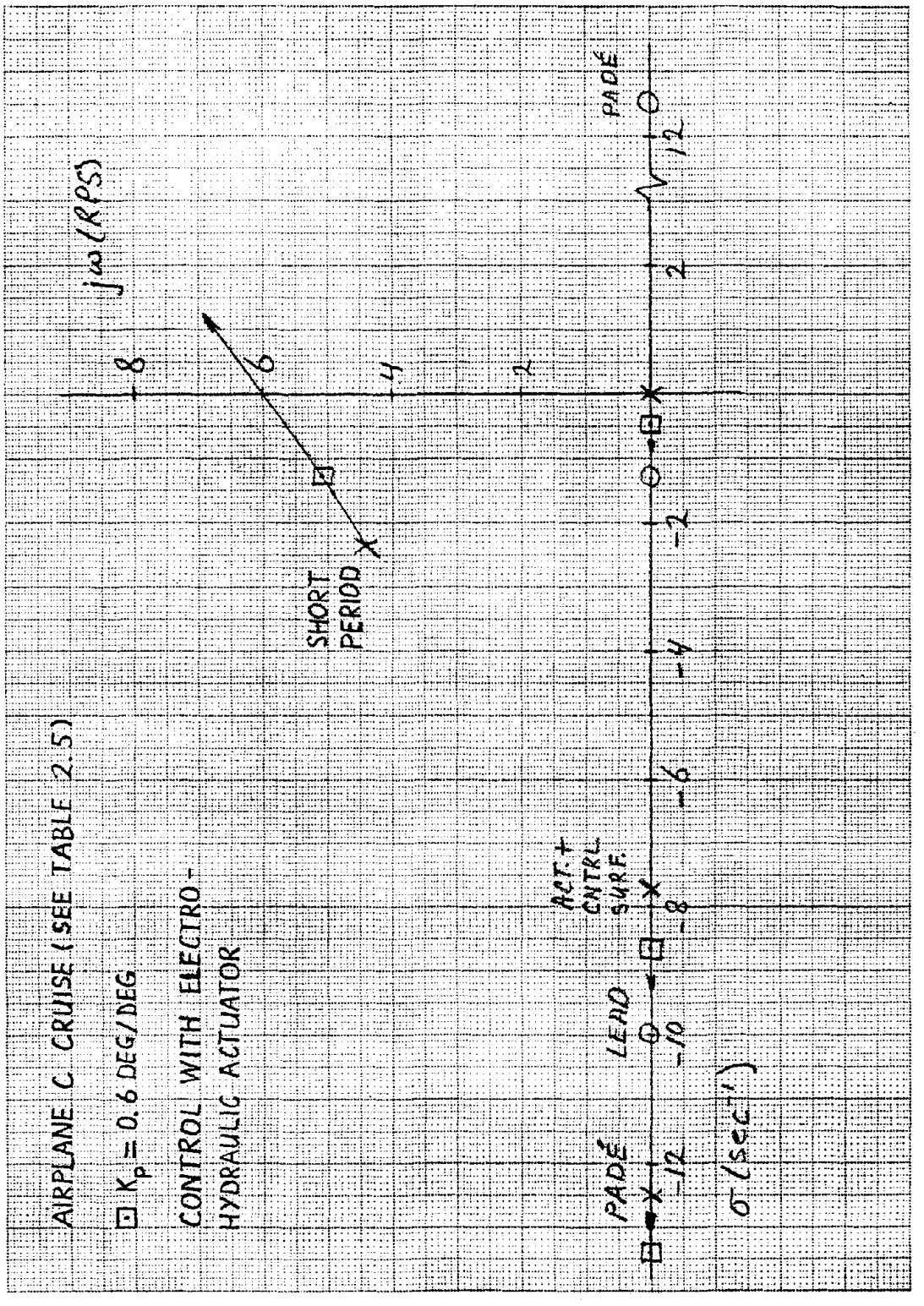


| | | | | | |
|---|---|---|---|---|---|
| CALC | HE | | REVISED | DATE | Figure 6.9: Theta Hold Airplane C, Cruise Electro-Hydraulic Actuator |
| CHECK | | | | | |
| APPD | | | | | |
| APPD | | | | | |
| | | | | | UNIVERSITY OF KANSAS |

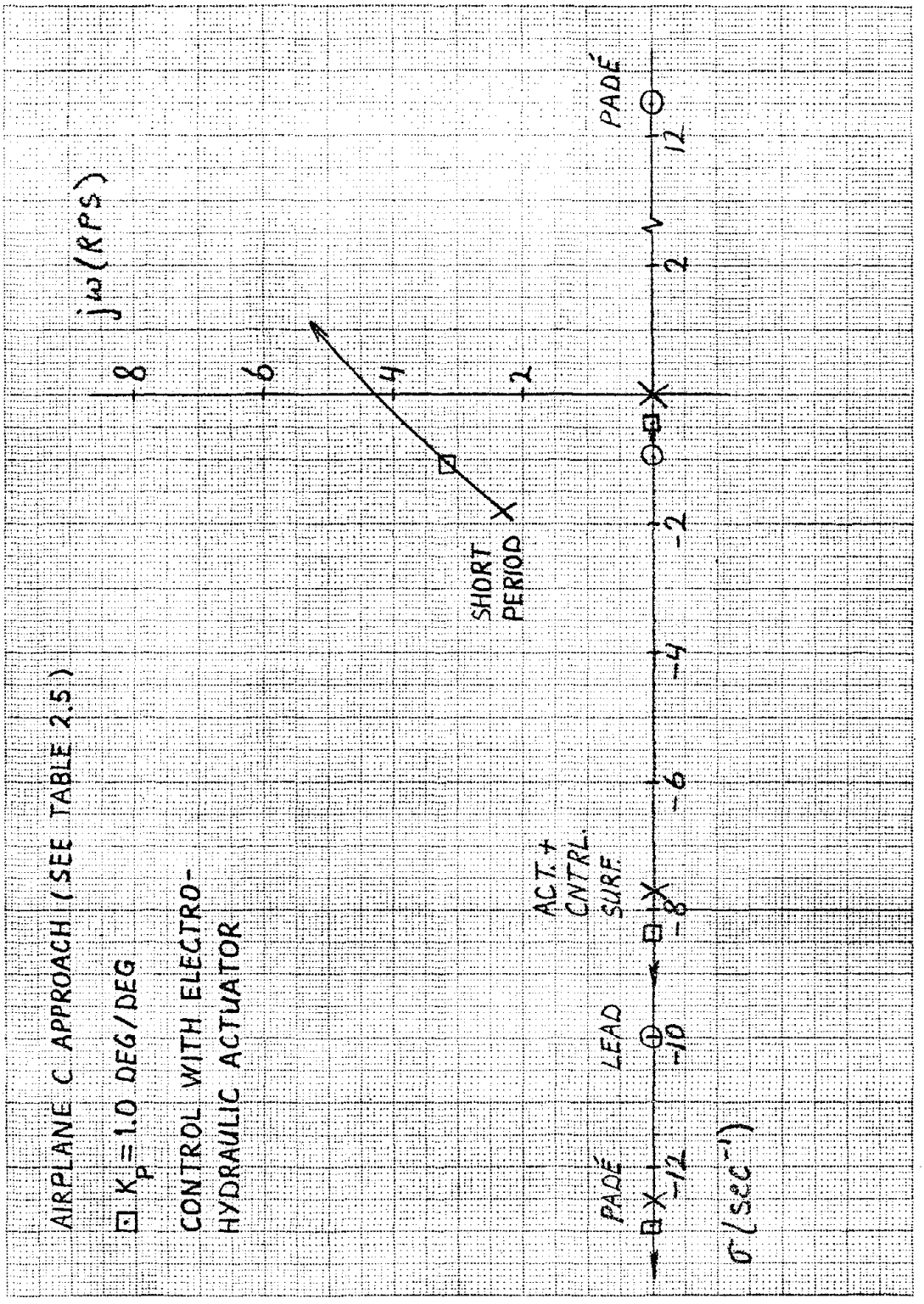


| | | | | | |
|---|---|---|---|---|---|
| CALC | HE | | REVISED | DATE | Figure 6.10: Theta Hold Airplane C, Approach Electro-Hydraulic Actuator |
| CHECK | | | | | |
| APPD | | | | | |
| APPD | | | | | |
| | | | | | UNIVERSITY OF KANSAS |

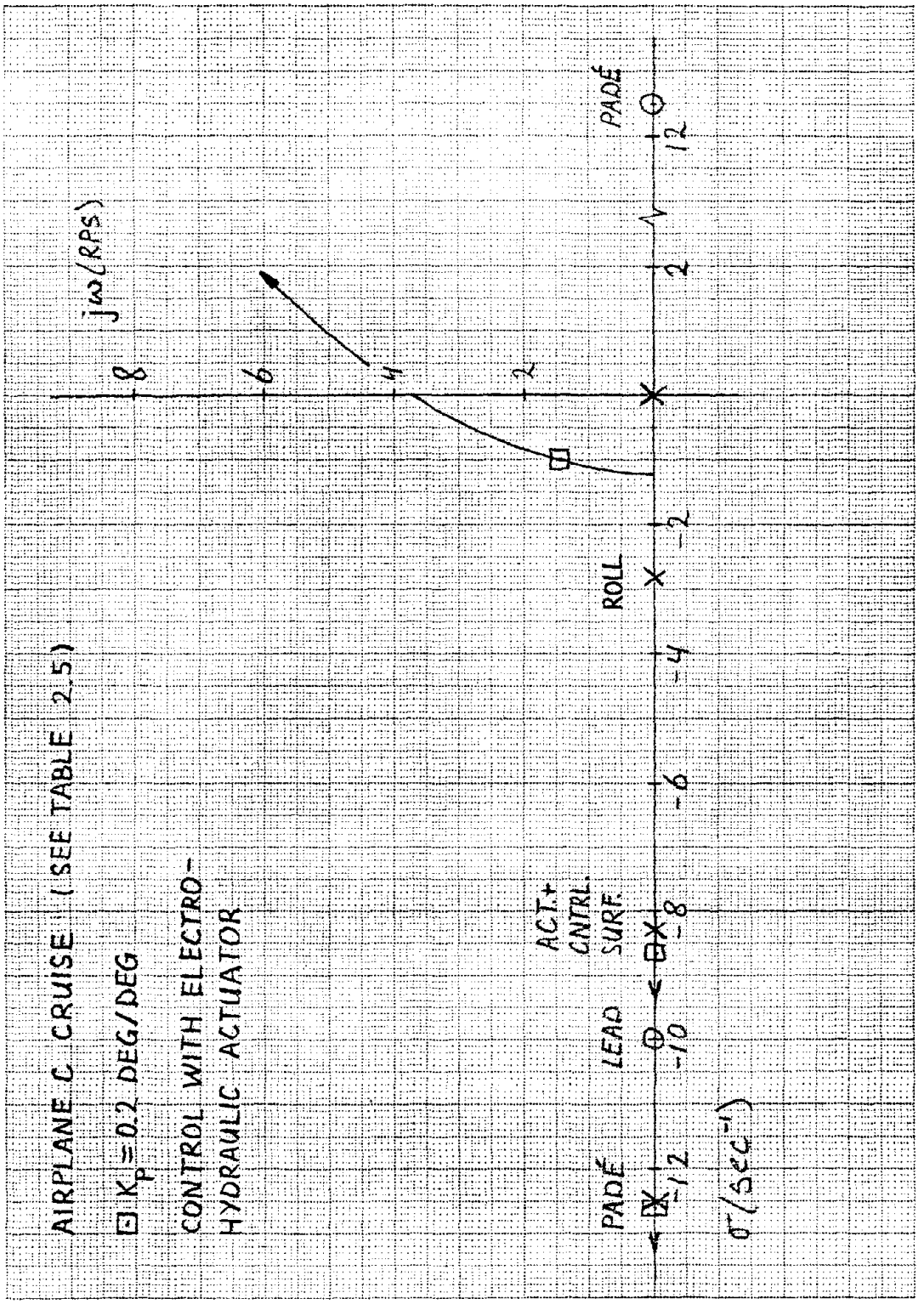


| | | | | |
|---|---|---|---|---|
| CALC | HE | 78-3-1 | REVISED | DATE |
| CHECK | | | | |
| APPD | | | | |
| APPD | | | | |
| | | | | |

Figure 6.11: Phi Hold Airplane C, Cruise Electro-Hydraulic Actuator

UNIVERSITY OF KANSAS

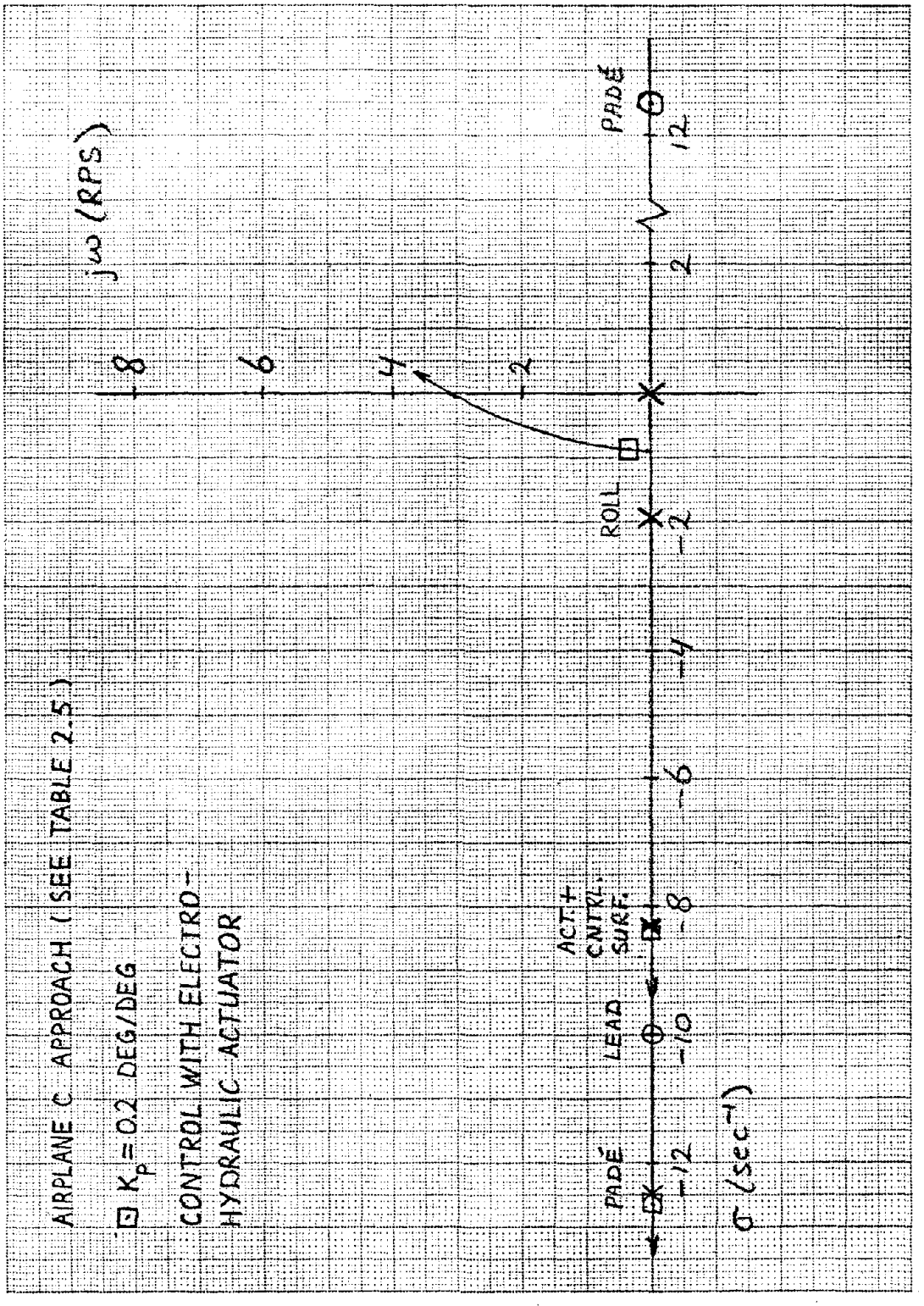


| | | | | | |
|---|---|---|---|---|---|
| CALC | HE | 78-2-20 | REVISED | DATE | Figure 6.12: Phi Hold Airplane C, Approach Electro-Hydraulic Actuator |
| CHECK | | | | | |
| APPD | | | | | |
| APPD | | | | | |
| | | | | | UNIVERSITY OF KANSAS |

in approach. These values are not too high and there are two ways to improve the situation: inner loop feedback of roll rate (which moves the roll pole to the left in the s-plane) or generation of more lead by the pilot. However, he would have to generate a rather large amount of lead (about 0.5 sec). This may be possible during approach, but it is not very likely to happen in cruise.

The electro-hydraulic actuator has good response characteristics and is therefore very suitable for autopilot systems. In fact it is widely used in transport aircraft, except for the smaller airplanes that do not have a hydraulic system.

## 6.5 SUMMARY

Three different types of actuators have been investigated for their suitability in a pilot-in-the-loop system. These types are electro-pneumatic, electro-mechanical and electro-hydraulic. All analyses have been carried out with pilot-in-the-loop operation on three different general aviation airplanes. The response of the electro-pneumatic actuator is rather poor; but the other two types are both very suitable for actuation requirements, the electro-mechanical actuator being somewhat better than the electro-hydraulic one. Since the performance of these types is good, choice of either one will depend on weight considerations and power requirements, which are discussed in Chapter 7. An advantage for the electro-mechanical actuator is that all general aviation airplanes have an electrical system, but not all of them--especially not the smaller ones--have a hydraulic system.

8. Wolowicz, C. H. and Yancey, R. B., "Longitudinal Aerodynamic Characteristics of Light Twin-Engine Propeller-Driven Airplanes," NASA TN D-6800, June 1972.

CHAPTER 7

# OPERATIONAL CHARACTERISTICS

This chapter discusses the operational characteristics of each type of actuator and its suitability for light aircraft applications. Section 7.1 covers weight and volume requirements with diagrams of several actuators showing their relative size. Section 7.2 covers cost and power requirements, and Section 7.3 shows installations of each of the three types of actuators with the control surface model.

Reference 1 presented a table showing the relative merits of mechanical, electro-mechanical, pneumatic and hydraulic systems and is shown in Table 7.1. Recent advances in the use of rare earth magnetic materials in electro-mechanical actuators should improve their ratings in torque, power, speed of response and compactness.

Table 7.1 - Comparison of Power Systems

| System | | |
|---|---|---|
| | M | Mechanical |
| | EM | Electro-Mechanical |
| | P | Pneumatic |
| | H | Hydraulic |

| Property | Best | Good | Fair |
|---|---|---|---|
| Torque/Inertia | H | P | M,EM |
| Power/Weight | H,P | - | EM,M |
| Steady State Rigidity | H | M | P,EM |
| Friction | EM | H,M | P |
| Dirt Vulnerabliity | EM,M | - | H,P |
| Speed of Response | - | H | P,M,EM |
| Compactness | - | H | P,M,EM |
| Ability to Work in Adverse Conditions | - | P,M,H | EM |
| Relative Cost | M,EM | H,P | - |

## 7.1 WEIGHT AND VOLUME REQUIREMENTS

In an aircraft, weight is a major consideration, as each pound of weight saved in the airframe is an additional pound in payload. Weight reduction can also lead to reduced engine size, less structural weight and increased performance. Volumetric requirements for components such as actuators are also important in an aircraft, as space is frequently at a premium, especially for wing installations. In the preliminary design stages of an aircraft, the weight and volume requirements of system components are normally the two most important considerations in the selection process.

Pneumatic actuators require a greater volume than their hydraulic counterparts. This is due to the reduced supply pressure which is normally 20 to 150 psi as compared to hydraulic which normally runs from 500 to 3000 psi. This reduced supply pressure requires a larger piston area for the same force and increases the overall volume. Reduction in supply pressure also decreases the oscillatory nature of the response as shown in Section 4.3. Figure 7.1 shows the pneumatic actuator used in the control surface model in Section 4.3. One reason for the high weight is the high service pressure which increases the thickness of the cylinder walls. Making the cylinder of aluminum instead of steel would reduce overall weight.

An autopilot currently in use for general aviation aircraft using pneumatic actuators uses two actuators for positive and negative displacements resulting in a large piston area. The actuators are installed on the aircraft's cable system, and the valves are controlled with a pulse modulation to position the actuator. The cable system provides more damping than a direct attachment of the actuator to the control

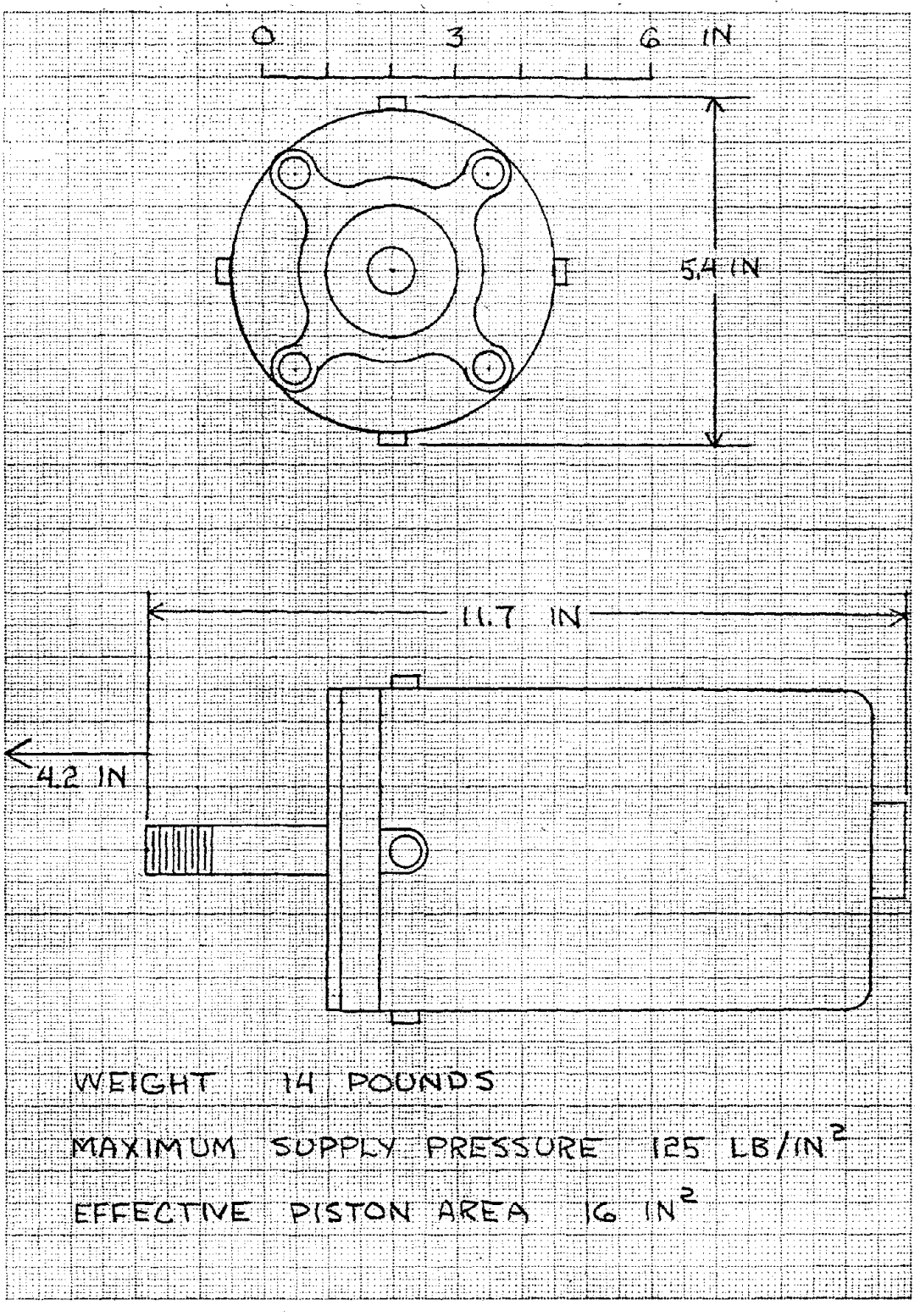


| | | | | | |
|---|---|---|---|---|---|
| CALC | | | REVISED | DATE | Figure 7.1: Linear Diaphragm Pneumatic Actuator |
| CHECK | | | MSR | | |
| APPD | | | | | |
| APPD | | | | | |
| | | | | | UNIVERSITY OF KANSAS |

surface. By keeping the supply pressure to 30 psi, the oscillations are minimized in the response. Valve areas and specific supply pressures must be tailored to each type of aircraft. A more detailed description of this system is found in Reference 2.

The hydraulic actuator used to evaluate the control surface model in Section 5.3 is shown in Figure 7.2. Weight is reduced in comparison to the pneumatic due to the smaller piston area, but overall length is increased. It should be added that the hydraulic actuator requires hydraulic fluid that has a weight of about 55 lbs/ft$^3$. A reservoir normally holds enough fluid for several minutes of rated flow (Section 5.1). For a flow rate of 20 in$^3$/sec which would be normal for 4 of the actuators used in the control surface model, this amounts to 113 pounds for 3 minutes at rated flow. A rotary hydraulic actuator is shown in Figure 7.3 that is used in industrial applications. High supply pressures require a thick walled housing which increases the weight. The example shown uses a steel housing, and aluminum would help in reducing the weight. Its size would also probably make a wing installation for the ailerons impractical for a small aircraft but could be fuselage mounted and mechanically linked.

Electro-mechanical actuators are frequently used on general aviation aircraft for flaps and landing gear retraction. Using conventional magnetic materials such as Alnico for the motor results in a size comparable to a pneumatic actuator as shown in Figure 7.4. This is an electro-mechanical used in industrial and agricultural applications. Figure 7.5 shows the electro-mechanical actuator used recently in the NASA Separate Surface Stability Augmentation Program. Recent advances in the use of rare earth magnets such as samarium cobalt has greatly reduced the motor

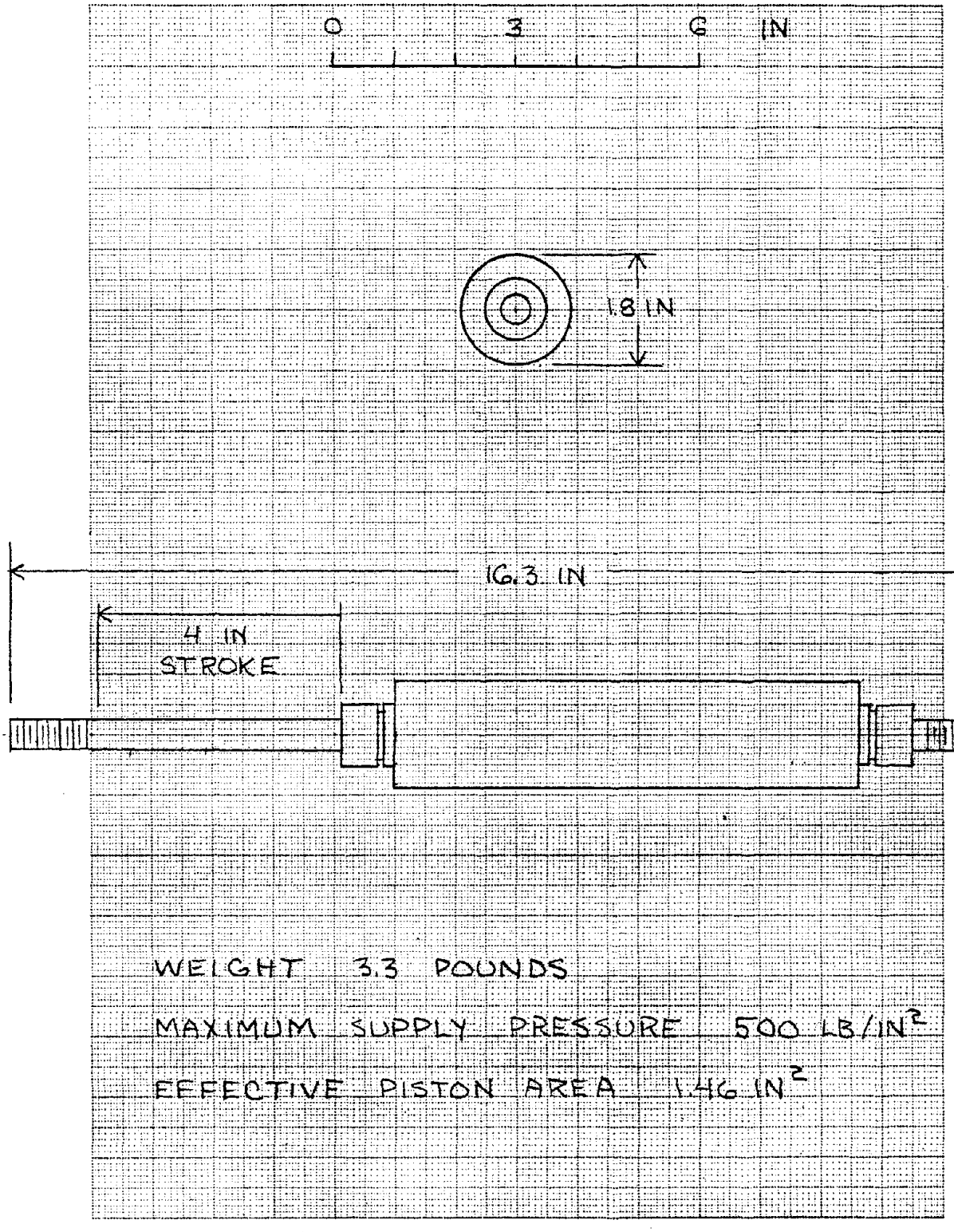


| | | | | |
|---|---|---|---|---|
| CALC | | | REVISED | DATE |
| CHECK | | | MSR | |
| APPD | | | | |
| APPD | | | | |
| | | | | |

Figure 7.2: Linear Hydraulic Actuator

UNIVERSITY OF KANSAS

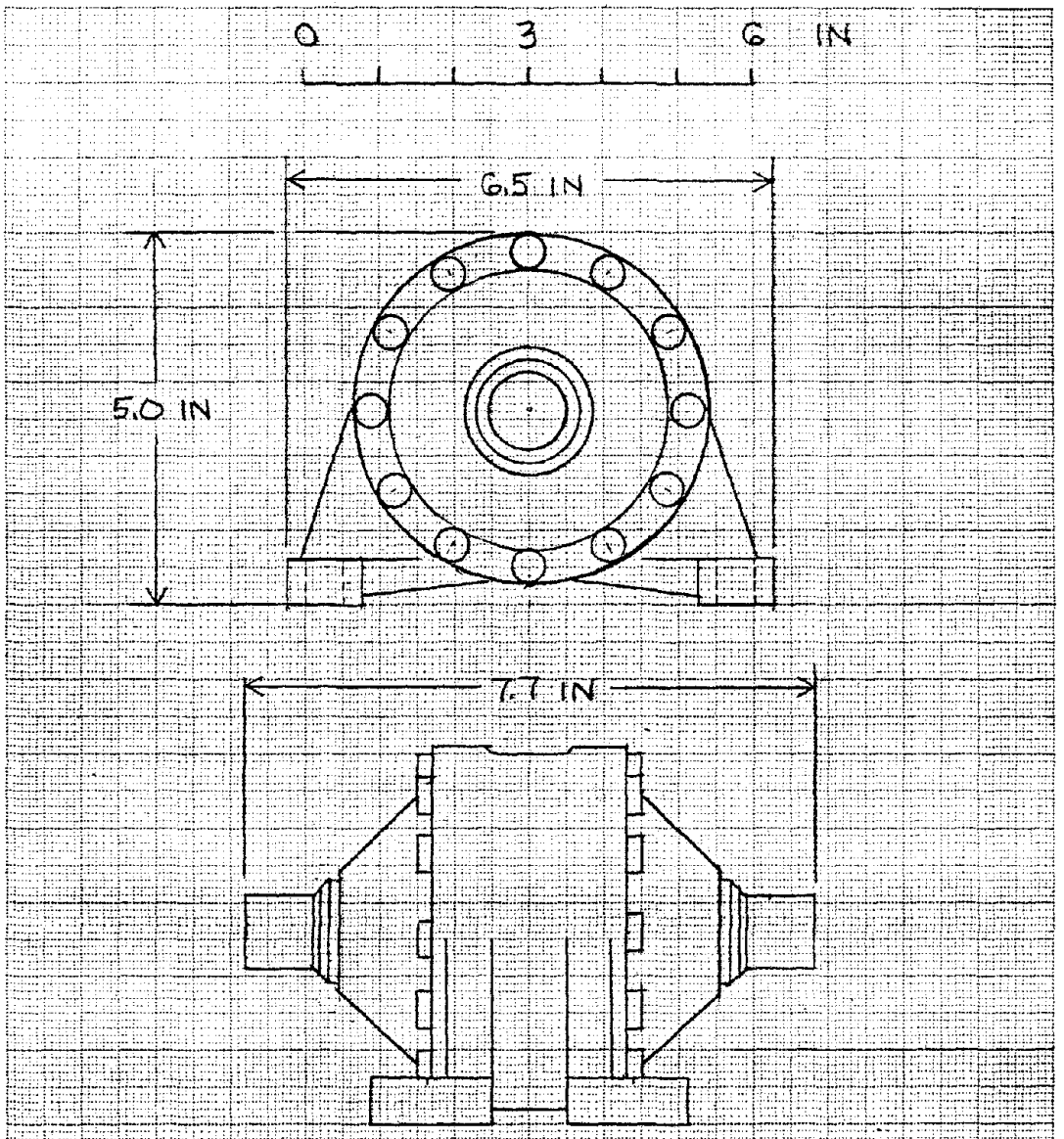


WEIGHT 16.5 POUNDS

SUPPLY PRESSURE 100 TO 3000 LB/IN$^2$

MAXIMUM TORQUE 3240 IN LB

ANGULAR DISPLACEMENT 280°

| | | | | |
|---|---|---|---|---|
| CALC | | | REVISED | DATE |
| CHECK | | | MSR | |
| APPD | | | | |
| APPD | | | | |
| | | | | |

Figure 7.3: Rotary Hydraulic Actuator

UNIVERSITY OF KANSAS

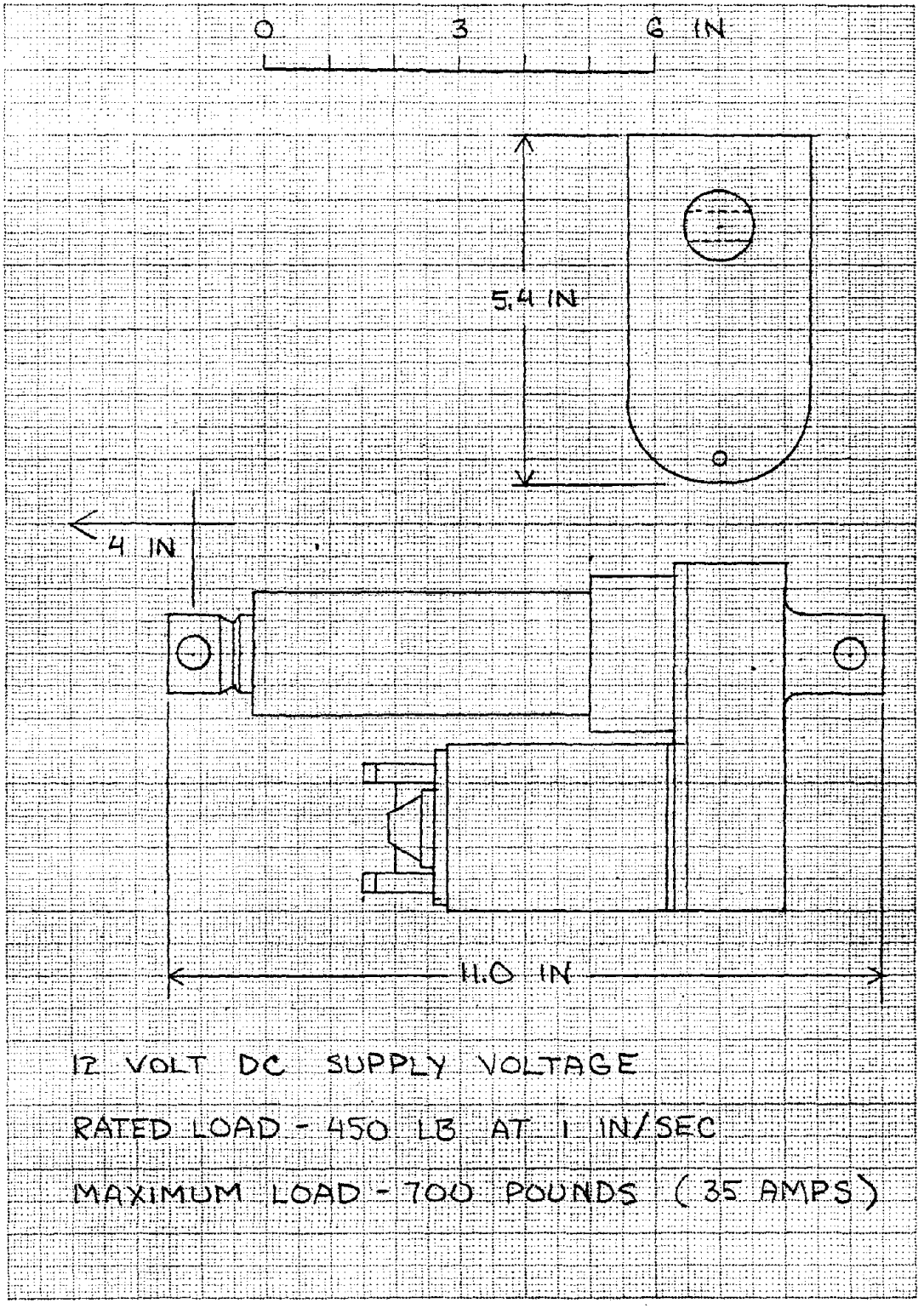


| | | | | |
|---|---|---|---|---|
| CALC | | | REVISED | DATE |
| CHECK | | | MSR | |
| APPD | | | | |
| APPD | | | | |
| | | | | |

Figure 7.4: Linear Electro-Mechanical Actuator

UNIVERSITY OF KANSAS

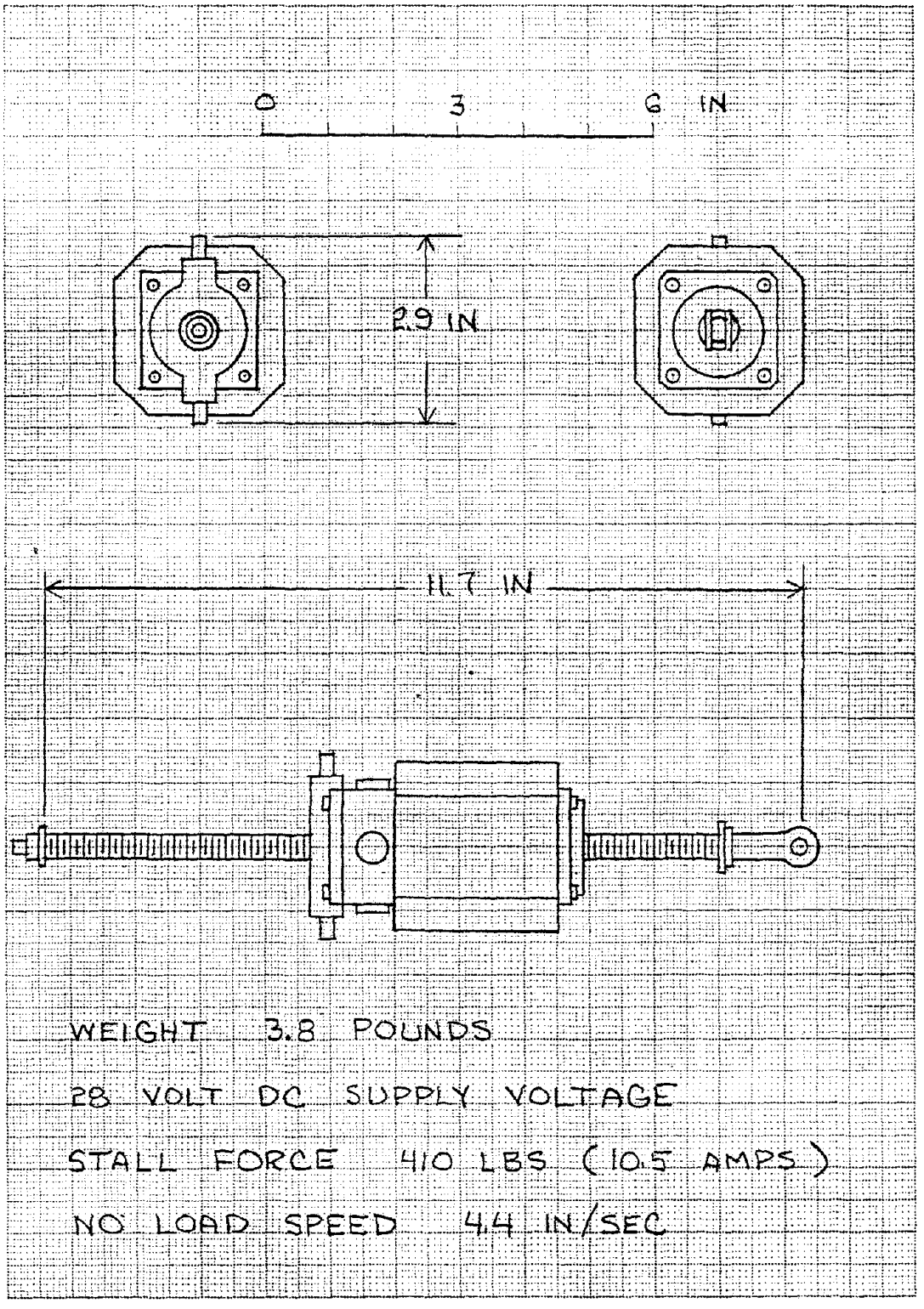


| | | | | |
|---|---|---|---|---|
| CALC | | | REVISED | DATE |
| CHECK | | | MSR | |
| APPD | | | | |
| APPD | | | | |
| | | | | |

Figure 7.5: Linear Electro-Mechanical Actuator for Aircraft Usage

UNIVERSITY OF KANSAS

size necessary for a required torque. Figure 7.6 shows a motor recently developed for aerospace applications. The gearbox necessary to connect the motor to the control surface is not shown, but a possible configuration is shown in Section 7.3. The weight of the gearbox should not be a great deal larger than that of the motor making this type of actuator very suitable for small aircraft applications.

It should be added that the weight of the actuator is not the only weight involved in the system. A pneumatic system requires a compressor and valves and the other components outlined in Section 4.1. If the aircraft is pressurized, an expansion of the present system is all that is necessary. System weights vary according to the aircraft requirements but typically run from 20 to 40 pounds for a small aircraft (Reference 2). Hydraulic system weights should be comparable to pneumatic system weights exclusive of the weight of the fluid. In a small aircraft that does not already have a hydraulic system, this weight may be prohibitive. Electro-mechanical actuation of secondary control surfaces is already common practice, and actuation of the primary surfaces would only require expansion of the present system with a minimal increase in weight.

## 7.2 COST AND POWER REQUIREMENTS

A complete aircraft actuation system is normally not an off-the-shelf, fixed-price item and is usually designed by the aircraft company or subcontracted. For a small single-engine aircraft an actuation system exclusive of an autopilot costing much more than several thousand dollars would probably be prohibitive.

For pneumatic and hydraulic systems the control valves require the closest tolerances and tend to be the most expensive items in the

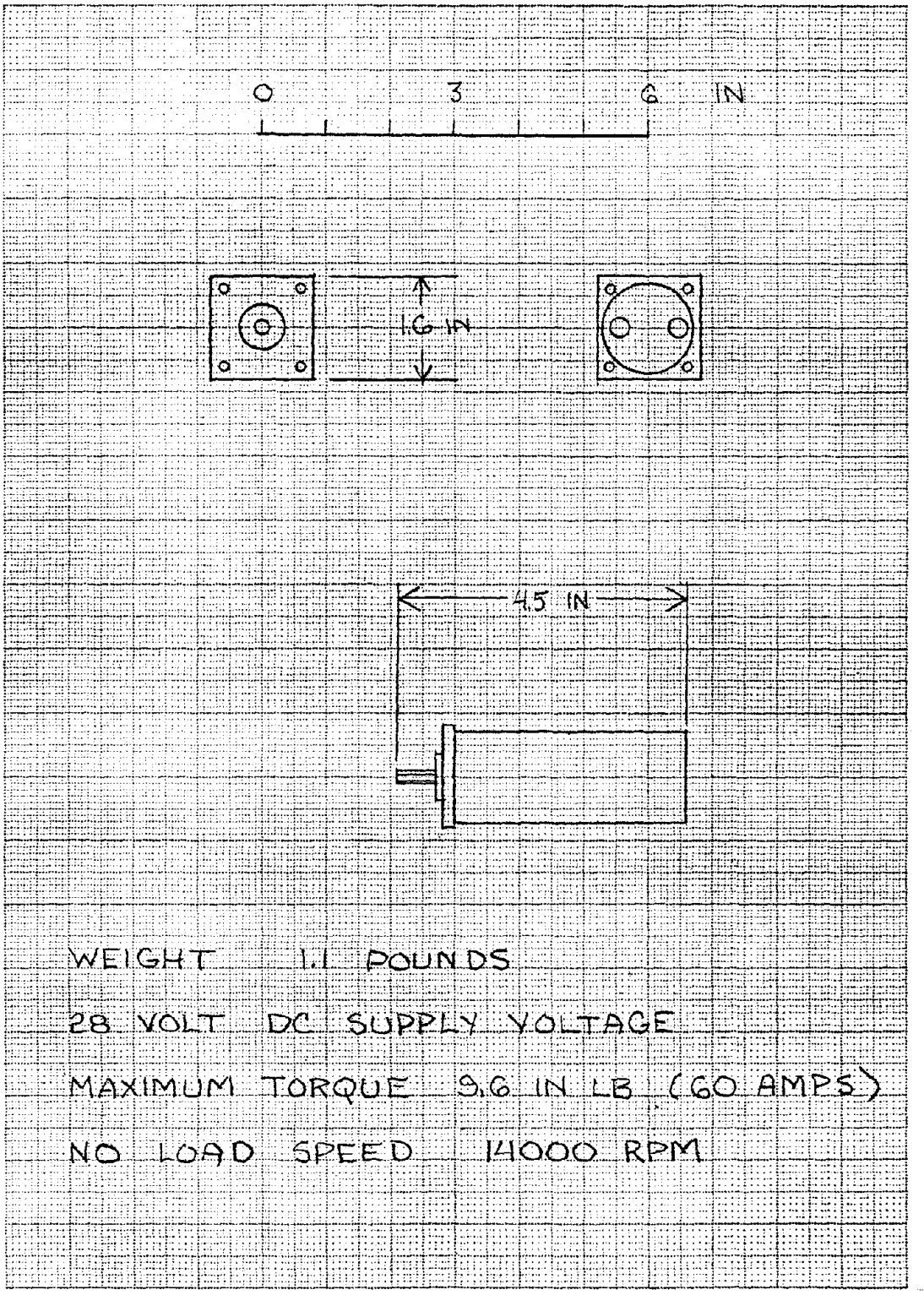


| | | | | | |
|---|---|---|---|---|---|
| CALC | | | REVISED | DATE | Figure 7.6: Samarium Cobalt DC Electric Motor |
| CHECK | | | MSR | | |
| APPD | | | | | |
| APPD | | | | | |
| | | | | | UNIVERSITY OF KANSAS |

system. To protect the valves from erosion, damage filters are necessary. Hydraulic systems require filtration levels of 5 microns due to the small valve openings and are more expensive than the 40 micron filters used in pneumatic systems. Hydraulic and pneumatic components currently in use for military vehicles could be converted for use in general aviation aircraft with some reduction in environmental and performance requirements to reduce cost.

Cost is a primary reason for the current popularity of electro-mechanical actuation for secondary control functions in general aviation aircraft. No additional systems need to be added to the aircraft; the electrical system of the aircraft only needs to be large enough to handle peak loads. The new rare earth magnets are currently in the developmental stages, and costs are relatively high; but continued research should bring prices down to an acceptable level.

Power requirements of an actuator are related to the life cycle costs of the system in that a certain percentage of aircraft engine power is used to power the aircraft systems, and any reduction lowers the fuel consumption. To evaluate the power requirements of fluid actuators, the following equation has been used:

$$HP = \frac{qP_s}{6600\eta} \tag{7.1}$$

where 6600 is the conversion factor from in lbs/sec to horsepower. For an electro-mechanical actuator the following equation is used:

$$HP = \frac{V_{max}\ I_{max}}{745.7\eta} \tag{7.2}$$

where 745.7 is the conversion from watts to horsepower. Power requirements for the three types of actuators used for the control surface model are shown in Table 7.2. An overall efficiency of 80% is used

and is typical for fluid and electro-mechanical systems (Reference 1 and 3). Power requirements for an aircraft system would be approximately 4 times the requirements shown in Table 7.2. The table shows the pneumatic and hydraulic systems approximately equal in power requirements and superior performance for the electro-mechanical. Use of conventional magnetic materials would degrade the performance of the electro-mechanical actuator.

Table 7.2 - Actuator Power Requirements

Pneumatic Actuator

100 psi supply pressure
16 square inch piston area
5 inch/sec velocity
80% efficiency
1.5 horsepower power requirement

Hydraulic Actuator

1000 psi supply pressure
1.46 square inch piston area
5 inch/sec velocity
80% efficiency
1.4 horsepower power requirement

Electro-Mechanical Actuator

Samarium Cobalt Magnet
28 volts maximum voltage
20 amps maximum current
80% efficiency
0.9 horsepower power requirement

## 7.3 INSTALLATION AND MAINTENANCE

The actuation system should be installed on the aircraft so that components requiring maintenance are easily accessable. Volumetric

requirements and the location of structural members for attachment are limitations on the placement of the actuators.

Figure 7.7 shows an installation for a pneumatic actuator. The actuator's volume requires that it be installed in the fuselage tail-cone for an elevator application, and this would also be necessary for the rudder. For the ailerons the actuator would probably have to be fuselage mounted and linked mechanically to the ailerons. This would allow synchronization of the right and left ailerons mechanically.

Figure 7.8 shows an installation for a hydraulic actuator to the control surface model. The reduced volume would allow a wing installation using an aerodynamic fairing in an aileron application. Figure 7.9 shows an electro-mechanical actuator installation using the actuator evaluated in Section 3.3. By having the gearbox act as the hinge for the control surface, the entire actuation system can be contained in the wing. This type of installation was also used in Reference 3. Maintenance for an electro-mechanical system should be minimal as the components can be sealed from environmental contamination.

Conclusions on the suitability of each type of actuator for aircraft applications are discussed in Chapter 8. Weight and volumetric requirements are normally critical in the early design stages with volumetric requirements important with regard to installation ease.

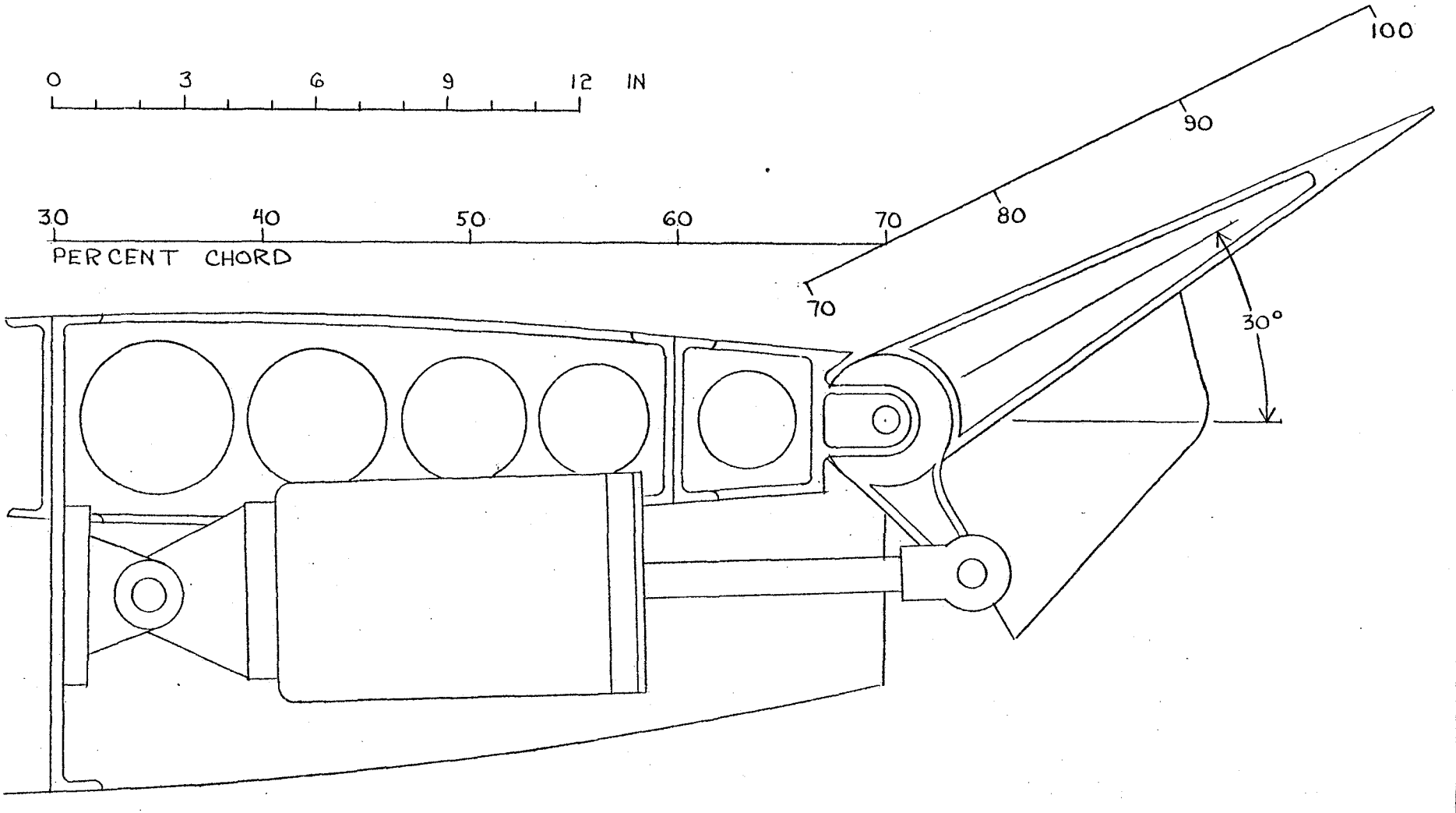


| | | | | |
|---|---|---|---|---|
| CALC | | | REVISED | DATE |
| CHECK | | | | |
| APPD | | | | |
| APPD | | | | |
| | | | | |

Figure 7.7: Pneumatic Actuator Installation Diagram

UNIVERSITY OF KANSAS

PAGE

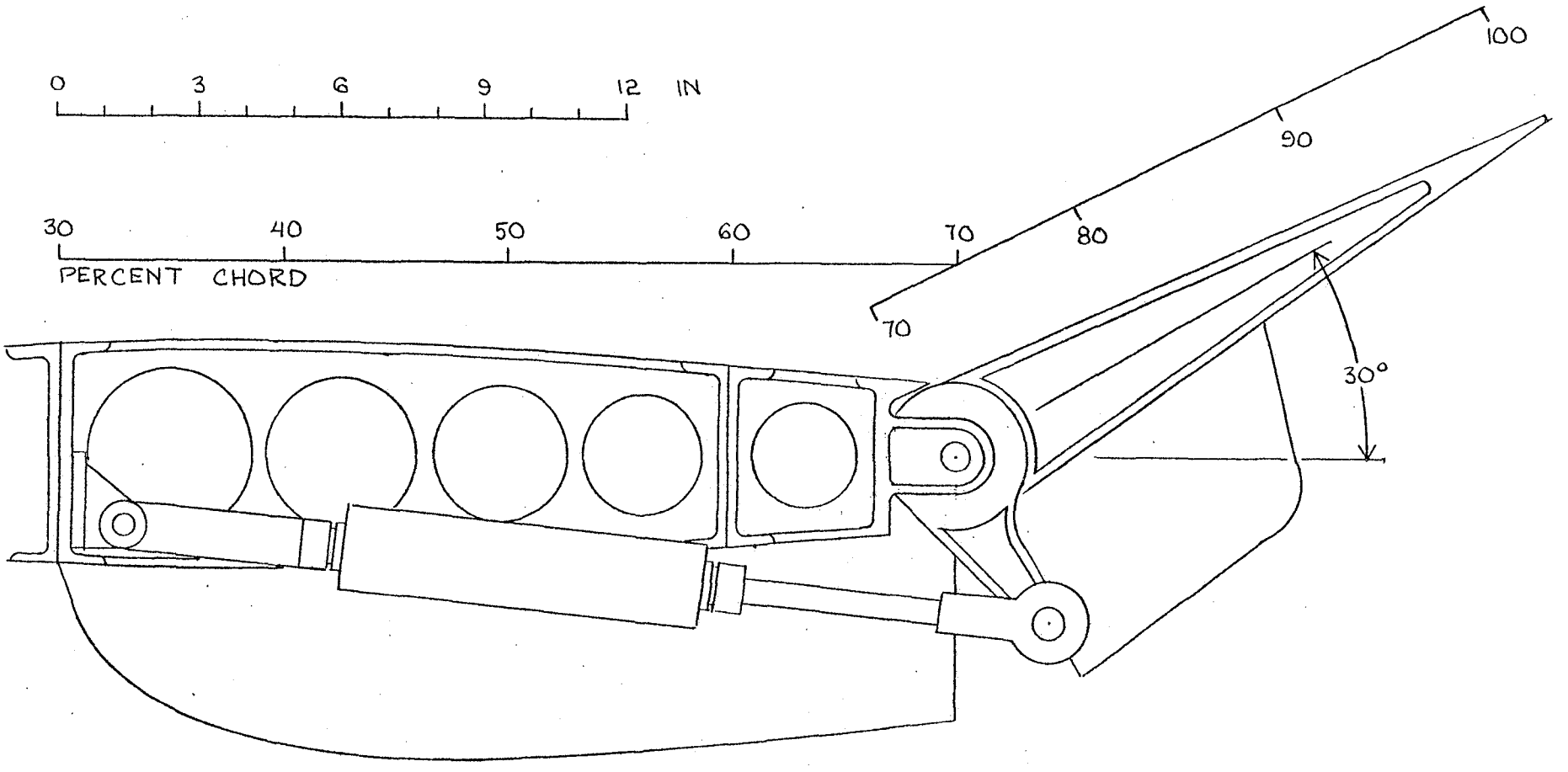


| | | | | |
|---|---|---|---|---|
| CALC | | | REVISED | DATE |
| CHECK | | | | |
| APPD | | | | |
| APPD | | | | |
| | | | | |

Figure 7.8: Hydraulic Actuator Installation Diagram

UNIVERSITY OF KANSAS

PAGE

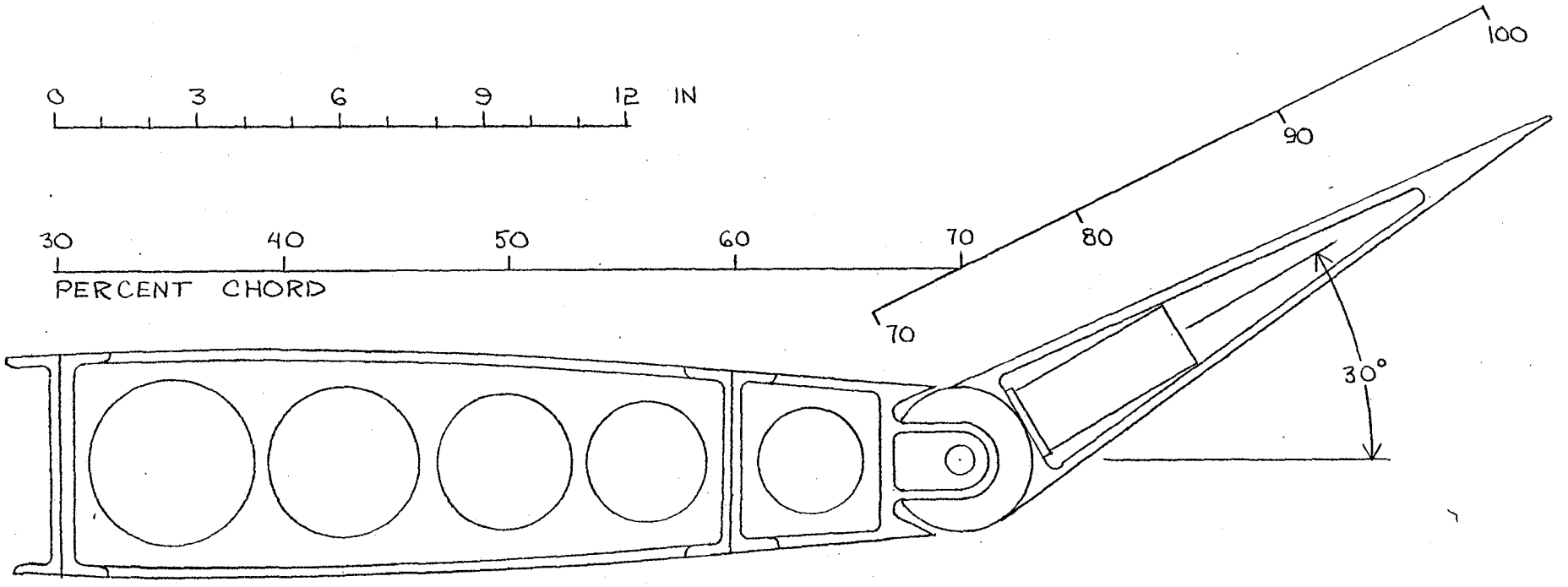


| | | | | |
|---|---|---|---|---|
| CALC | | | REVISED | DATE |
| CHECK | | | | |
| APPD | | | | |
| APPD | | | | |
| | | | | |

Figure 7.9: Electro-Mechanical Actuator Installation Diagram

UNIVERSITY OF KANSAS

PAGE

References for Chapter 7

1. McCloy, D. and Martin, H. R., "The Control of Fluid Power," John Wiley & Sons, 1973.

2. Roskam, Jan, "Flight Dynamics of Rigid and Elastic Airplanes," Volume 2, published by Roskam Aviation and Engineering Corporation, 519 Boulder, Lawrence, Kansas, 1972.

3. Wood, Neal E., Echols, E. F. and Ashmore, John H., "Electro-mechanical Actuation Feasibility Study," AFFDL-TR-76-42, 1976.

4. Andersen, Blaine W., "The Analysis and Design of Pneumatic Systems," John Wiley & Sons, 1967.

5. Hinson, M. L., "An Iron Bird for Static Test and Performance Evaluation of a Separate Surface Attitude Command System," M.S. Thesis, University of Kansas, 1973.

6. Prins, J. J. M., "Flight Hardware Design and an Analog Model of a SSSA Control System for a Beech Model 99 Aircraft," M.S., Thesis, University of Kansas, 1972.

# CHAPTER 8

## CONCLUSIONS

This chapter summarizes the suitability of each type of actuator for use in the primary flight control system of a single engine general aviation aircraft. A low cost electrical actuation system suitable for this type of aircraft would allow an automatic flight control system to be easily installed. With recent advances in micro-electronics, such a system could be developed at a reasonable cost within the next five to ten years.

With further development a pneumatic actuation system for a primary flight control system is feasible. Successful autopilots have been developed using this type of actuation system, and additional research could lead to one suitable for a single engine light aircraft. Electronics may be able to reduce the oscillatory nature of the response characteristics. It is difficult to determine if this type of system can be developed more economically than the other types.

Hydraulic systems are necessary for very high power requirements such as those encountered in airline and military applications. A hydraulic system for a small single engine aircraft could easily be developed with today's technology. The fact that high power requirements are not present in this type of aircraft lessens the need for this type of system.

Electro-mechanical actuation shows promise in that it is already in use for this class of aircraft; and recent advances in magnetic materials such as samarium-cobalt have the potential for greatly increased performance, similar to that obtained from hydraulic systems.

It will be necessary to reduce costs for these materials, as they are now only practical for military and space applications.

This report is a preliminary analysis; and though one type of system seems more suitable than the others, none should be ruled out. Advances are continually being made into all the systems covered, and new solutions to existing problems are continually being found.